Fall 12-14-2018

Towards An In Vitro Model of Testing Osteoblast Cellular Function In Contact With Various Surfaces

Raheleh Miralami
University of Nebraska Medical Center

TOWARDS AN IN VITRO MODEL OF TESTING OSTEOBLAST CELLULAR

FUNCTION IN CONTACT WITH VARIOUS SURFACES

by

Raheleh Miralami

A DISSERTATION

Presented to the Faculty of

the University of Nebraska Graduate College

In Partial Fulfillment of Requirements

For the Degree of Doctor of Philosophy

Medical Science Interdepartmental Area Graduate Program

(Orthopedics)

Under the Supervision of Professor Geoffrey M. Thiele

University of Nebraska Medical Center
Omaha, Nebraska

November 2018

TOWARDS AN IN VITRO MODEL OF TESTING OSTEOBLAST CELLULAR

FUNCTION IN CONTACT WITH VARIOUS SURFACES

Raheleh Miralami, Ph.D.

University of Nebraska, 2018

Supervisor: Geoffrey M Thiele, Ph.D.

Past studies have shown that the success of total joint replacements depends on the biocompatibility of orthopaedic materials, which can be improved by modifying the implant surface. However, the exact roles of these modifications and their effective mechanisms are poorly understood. The objective of this study was to develop and evaluate a model system to investigate the impact of nano-structured surfaces, produced by the ion beam-assisted deposition (IBAD) technique, on biomarkers of osteointegration using an *in vitro* model. The IBAD technique was employed to deposit zirconium oxide (ZrO_2), Titanium oxide (TiO_2), and Titanium (Ti) nano-films on glass or Ti substrates. Essential cellular functions including adhesion, proliferation, differentiation, and apoptosis of a human osteosarcoma cell line (SAOS-2) were compared on coated *vs.* uncoated surfaces at both molecular and gene levels.

Our studies have resulted in several novel observations, including enhanced cell adhesion on nano-coated surfaces assessed by the number of DAPI-stained cells along with monitoring cell morphology (actin stress fiber remodeling at focal adhesion sites) on the surfaces using immunofluorescence techniques. Similarly, we reported that IBAD nano-modifications increased cell proliferation on nano-surfaces measured by mitochondrial dehydrogenase activity and a nuclear cell proliferation-associated antigen. Moreover, enhanced cell differentiation on IBAD-produced surfaces was determined by ALP activity and the rate of calcium deposition in alizarin red assays that are *in vitro* indicators of the successful bone formation. In addition, programmed cell death and necrosis assessed by annexin V staining and flow cytometry observed to be higher

on uncoated surfaces compared to nano-surfaces. Finally, there was a correlation between IBAD-modifications and enhanced bone-associated gene expression at cell adhesion, proliferation, and differentiation as assessed by polymerase chain reaction (PCR) techniques.

In summary, our studies using an *in vitro* model system showed that nano-coated surfaces produced by the IBAD technique are superior to uncoated surfaces in supporting bone-cell adhesion, proliferation, differentiation, and reducing apoptosis at both molecular and gene levels. Therefore, increased osteoblast cellular functions and enhanced bone formation with stronger attachments would be expected from these surfaces in bone-cell applications. In contrast, as anticipated by design, polish uncoated metallic surfaces, e.g., cobalt-chromium inhibited such interactions.

DEDICATION

To my mother, whose patience and constant love sustained me throughout my life, to the memory of my father who always had confidence in me and I feel his presence that used to urge me to strive to achieve my goals, to my loving husband, whose has been a constant source of support and encouragement during the challenges of graduate school and life, and to my son, who came into my life during this journey but unfortunately didn't stay in this world long enough to see me accomplish it.

AUTHOR ACKNOWLEDGMENTS

I am thankful to the lab members from Rheumatology & Immunology Division of the Department of Internal Medicine, specifically Karen Easterling, Carlos Hunter, and Michel Duryee for their help and instructions in lab protocols.

Additionally, I would like to thank Biomechanics lab members from Orthopaedic Department especially David Lusk, Kevin Swierczek, and Joel Weisenburger for all of their help whenever needed. My special thanks go to Eileen Rooney and David Staiert from the Orthopaedic Department for their excellent help during my entire Ph.D. program.

And, finally, I would also like to extend my gratitude to Dr. Davis (Vice Chancellor of Academic Affairs and Dean of Graduate Studies) who has always provided me the best possible support at any time.

TABLE OF CONTENTS

LIST OF FIGURES

LIST OF TABLES

LIST OF ABBREVIATIONS

ALP Alkaline Phosphatase

Ar Argon

BCA Bicinchoninic Acid

BSA Bovine Serum Albumin

CoCr Cobalt Chromium

DAPI 4′,6-Diamidino-2-Phenylindole

FBS Fetal Bovine Serum

FN Fibronectin

IBAD Ion Beam Assisted Deposition

IBSD Ion Beam Sputtering Deposition

N Nitrogen

NaN3 Sodium Azide

O Oxygen

PBS Phosphate Buffered Saline

PCR Polymerase Chain Reaction

PI Propidium Iodide

PNPP P-Nitrophenyl Phosphate

PS   Phosphatidylserine

TA   Tantalum

THA   Total Hip Arthroplasty

Ti   Titanium

TiO2   Titanium Oxide

TJR   Total Joint Replacement

TKA   Total Knee Arthroplasty

ZrO2   Zirconium Oxide

1 CHAPTER ONE: INTRODUCTION

1.1 BACKGROUND

1.1.1 Joint and Related Problems

As defined in a medical dictionary (1), "a joint is a physical point where two or more bones meet." The main components of a joint are cartilage that covers the surface of the bones, fibrous connective tissue that connects the bones together, and tendons that connect muscles to the bones. Some joints are sealed by the synovial membrane that forms a joint capsule and is filled by synovial fluid for lubrication. Joints are grouped based on their mobility as immovable, slightly movable, or freely movable. Movable joints mainly include ball-and-socket joints, hinge joints, pivot joints, and ellipsoidal joints. There are certain diseases affecting joints including osteoarthritis, rheumatoid arthritis, gout, rheumatic fever, etc. Also, joints are subjected to injuries and inflammation based on their location. Aging, continual wear, excess weight, and stress also cause irreversible damage and cause joints to deteriorate. Besides pain, these problems limit ranges of motion and activities. There are drugs that reduce inflammation based on the extent of the problem, but they may have serious side effects such as bone loss, toxicities, or addiction. In addition, patients with end-stage joint deterioration usually do not receive adequate relief or functional improvement from medications and seek out a surgeon for operation options. Due to the progressive nature of their disease, arthroscopy or osteotomy is not usually an option for these patients, and the ultimate approach to cure the problem is joint replacement surgery (2).

1.1.2 Arthroplasty as a Solution

Arthroplasty or total joint replacement (TJR) is a major surgery that removes the damaged joint and replaces it with a new, artificial one. Knees and hips are more often subjected to TJR, but surgeries are not limited to them and include other joints such as shoulders, fingers, ankles, etc. In 2003 in the United States, 202,500 primary total hip arthroplasty (THA) and 402,100 primary total

knee arthroplasty (TKA) procedures were performed (3). Annually, more than 1.5 million TJRs are performed globally, and the expected number for 2030 is expected to increase to 4 million (4). Projected numbers for the United States, specifically, would be 3.48 million TKAs and 572,000 THAs by 2030 (5).
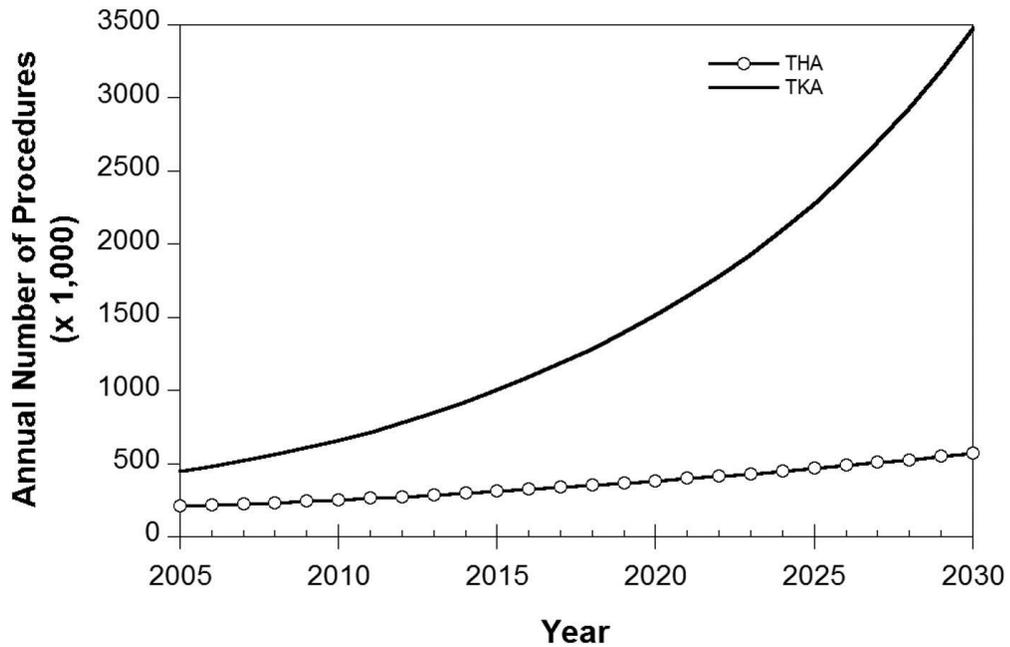
Figure 1-1: The projected number of primary THA and TKA procedures in the United States from 2005 to 2030 (3)

Based on increasing procedure volumes, Wilson *et al.* (6) estimated that the Medicare expenditures of TJA would increase from $5 billion in 2006 to $50 billion in 2030 (5).
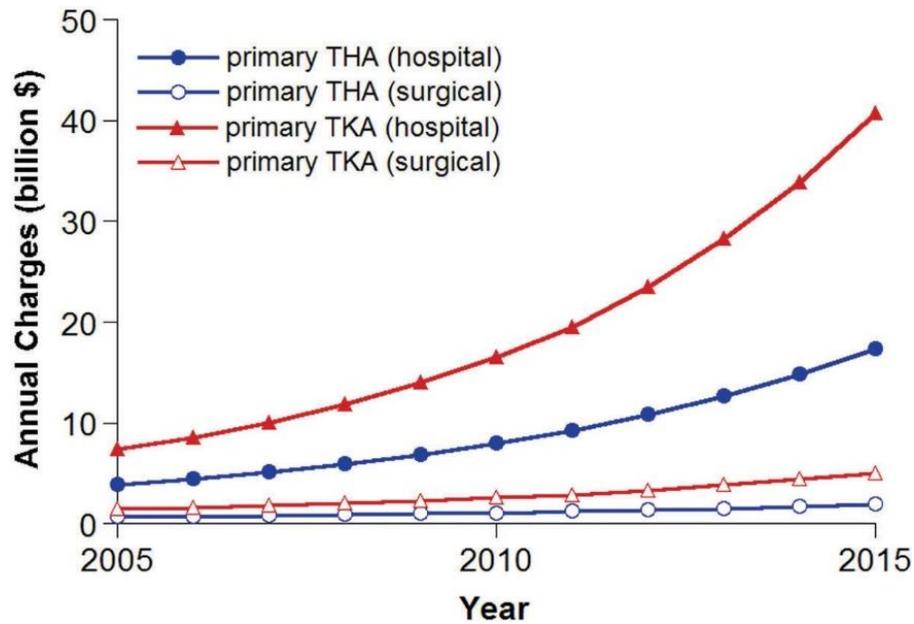
Figure 1-2: Projected costs for primary THA and TKA procedures (7)

Although TJR can successfully restore patients' mobility, currently the lifetime of orthopedic implants are only 10–15 years (8). Therefore, 10-20% of surgeries will need revision due to implant failure (3) resulting from infection, poor osseointegration, aseptic loosening, and inflammation caused by wear particles. (4, 7). In 2003, in the United States, 36,000 THA revisions and 32,700 TKA revisions were performed (3). As the number of primary procedures grows, the number of revisions is also expected to expand (2).
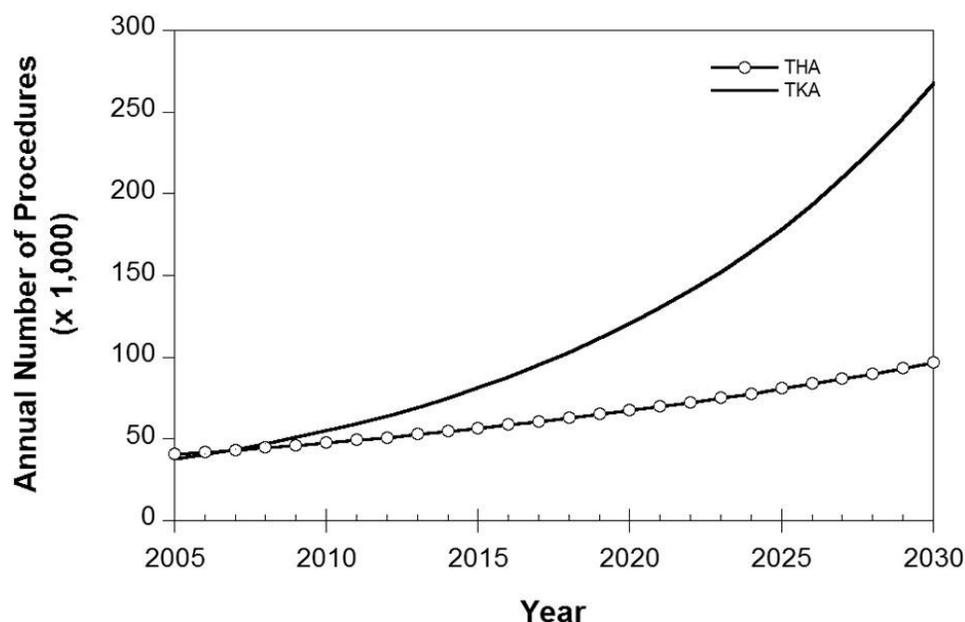
Figure 1-3: The projected number of revision THA and TKA procedures in the United States from 2005 to 2030 (3)

These projections are based on historical data. However, improvements in implant technology or orthopaedic treatments have the potential to reduce the need for revision surgeries (3). Therefore, improving outcomes by developing better technologies for arthroplasty can make a substantial savings of health care dollars and significantly reduce future Medicare costs.

1.1.3 Biological Events Happening after Surgery

When the implant is placed in the body, a series of events occur. First of all, there is an interaction between the implant surface and bloodstream that leads to an exchange of proteins and ligands. The subsequent healing process that starts around the implant has three phases, osteoconduction, bone formation, and bone remodeling. Osteoconduction starts with platelet activation that results in migration of osteogenic cells to the implant surface. Next, the osteogenic cells differentiate to bone-forming cells (osteoblasts), which start to secrete the matrix and

mineralize it. Lastly, bone remodeling happens, which is a slow process and needs multiple cycles to give bone-implant complexes the appropriate mechanical strength (9). However, this healing process does not always happen, and sometimes the host system forms a fibrous capsule to protect itself from the foreign body (implant); this is termed fibrosis. This capsule cannot remove dead cells (apoptotic or necrotic cells) and these may lead to inflammation. Also, matrices generated by fibroblasts are entirely different from bone matrix (10).
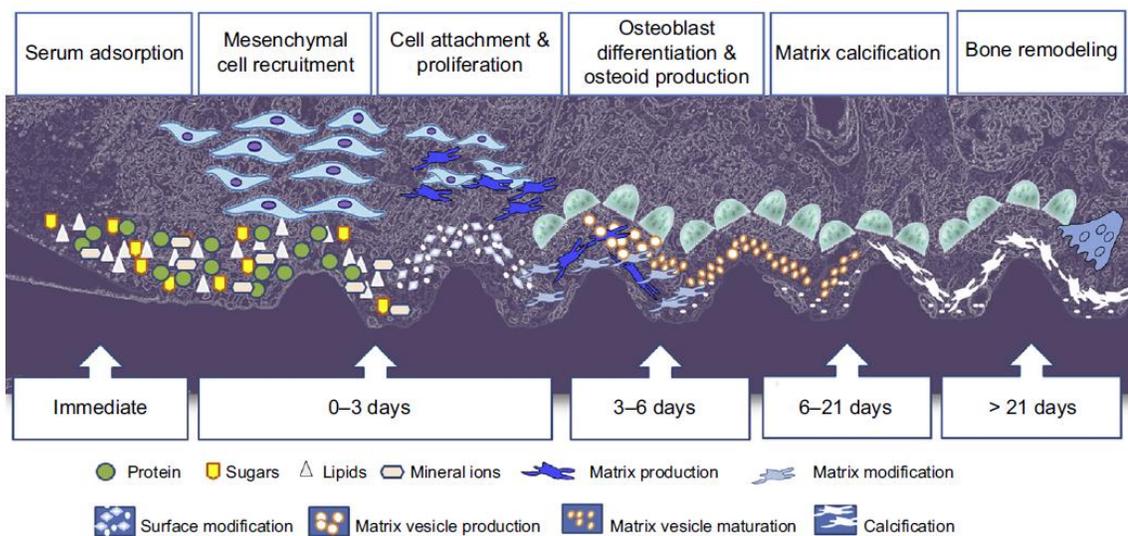
Figure 1-4: Cellular events during the implant healing process (11)

Implant osseointegration properties directly affect the outcomes of the healing processes. Also, implant surface properties such as chemical properties, physical properties, roughness, and hydrophilicity (wettability) directly influence the rate and quality of the healing processes (9). Note that, effective osseointegration is essential to fixation of that part of the prosthesis in contact with bone and is not required or even desirable for the articulating surfaces of the prosthesis that are designed to minimize the cellular adhesion.
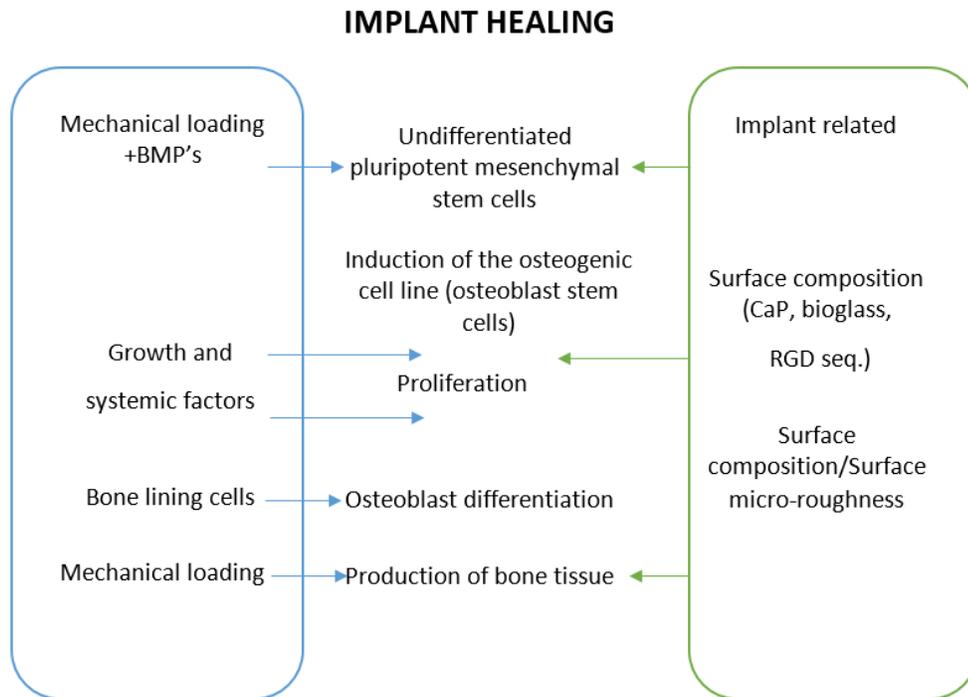
IMPLANT HEALING

Figure 1-5: The implant healing process reflects surface composition and surface roughness that influence osteoblasts responses (11)

1.1.4   Implant Properties

The properties that determine if a material is suitable to be used as an implant are mechanical and chemical, as listed below:

Modulus of elasticity: The elasticity module of the implant material should be equivalent to that of bone to ensure a uniform stress distribution (12).

Tensile, compressive and shear strength: High tensile, compressive and shear strengths prevent the transfer of fractions and lower stress to the bone (12).

Yield and fatigue strength: High yield and fatigue strengths protect the implant from fracture under cyclic loading (12).

Hardness and Toughness (wear resistance): Increased hardness decreases wear, and increased toughness prevents fractures (12).

Biocompatibility: implant materials should be non-toxic and must not trigger inflammatory or allergic responses (13).

Surface energy and tension: This determines implant wettability and affects protein absorption (increased osteoblast adhesion is expected from hydrophilic surfaces) (9, 12).

Surface roughness: Increased roughness provides extra surface area for cells to attach (12). Micro- and nano-roughness are mainly used for implants and are believed to affect wound healing and osseointegration (9).

Corrosion resistance: Higher corrosion resistance equals to lower ion transfer from the implant surface to the surrounding environment (12).

Osseointegration: Integration of implant surface with surrounding bone and tissue is necessary for the non-articular component of the prosthesis (13).

Thus the development of implants with optimal chemical and mechanical properties, especially corrosion and wear resistance, is significant for the longevity of the implant.

1.2   PROBLEM STATEMENT

1.2.1   Implant Failures

Like all biomedical devices, implants can also fail over time, because of trauma, chronic joint disease, prosthetic loosening, and infection of the joint. Joint replacement is usually a success, but possible problems occur, such as infection or aseptic loosening.

Infection: Areas in the wound, or around the new joint, may get infected. It may happen during surgery, hospital stay, or after discharge. It may even occur years later. Minor infections in the wound are usually treated with drugs. Deep infections may need a second operation to treat the infection or replace the joint (revision surgery).
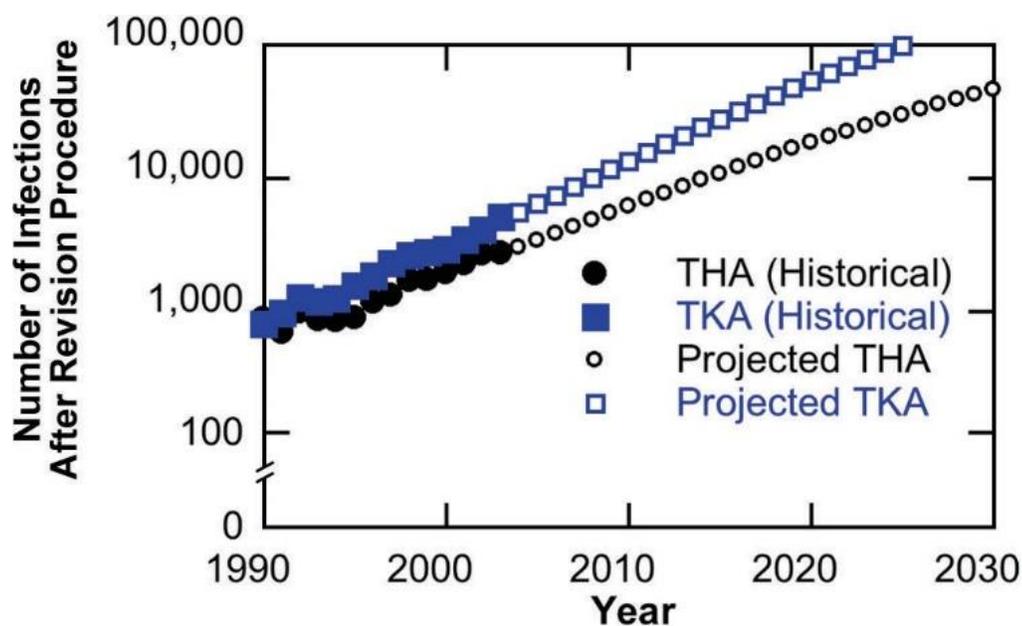
Figure 1-6: The projected number of infected revision THA and TKA procedures (7)

Aseptic loosening: The new joint may loosen, causing pain. If the loosening is very significant, another operation may be needed. Aseptic loosening can be explained by four concepts, including wear particle disease, interface sealing effects, hydrostatic fluid pressure concepts, and the bacterial endotoxin theory (14).

Wear particles: Some wear can be found in all joint replacements. The amount, type, and size of wear particles depend on the particles materials, the orientation, and the position of the joint.

These particles activate macrophages and cause secretion of proinflammatory enzymes that may lead monocytes/macrophages to differentiate to bone-resorbing osteoclasts (14). Characteristics of wear particles such as size, shape, material and amount, directly affect this procedure. For example, only particles from 0.3 to 10 μm can be phagocytosed by macrophages and activate them, thus increased proinflammatory reactions would be expected from these size-range particles (14).

1.2.2 Current Implant Materials

The artificial joint known as the prosthesis is usually made of metal or a combination of metals and plastic. It is usually cemented into place, and bone adjacent will grow into it.

Polymers: Polymers are reported to be biologically tolerable substances and are selected for implant technology because their physical characteristic can be easily altered and microscopically evaluated. They show fibrous connective tissue attachments, and unlike metals, they do not generate microwaves or electrolytic currents. However, there are some disadvantages, such as low-quality mechanical properties, low adhesion to living tissues and adverse immunologic reactions (12). Polyethylene, which is commonly used, showed low wear particle production (7 % of the revisions related to PE wear), and its fracture is rare (15).

Stainless steel: Stainless steel is used for iron-based alloys containing chromium and sometimes nickel. Stainless steel is readily available with low cost that possesses acceptable biocompatibility and suitable hardness and corrosion resistance. However, it has low fatigue behavior that makes it improper for long-term implants. Also, excessive iron released from the implant may cause reactions in blood or damage cellular components. Moreover, added nickel is toxic to the human body (16).

Cobalt-chromium: CoCr alloys are among the oldest implant materials and orthopedic implants used to be made out of cobalt, chromium, molybdenum, and nickel (17). Cobalt provides

a continuous phase for basic properties, chromium is added to increase corrosion resistance via its oxide surface, molybdenum is added for higher strength and corrosion resistance, and nickel enhances mechanical properties (12). The articular surfaces is usually polished.

Because of the high fatigue resistance, it is an excellent choice for TJR although CoCr alloys are expensive and difficult to machine (16). The primary concerns with CoCr are wear particles, stress shielding effects because of the high Young's modulus, metal toxicity, and the risk of hypersensitivity that may cause systemic allergic reactions and inflammation in the host body (16, 18).

Titanium: Ti is biocompatible because of the thin oxide layer on its surface. Ti alloys also show high strength and good corrosion resistance. In Ti alloys, Iron provides corrosion resistance, aluminum provides increased strength and decreased density, and vanadium prevents corrosion (12). As for disadvantages, they have low wear resistance properties, and vanadium used in Ti alloy is cytotoxic. Also, there is no proper equivalent elastic modulus between Ti implants and the bones, which passes stress to the bone and is associated with bone resorption (19).

Properties	Stainless steel	Cobalt–chrome	Titanium
Stiffness	High	Medium	Low
Strength	Medium	Medium	High
Corrosion resistance	Low	Medium	High
Biocompatibility	Low	Medium	High

Figure 1-7: Properties of stainless steel, CoCr, and Ti implants (84)

Magnesium: Mg has high malleability and can be tolerated by the body at relatively high levels, thus it has been used mainly in pediatric orthopaedics or devices for the internal fixations.

However, it is highly corrosive and absorbable with low rigidity and toughness that limits its application (17).

Ceramics: Zirconium is a less allergenic material and is used as ZrO_2, also known as zirconia, by the implants industry. Ceramic implants are known for good osseointegration, strength, and physical properties (12). ZrO_2 knee implants produce less PE wear compared to CoCr, but the surface roughness of ZrO_2 is lower than that CoCr (18).

Tantalum: Ta has some common characteristics with Ti such as high biocompatibility, flexibility, and corrosion resistance, but it is costly. Also, because Ta is highly porous, fracturing can be an issue (17).

1.2.3   Surface Modifications as a Solution

To facilitate healing processes and reduce the rejection rates, osseointegration and osteoinduction of implant materials should be improved (20). Improving the bone-implant interface can be achieved via physical or chemical techniques (10). The physical methods modify the implant surface by modifying surface morphology, topography, and organization, via different methods such as etching, plasma spraying, sintering powders, grit-blasting, anodization, and machining/micro-machining (10, 20). The rationale behind physical approaches is increasing surface roughness that provides higher surface energy levels that improve protein adsorption and osteoblast functions (10). It has been shown that micro-topography and nano-topography influence cell adherence and spreading. The chemical methods create a bioactive surface by applying different coatings onto the implant layer via biochemical and physicochemical techniques. The only difference between biochemical and physicochemical coatings is the use of organic materials (growth factors, peptides, or enzymes) or inorganic (i.e., calcium phosphate) materials. Some modifications may also combine both physical and chemical coatings (10).
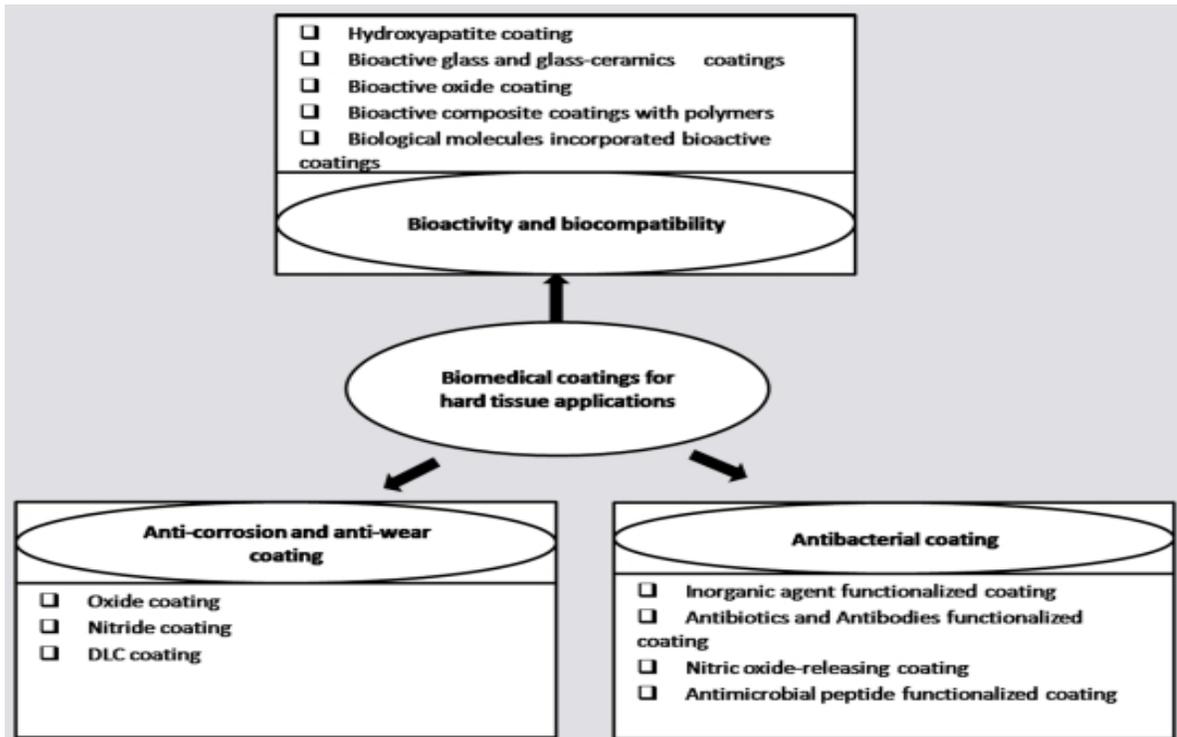
Figure 1-8: Biomedical coating for implants (21)

Among the techniques that are used to improve bioactivity and biocompatibility, ion beam techniques including ion beam sputtering deposition (IBSD) and ion beam assisted deposition (IBAD) can be beneficial. These techniques are used to deposit thin and homogeneous films on the metallic substrates with high adhesive strength. The only difference between the IBSD and IBAD is ion bombardment in the IBAD technique that leads to a higher adhesive strength (21).
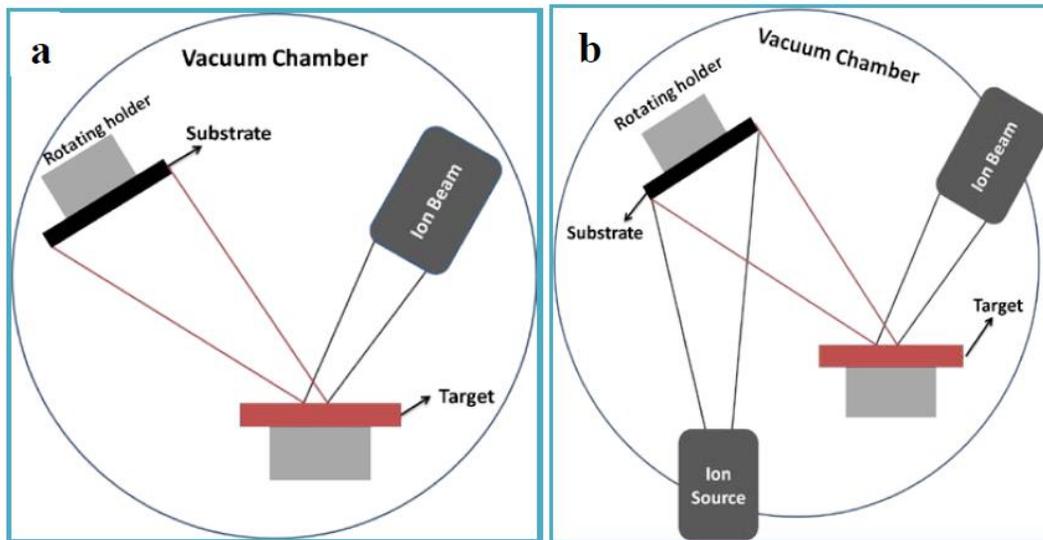
Figure 1-9: Schematic of (a) IBSD and (b) IBAD (22)

It has been shown that by controlling IBAD processing parameters, specifically the ion beam current density, and the coating chemical composition can be controlled. Therefore, IBAD is an excellent technique for implant coating because of the high adhesive strength, low substrate temperature, high reproducibility, and controllability of microstructure and chemical composition (21).

1.3   RESEARCH QUESTIONS AND BACKGROUND OF THE PROJECT DESIGN

1.3.1   Surfaces with Increased Biocompatibility, Resistance to Wear, and Anti-infective Properties

Nano-technology is defined by the National Aeronautics and Space Administration as "the creation of functional materials, devices, and systems through control of matter on the nanometer length scale (1–100 nm), and exploitation of novel phenomena and properties (physical, chemical,

and biological) at that length scale" (p. 187). Nano-technology involves materials with nano-sized topography that plays an essential role in the protein adsorption, osteoblasts adhesion, and osseointegration. However, producing such surfaces are challenging (9). The nano-technology laboratory of the Department of Orthopaedic Surgery and Rehabilitation at the University of Nebraska Medical Center (UNMC) was inaugurated in 2004 with the core technology of IBAD to produce nano-crystalline coatings for reducing the wear of artificial orthopaedics implants. In 2008, Namavar *et al.* reported transparent nano-crystalline ZrO_2 films possessing combined properties of hardness and wetting behavior to benefit wear reduction and biomedical applications (22). To evaluate the osseointegrative properties of the ZrO_2 coatings, they performed a series of biological experiments including alamar blue assays and direct cell counting methods (using a hemocytometer) to determine the growth of mesenchymal stromal cells (OMA-AD) on different nano-engineered surfaces. The *in vitro* experimental results indicated that the nano-engineered ZrO_2 was superior in supporting adhesion, and proliferation (23).
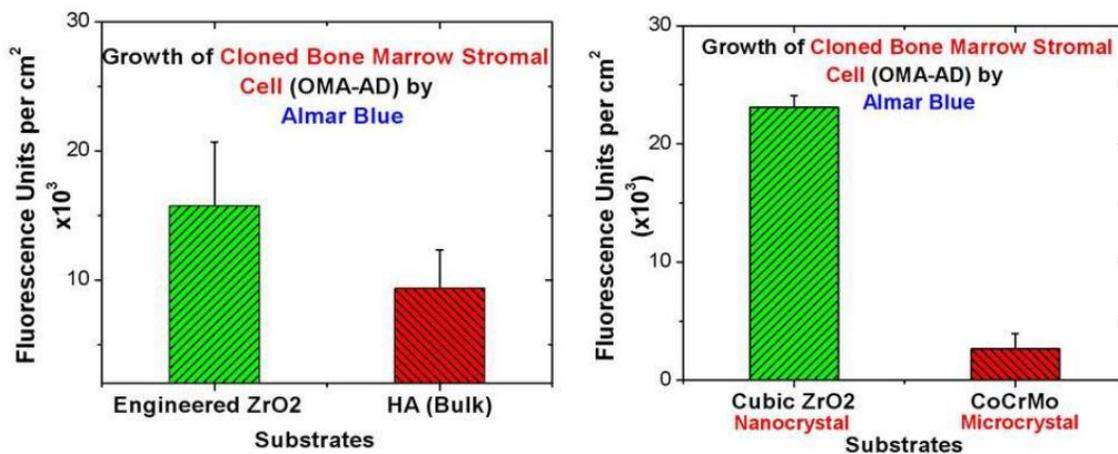
Figure 1-10: OMA-AD growth on nano-crystalline ZrO_2 compared with HA and CoCrMo (23)

They also performed a comparative analysis of absorption energies of fibronectin (FN) fragments using quantum mechanical calculations and Monte Carlo simulations on different surfaces to elucidate why cells attached more effectively to ZrO_2 nano-structures (23-25). During their ongoing search for durable coatings to promote bone marrow stromal cell growth, they also investigate if the IBAD-produced coatings could prevent biofilm formation and the preliminary results showed reduced staphylococcus aureus attachment and growth on nano-structures (26). Limited *in vivo* experiments indicated that IBAD nano-structured surfaces not only did not elicit any excessive inflammatory responses that inhibited new bone formation but also counteracted deficiencies in converting woven bone to mature bone (27). Based on these preliminary data, Dr. F Namavar (emeritus professor in the Department of Orthopaedic Surgery and an expert in material sciences and nano-technology) proposed the idea of producing "triple smart" surfaces for implants that possess optimized wear resistance, anti-infective and osseointegrative properties.

The author joined the team in 2012 as a volunteer and started her Ph.D. program the same year. This research proposal was focused on one aspect of triple smart surfaces, i.e., their osseointegration. The plan was to develop a model system to study osteoblast functions including cell adhesion, proliferation, and differentiation on different nano-sample and micro-sample surfaces to investigate the differences between nano-materials *vs.* bulk materials mainly, along with the effects of coating chemistry and substrates on the outcomes of bone-forming (osteogenic) cells behaviors.

1.3.2 OMA-AD Stem Cells

Namavar *et al.* used a murine mesenchymal stem cell (MSC) cell line OMA-AD for the *in vitro* experiments to determine the effect of nano-structures coatings on cell growth. OMA-AD was derived from the bone marrow of a female C57Bl/6 mouse by repeated trypsinization of the adherent layer of a long-term bone marrow culture (28). OMA-AD cells represent a spontaneously

immortalized mouse MSC line and are capable of differentiating to all of the primary cell lineages of mesenchymal (connective) tissue lineages such as osteoblasts. These cells also supported primitive mouse hematopoietic stem cells and hematopoietic cells in culture (28). Obviously, using them is more efficient and less costly than primary cells. However, the cell line was generated from mice, thus there are potential interspecies differences, genomic differences and cell phenotypes that are sensitive to age and site of isolation factors (29). Also, OMA-AD cells are stem cells and their application in experiments needs extra time for differentiation into osteoblasts. Therefore, after a comprehensive search, the author decided to use SAOS-2 cells instead. These cells are well differentiated human osteosarcoma cell lines, showing mature osteoblast phenotypes (for more details see Chapter 2).

1.4 LIMITATIONS

1.4.1 Standardization of Methods to Test and Compare Surfaces

All new materials or new coatings for implants first need *in vitro* and later, *in vivo* evaluations before they seek approval for clinical trials. These tests are generally used to compare the new surfaces with known and FDA approved orthopaedic materials in order to investigate any enhanced properties. *In vitro* experiments are mainly focused on evaluating cell morphology, adhesion, migration, proliferation, differentiation, and gene expression. Although these are considered the first steps to monitor biological events for the new surfaces, they cannot provide an evaluation as complete as *in vivo* experiments. The bone-implant environment is dynamic and only animal models, and later clinical trials can confirm the efficiency of new implant surfaces (9). Therefore, it was initially necessary to test nano-surfaces *in vitro*. Namavar's team had been using limited *in vitro* techniques (alamar blue and FN staining) to show differences between nano-surfaces with other orthopedic materials. Their focus was on initial adhesion and proliferation, and mainly, they were interested in FN effects. However, the new experimental design proposed for

this study was to develop and evaluate a model system that investigates all essential cellular events including adhesion, proliferation, cell morphology, apoptosis, necrosis, and differentiation. The techniques used to test these features are in development and currently, there is no standard for such analyses. A comprehensive research plan had to be devised and modified to identify the best techniques to establish the criteria necessary to achieve this objective. The methods, results, and conclusions of this research are described following.

1.5   DISSERTATION ORGANIZATION

This dissertation is organized into six chapters as follows:

- Chapter 1: presents background information, the statement of problems, research questions, and background to project design, methods limitations, and organization of this dissertation.
- Chapter 2: presents methods for designing and implementing tools used in the experiments
- Chapter 3: provides the data from the first paper
- Chapter 4: provides the data from the second paper
- Chapter 5: provides the data from the third paper
- Chapter 6: is a summary of the conclusions of papers and general discussion of all of the studies along with suggestions for future work.

Chapters 3, 4, and 5 are duplication of published papers during this study.

2 CHAPTER TWO: MATERIAL AND METHODS

2.1 NANO-FABRICATION

2.1.1 IBAD Technology

Depositing thin metallic or ceramic films on different surfaces was performed by the IBAD technique that allows designing and engineering nano-crystalline coatings with distinct structures, chemistry, and morphology. The IBAD combined evaporation with concurrent ion beam bombardment (e.g., N, O, and Ar) in a high vacuum stainless steel water-cooled vacuum chamber. The base pressure was about $5*10^{-8}$ torr, and the operating pressure was in the range of 10^{-4} to 10^{-6} torr. The IBAD was equipped with an RF 12 cm Ion gun that generated a maximum current of 500 mA at 1500 eV ion energies, an electron-beam evaporation source that provided evaporation temperature up to 2500°C, a residual gas analyzer, and a 10 kW electron gun with a programmable sweep multi-pocket four electron beam evaporation source. During the process, a vapor flux of atoms was generated with an electron beam. Ions of a particular gas simultaneously were extracted from plasma, and the bombardment of these energetic ions was employed, like a hammer, to stitch nano-films to the substrate. Ion bombardment, the critical factor in controlling film properties, along with other processing properties including coating material, evaporation rate, ion species, ion energy, and ion beam current density, substrate temperature, and orientation, made the IBAD technique capable of producing materials with exceptional chemical, physical, mechanical properties.
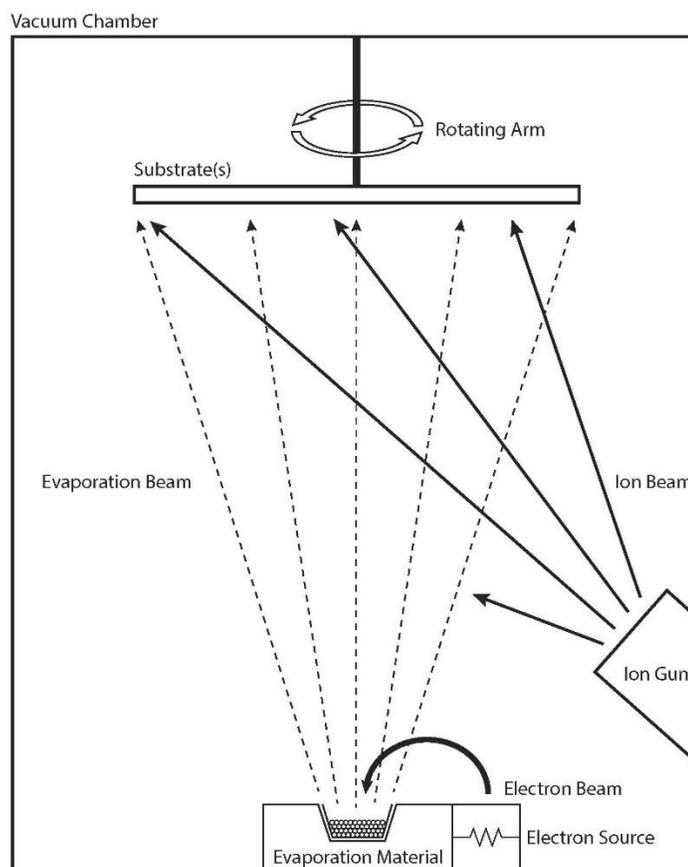
Figure 2-1: Schematic of the IBAD system

2.1.2 Chemistry of Coatings

IBAD is capable of producing different nano-films on surfaces. Candidates for biomedical applications are nano-crystalline coatings of pure cubic ZrO_2, TiO_2, Ta oxides, cerium oxides, Ti nitrides, aluminum oxides, and silver. Based on the preliminary data, for this study, pure cubic ZrO_2 and Ti were chosen.

2.1.3 Nano-crystalline Properties and Tests Performed on Surfaces (Wettability and Roughness)

Transparent nano-crystalline cubic ZrO_2 films were produced by IBAD with hardness as high as 16 GPa and a bulk modulus of 239 (12 GPa). Source material for deposition was 99.7%

pure ZrO$_2$ with a monoclinic crystal structure, and evaporation rate ranged from 1 to 4 Å/s, ion energy from 0 to 600 eV, ion current density from 0 to 500 µA/cm^2, and the substrate temperature from room to 550°C. The ion beam was compromised of O, N, Ar ions, or mixtures and the average nano-crystalline grain size increased from 5 to 70 nm as the deposition temperature increased from room temperature to 550°C. These ZrO$_2$ films were maximally wettable by water and demonstrated from zero to several degrees contact angles with adequate surface energy 22–24 of 82 dynes/cm (22).
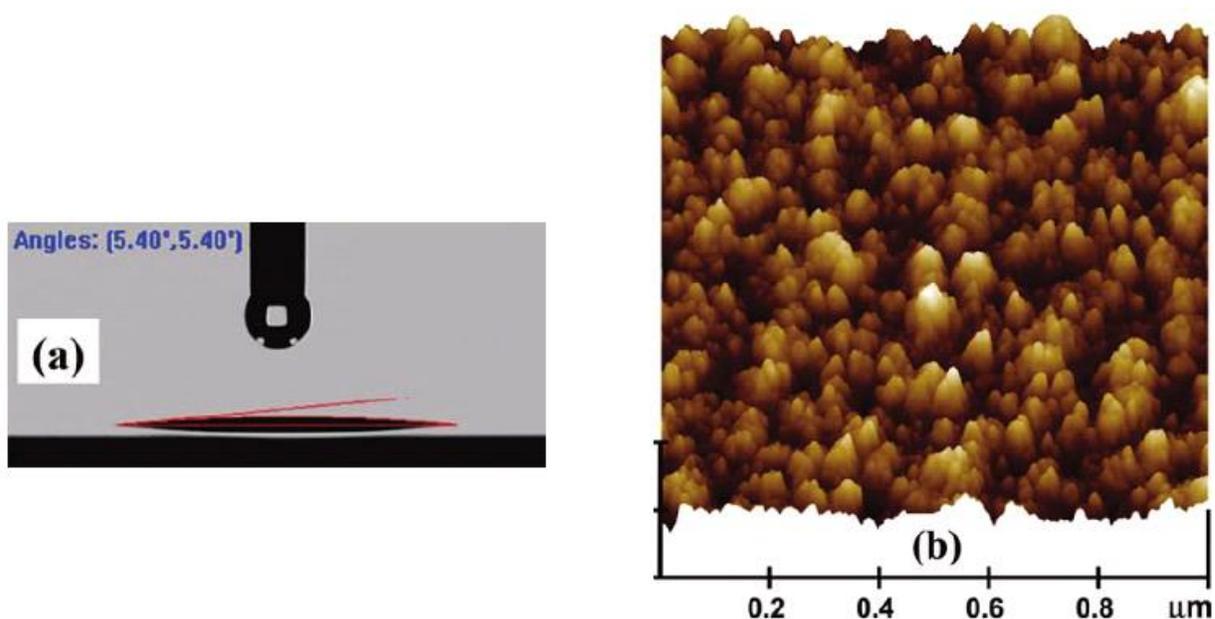
Figure 2-2: a) Contact angle of cubic ZrO$_2$ that indicated a contact angle of about 5° for deionized water (b) AFM of the same sample measured the roughness of about 7 nm (22)

Source material for IBAD TiO$_2$ films was 99.9 % pure rutile TiO$_2$ and evaporation rate ranged from 2 to 3 Å/sec, ion energy from 100-120 eV, and the substrate temperature from room to 610°C. Ion beam was compromised of O, N, or Ar and the thickness of the deposited films was about 1 µm. The IBAD TiO$_2$ films made with Ar, O, and N ion beams showed roughness values of

64.4 nm, 20.4 nm, and 19.4 nm relatively. Different ranges of grain sizes were obtained with different chemical ion beams in the IBAD process. TiO_2 films made with Ar, O, and N ion beams have roughness values of 64.4 nm, 20.4 nm, and 19.4 nm respectively. All these values showed greater roughness than the usual films made with other techniques (30).
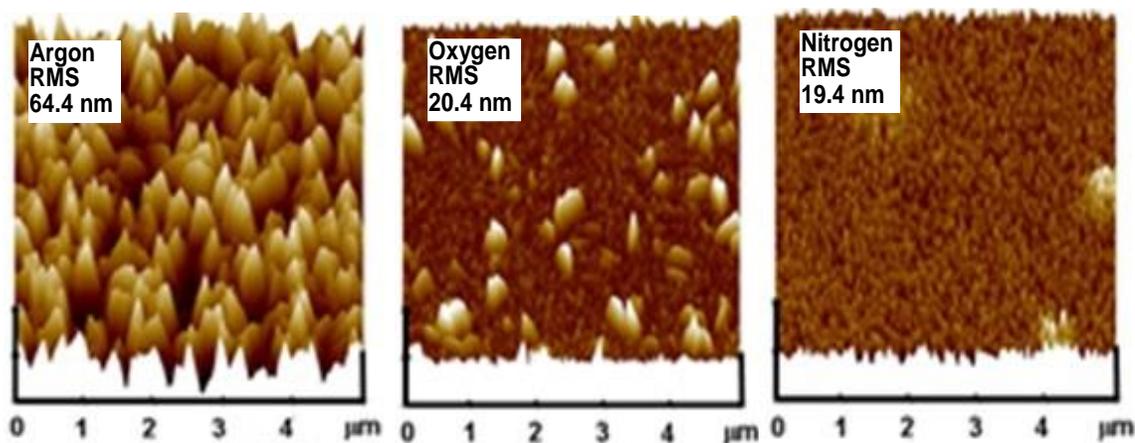
Figure 2-3: Morphology of nano-crystalline TiO_2 determined by atomic force microscopy (AFM) for a 5-micron scan size. IBAD-produced TiO_2 films showed different roughness by varying ion species (30)

2.1.4   Substrate Materials

Glass and Ti were used as substrates for nano-coating. Ti is a material with a microstructure that is used for orthopaedic purposes because of its enhanced biocompatibility. Glass substrates were used to eliminate inherent surface properties of metal surfaces, allowing a focus solely on the specific nano-coating properties. ZrO_2 deposited onto glass and Ti and TiO_2 deposited on Ti were used in this study.

2.1-5 Samples preparation

Both nano-coated surfaces and control glass surfaces were cut into 10 mm by 10 mm squares (area = 100 mm^2), and CoCr samples were cut into disks with 12.7 mm diameter (area = 127 mm^2), sonicated for 1 to 2 hours in a 50:50 acetone:methanol mixture, wrapped in aluminum foil and autoclaved to ensure clean, sterile surfaces for cell culture studies.

2.2   CELL LINES

2.2.1   Osteosarcoma Cell Line

SAOS-2 is a human osteosarcoma cell line isolated from an 11-year old Caucasian female in 1975 and was selected for use in the model system of osteoblast functions.
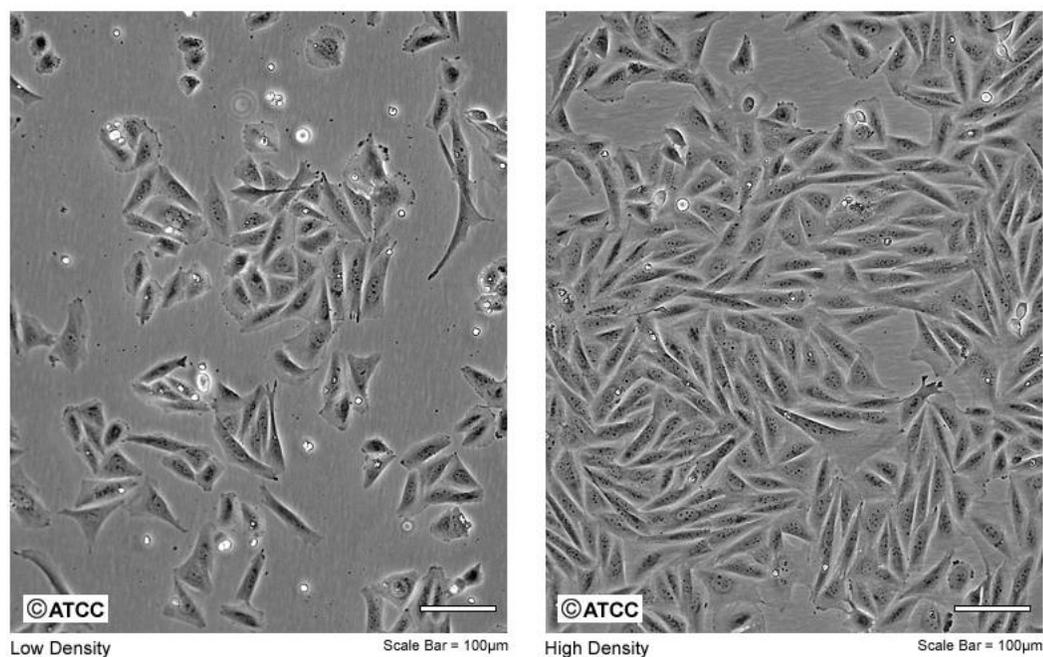
Figure 2-4: SAOS-2 cells in culture

These cells show a mature osteoblast phenotype and production of mineralized matrixes and high levels of alkaline phosphatase (ALP) activity are major characteristic (29, 31). They are

able to form a calcified matrix typical of woven bone, and their synthesized collagen structures and cytokine and growth factor production are similar to human primary normal osteoblast cells (29). These properties make them a chosen model for studies of osteoblast functions. However, they are osteosarcoma cells and were derived from malignant bone tumor thus their chromosomal alterations may lead to abnormal molecular and cellular functions that may not mirror the whole range of osteoblast phenotypic properties (29, 32). The SAOS-2 cells were obtained from the ATCC and based on their protocol were, cultured in McCoy's 5A medium, supplemented with 15% heat-inactivated FBS and 1% gentamycin in a humidified 5% CO_2 atmosphere at 37°C. The differentiation medium, used for ALP and PCR experiments, employed the same medium as above, supplemented with 0.3 mM ascorbic acid and 10 mM glycerol phosphate.

2.3   ADHESION

For quantifying adherent cells and morphology of focal adhesions, SAOS-2 cells at a density of 100,000 cells per 2 ml were cultured on surface samples in 12-well plates for 2 hours. The medium was removed from the samples, washed with PBS/1%BSA, transferred to fresh 12-well plates, 2 ml of fresh medium was added, and incubated for 24-48 hours. Samples were washed with 1x PBS containing 1% BSA, fixed with 1 ml of 4% formaldehyde for 10 minutes, and permeabilized with 1 ml of 0.1% Triton-X-100 for 5 minutes, all at room temperature. Samples were stained first with actin (5 µl of stock solution into 200 µl PBS/1%BSA, Alexa Fluor 546 Phalloidin) for 30 minutes and rinsed with PBS 3 times for 5 minutes at room temperature. DAPI (1 ml of a 300 nM stock solution of 4', 6- diamidino-2-phenylindole dihydrochloride in PBS per sample) was added to each sample for 5 minutes in the dark at room temperature. Between all steps above, cells were washed twice with PBS/1% BSA buffer. Samples were fixed to the slides and coverslips were attached with Fluormount-G. From each sample, 10 digital images were randomly taken with a Nikon camera using a planar 10x/0.25 objective. The morphology of focal adhesions

and actin of SAOS-2 cells cultured on the samples were characterized by microscopy after immunofluorescent staining and random images from samples were analyzed. DAPI-stained cells were automatically counted after single-channel image segmentation and binary masking. Cells were quantified using ImageJ software (IJ 1.45 m) and Metamorph software, and data were expressed as the average number of DAPI-stained cells in 15 random fields captured at 10x magnification.

2.4   PROLIFERATION

2.4.1   Metabolic Activity

As an indicator of cell viability and proliferation, the metabolic activity of SAOS-2 cells on coated and uncoated surfaces was determined using a MTS assay. The original form of this assay was described by Mosmann and improved by several other investigators subsequently (33-37). Our study employed the method described as follows. Briefly, 500,000/ml cell with 2 ml of suspension were cultured as outlined above on different surfaces. After 24 hours, all samples were transferred to a fresh 12-well plate, fresh medium was added, and incubated for 3 more days. At day 4 after plating, the medium was removed from the samples, 200 µl of fresh medium, and 40 µl MTS dye solution was added to each sample. The plates were incubated in a CO_2 incubator at 37°C for 3 hours. After this incubation period, 100 µl of supernatant was transferred into each well of a 96-well plate and absorbance of the MTS formazan dye product was measured photometrically at 490 nm using an Infinite M200 plate reader.

Figure 2-5: MTS plate after the incubation period, ready for measuring by a plate reader

The cells in each well were stained with DAPI and visualized at 10x by fluorescence microscopy as described in the cell counting section.

2.4.2 Ki-67

In order to compare osteosarcoma cell proliferation on different surfaces, the Ki-67 assay was applied using PE mouse anti-human Ki-67 Set (RUO) from Biosciences (38). Ki-67, a nuclear cell proliferation-associated antigen, expressed by all human proliferating cells, can be recognized at all stages of the cell cycle (late G1, S, M, and G2 phases) except for G0 phase (39, 40). Approximately 30 flasks of cells were harvested at 50% confluency using trypsin, and detached cells were adjusted to 500,000 cells per 2 ml (250,000/ml), 3 samples of each surface were placed in a 12-well plate, and each sample was seeded with 500,000 cells (2 ml for each well), and incubated for 24 hours. After 24 hours, samples were transferred to a fresh 12-well plate; fresh medium was added and incubated for 3 more days. At day 4 after plating, samples were washed

with 1 ml PBS once, 500 µl of accutase were added to each well (see Appendix for details of optimization of this procedure), and incubated for 10 minutes at room temperature. After 10 minutes, 2 ml of medium was added to the each well, detached cells were collected in separate 15-ml conical tubes, centrifuged at 200 g for 5 minutes, the supernatant was discarded, 5 ml of cold 70% - 80% ethanol was added drop by drop onto the cell pellet in each tube, mixed well and were incubated at -20°C for 24 hours. For Ki-67 staining by flow cytometry,10 ml wash buffer (PBS with 1% FBS, 0.09% NaN$_3$ pH7.2) was added to the fixed cells in each tube, centrifuged for 5 minutes at 200 g and supernatant was aspirated. Another wash was performed as described, cells were resuspended in 100 µl wash buffer, 20 µl of antibody was added into the tubes, and mixed gently. Tubes were incubated at room temperature for 30 minutes in the dark, washed with 2 ml of PBS washing buffer, centrifuged at 200 g for 5 minutes, and 0.5 ml of PBS wash buffer was added into each tube. The samples were analyzed by FACS.
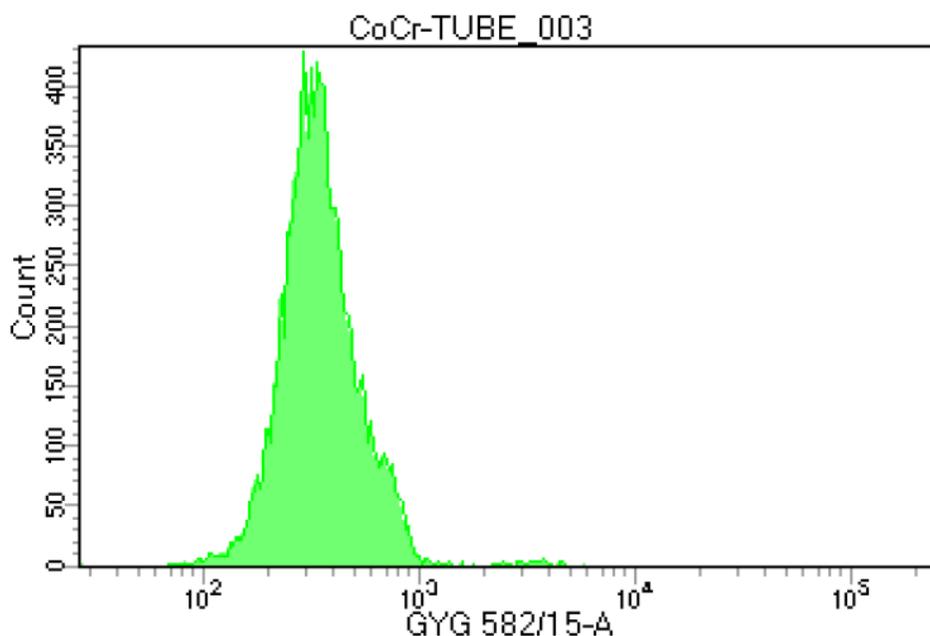
Figure 2-6: An example of the Ki-67 flow cytometry batch analysis

2.5   DIFFERENTIATION

2.5.1   Alizarin Red

To determine calcium deposition, SAOS-2 cells were cultured as described previously, incubated on the different surfaces for 7 and 14 days in 24-well plates, and alizarin red staining was performed following the standard protocol as described in the Osteogenesis Assay Kit (ECM815, Millipore). After removing medium from the samples and rinsing with PBS, samples were transferred to fresh plates and fixed with 10% formaldehyde at room temperature for 15 minutes. Samples were rinsed 3 times with de-ionized water, 1 ml alizarin red stain solution was added to each well, followed by incubation at room temperature for 20 minutes. Excess dye was removed by 4 washes with de-ionized water, 400 µl of 10% acetic acid was added to each well, the plates were incubated for 30 minutes with shaking, and the mixtures were transferred to 1.5-ml centrifuge tubes. To remove the cell monolayer, samples were vortexed for 30 seconds and then incubated at 85°C for 10 minutes in a block heater. Tubes were placed on ice for 5 minutes and then centrifuged at 20,000 g for 15 minutes. A 400-µl portion of the supernatant was transferred to a fresh 1.5-ml centrifuge tube and the pH was neutralized with 150 µl of 10% ammonium hydroxide (pH 4.1-4.5). Finally, 150 µl of the mixture in each tube was transferred to one well of a 96-well plate, and the absorbance at 405 nm was quantified.

2.5.2   Bone-specific Alkaline Phosphatase

In order to compare osteosarcoma cell differentiation on the different surfaces, an alkaline phosphatase (ALP) assay was used. A bone-specific isoform of ALP is found on the cell surface of osteoblasts that are responsible for the synthesis of the new bone matrix and its mineralization. The SensoLytepNPP ALP assay kit can detect ALP by ELISA using colorimetric pNPP (p-Nitrophenyl phosphate) phosphatase substrate at absorbance 405 nm. The study employed the ALP assay as described by Lin and modified as follows (41). About 30 flasks of cells were harvested at

50% confluency using trypsin, and detached cells were brought to the 500,000 cells per 2 ml (250,000/ml) density, 3 samples of each surface were placed in a 12-well plate, and each sample was seeded with 500,000 cells (2 ml for each well), and incubated for 24 hours. After 24 hours, samples were transferred to a fresh 12-well plate. Fresh medium was added and incubated for another day. At day 2 after plating, differentiating medium was added and incubated for 3 more days. At day 5 after plating, 1X assay buffer, pNPP ALP substrate working solution, and Triton X buffer were prepared according to the manufacturer's instructions. To prepare cell extracts, 500 µl of the Triton X buffer was added to each sample, cell suspensions were incubated the at 4°C for 10 minutes under agitation (100 rpm), collected in a microcentrifuge tube, centrifuged at 2500 g for 10 minutes at 4°C, and the supernatant was collected for ALP assay.

Figure 2-7: Samples for an ALP experiment, 5 days after plating

To detect ALP activity, 100 µL of pNPP substrate working solution was added into each well, mixed by gently shaking the plate for 30 seconds, and incubated at room temperature for 60 minutes in the dark. After the incubation period, 50 µL of stop solution was added into each well, and the absorbance was measured at 405 nm using Epoch microplate spectrophotometer
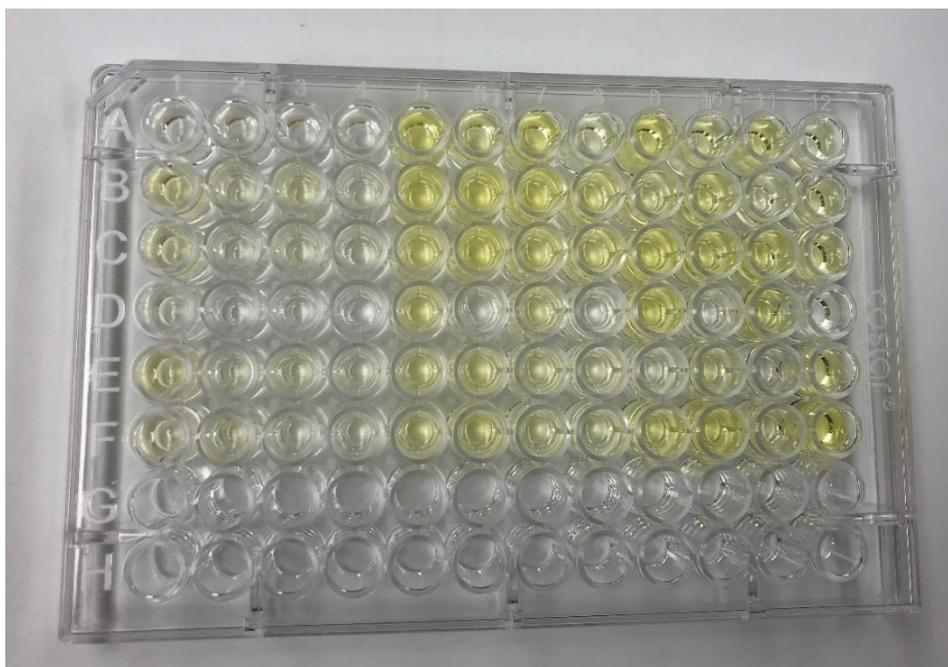
Figure 2-8: ALP plate after the incubation period, ready for measuring by a plate reader

ALP activity of cell lysates was extrapolated from the ALP standard curve, and the ALP activity was normalized according to the number of cells in the cell lysates using a BCA protein assay. This assay is based on bicinchoninic acid (BCA) for the colorimetric detection and quantitation of total protein. One cuprous ion forms a complex with two BCA molecules, producing a purple-colored, water-soluble complex that absorbs light at 562 nm. The absorbance data were plotted against the standard curve to calculate the concentration of protein in samples.

2.6 APOPTOSIS

Cell death can be classified into non-programmed (in injury or trauma) and programmed (in apoptosis and autophagy) groups, and losing plasma membrane integrity is the first element to determine the nature of the cell death. In the early stages of apoptosis, phosphatidylserine (PS) is translocated from the inner to the outer layer of the cytoplasmic membrane. This translocation

marks the cell for recognition and phagocytosis by macrophages and other cells (42). To compare

programmed cell death of SAOS-2 cells on different surfaces, an annexin V kit with PI (propidium

iodide) staining was used. Annexin V is a protein with high affinity for PS, which is labeled with

a fluorophore. This kit also includes red fluorescent propidium iodide (PI) nucleic acid binding dye

that is impermeable to live cells and apoptotic cells, but stains dead cells with red fluorescence.

Therefore, apoptotic cells show green fluorescence, dead cells show red and green fluorescence,

and live cells show little or no fluorescence.
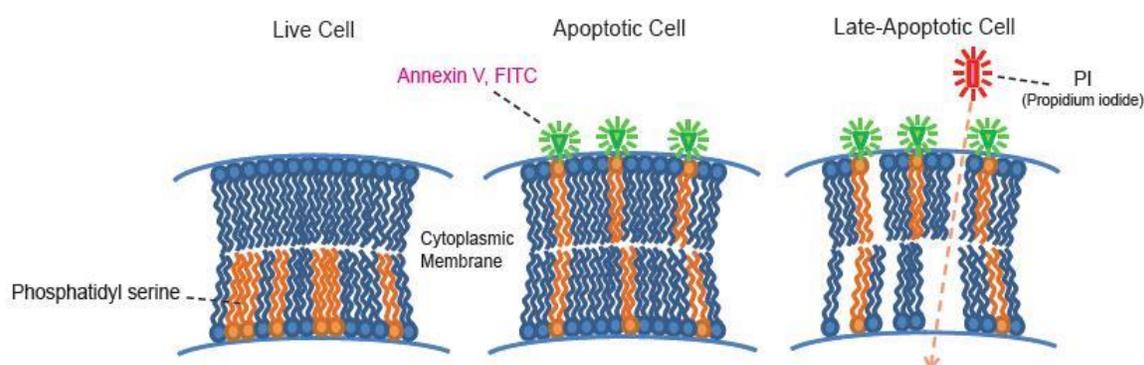
Figure 2-9: Apoptosis Detection Assay (83)

These populations can be distinguished using a flow cytometer with a 488 nm excitation

laser. The assay was mentioned by Koopman and have been optimized by Invitrogen (43, 44).

Some modifications applied for use with our *in vitro* model mentioned as follows. Approximately

30 flasks of cells were harvested at 50% confluency using trypsin and the detached cells were

adjusted to 1,000,000 cells per 2 ml (500,000/ml), 3 samples of each surface were placed in a 12-

well plate and each sample was seeded with 1,000,000 cells (2 ml for each well), and incubated for

24 hours. After 24 hours, samples were transferred to a fresh 12-well plate; fresh medium was

added and incubated for 3 more days. At day 4 after plating, 1X annexin-binding buffer, and PI

working solution were prepared based on the manufacturer's protocol. Subsequently, samples were

washed with 1 ml PBS, 500 µl of accutase was added to each well and incubated for 10 minutes at room temperature. After 10 minutes, 2 ml of medium was added to each well; detached cells were collected in separate 15-ml conical tubes, centrifuged at 200 g for 5 minutes, supernatant was discarded, cells were washed with cold PBS, and resuspended in 1X annexin-binding buffer, and 5 µL alexa fluor 488 annexin V and 1 µL 100 µg/mL PI working solution were added to each 100 µL of cell suspension and incubated at room temperature for 15 minutes in the dark. After the incubation period, 400 µL 1X annexin-binding buffer was added to the samples, mixed gently, and kept on ice for analysis within 1 hour, by flow cytometry, measuring the fluorescence emission at 530 nm and 575 nm or equivalent, using 488 nm excitation. From each sample, 10,000 events were collected, and the population was separated into three groups: live cells (little or no fluorescence), apoptotic cells (green fluorescence), and dead cells (red and green fluorescence). Data are expressed as the average percent viability. Controls that were used included unstained cells, cells stained with annexin V conjugate only (no PI), and cells stained with PI only (no annexin V conjugate).

Figure 2-10: Flow cytometric analysis of the SAOS-2 cells using apoptosis detection kit

2.7   RNA EXTRACTION / QUANTITATIVE REAL-TIME PCR

In order to determine the responses of human osteoblast cells to implant surfaces, the gene expression profiles as modified by the cell to surface interactions such as initial adhesion, proliferation, and differentiation, were measured using PCR techniques. RNA from cells cultured on the various surfaces was extracted and evaluated by real-time PCR for the osteogenic markers and matrix proteins listed in Table 2-1. This table includes transcription factors and osteoblastic marker genes that are involved in osteoblast adhesion, growth, and differentiation (45-48).

Table 2-1: List of genes used for PCR experiment

Target Gene	Abbreviation	Implication
Fibronectin	EGFLAM	Promoting cell attachment and migration
Ki-67	MKI67	Proliferation marker
RUNX 2	RUNX 2	Early osteoblastic transcription factor
Alkaline phosphatase	ALPL	Marker for bone mineralization (initial stage)
Osteopontin	SPP1	Marker for middle stage osteogenic differentiation
Osterix	SP7	Transcription factor in osteoblast differentiation
Bone morphogenetic protein 2	BMP2	Stimulates the production of bone
GAPDH	GAPDH	Control (housekeeping gene)

About 130 flasks of cells were harvested at 50% confluency using trypsin and detached cells were adjusted to 500,000 cells per 2 ml (250,000/ml) density. For each adhesion, proliferation, and differentiation set, 3 samples of each surface were placed in separate 12-well plates. Each sample was seeded with 500,000 cells (2 ml for each well) and incubated for 24 hours. After 24 hours, the adhesion set samples were harvested, but the samples from proliferation and differentiation samples were transferred to fresh 12-well plates, and fresh medium was added. The proliferation samples were incubated for 3 more days and harvested on day 4. For differentiation samples, at day 2 after plating, differentiation medium was added, samples were incubated for 3 more days, and were harvested at day 5 after plating. Cells were harvested using accutase as previously described. Detached cells were placed in separate centrifuge tubes, centrifuged at 14,000 rpm for 5 minutes, and the supernatant was discarded. To isolate RNA, QIAGEN RNeasy mini kits were used. Cells were resuspended in 350μL RLT buffer, vortexed for 5 seconds, pipetted onto a

QIAshredder spin column, centrifuged at 14,000 rpm for 2 minutes and the lysate was transferred to a gDNA eliminator spin column, centrifuged at 10,000 rpm for 30 seconds, and the flowthrough was saved. Then, 350μL of 70% ethanol was added to the lysate, mixed well by pipetting, 700μL of the sample was applied to an RNeasy mini column, centrifuged at 10,000 rpm for 20 seconds and the flowthrough was discarded. Next, 700μL Buffer RW1 was added to the column, centrifuged at 10,000 for 20 seconds, the flowthrough was discarded, and columns were transferred to new 2-mL collection tubes. Subsequently, 500μL Buffer RPE was pipetted onto the column, centrifuge at 10,000 for 20 seconds, flowthrough was discarded, 500 μL buffer RPE was added to the column, centrifuged at 10,000 rpm for 2 minutes. Columns were transferred to a new 1.5-mL collection tube, 50μL RNase-free water was pipetted onto the column membrane and centrifuged at 10,000 rpm for 1 minute. RNA quantification was performed at this stage to confirm successful isolation. For reverse transcription, cDNA master mix was made by adding 6 μl of 10x RT Buffer, 6 μl of 10x Random Primer, 3 μl of Multiscribe, 2.4 μl of 25x dNTPs, and 12.6 μl of nuclease-free water per reaction. Then, 30 μl of RT master mix and 30 μl of each RNA sample were added in separate centrifuge tubes, incubated at room temperature for 10 minutes in an incubator at 37°C for 2 hours, and then on a heat block at 85°C for 5 minutes, and stored at 4°C in the dark. To achieve the desired volume for each PCR, 70 μl of nuclease-free water was added to each cDNA sample. The PCR master mix for each sample and each primer was generated by adding 50 μl of TaqMan Master Mix, 5 μl of specific primer, 10 μl of cDNA Sample, and 35 μl of Nuclease-free water to a small tube. Then, 25 μl of the mix was added into 96-well PCR plate in triplicate, the plate was covered with an optical cover, centrifuged at 520 rpm for 30 seconds, and placed in the PCR machine. Relative quantification was used, and the primers that correspond to the plate were chosen (GAPDH as the endogenous control). After reading the plate, the PCR program was used for analyzing the data. The baseline was set for CoCr, and the amplification plots were acquired. The outliers/missing wells were omitted during the analysis.

2.8 DATA ANALYSIS AND STATISTICS

Statistical analysis was performed using data from three independent experiments (n = 3) and the results are presented as means ± SD. The statistical significance of differences between surfaces was evaluated using the ANOVA with post-hoc Bonferroni's multiple comparison tests, Mann-Whitney test, or a 2-sample t-test with independent samples.

3   CHAPTER THREE: COMPARING BIOCOMPATIBILITY OF NANO-CRYSTALLINE TITANIUM AND TITANIUM-OXIDE WITH MICRO-CRYSTALLINE TITANIUM

ABSTRACT

Ti is the material of choice for orthopaedic applications because it is biocompatible and encourages osteoblast ingrowth. It was shown that the biocompatibility of Ti metal is due to the presence of a thin native sub-stoichiometric Ti oxide layer which enhances the adsorption of mediating proteins on the surface (49). The present studies were devised to evaluate the adhesion, survival, and growth of cells on the surface of new engineered nano-crystal films of Ti and TiO_2 and compare them with orthopaedic-grade Ti with micro-crystals. The engineered nano-crystal films with hydrophilic properties are produced by employing an IBAD technique. IBAD combines physical vapor deposition with concurrent ion beam bombardment in a high vacuum environment to produce films (with 3 to 70 nm grain size) with superior properties. These films are "stitched" to the artificial orthopaedic implant materials with characteristics that affect the wettability and mechanical properties of the coatings.

To characterize the biocompatibility of these nano-engineered surfaces, we have studied osteoblast function including cell adhesion, growth, and differentiation on different nano-structured samples. Cell responses to surfaces were examined using SAOS-2 osteoblast-like cells. We also studied a correlation between the surface nano-structures and the cell growth by characterizing the SAOS-2 cells with immunofluorescence and measuring the amount alizarin red concentration produced after 7 and 14 days. The number of adherent cells was determined by means of nuclei quantification on the nano-crystalline Ti, TiO_2, and micro-crystalline Ti and analysis were performed with Image J. Our experimental results indicated that nano-crystalline TiO_2 is superior

to both nano- and micro-crystalline Ti in supporting growth, adhesion, and proliferation. Improving the quality of surface oxide, i.e., fabricating stoichiometric oxides as well as nano-engineering the surface topology, is crucial for increasing the biocompatibility of Ti implant materials.

INTRODUCTION

Osseointegration of orthopaedic implants is dependent upon different parameters of the implant surface such as surface properties and physicochemical properties including surface energy, charge, wettability, chemistry, and topography. Surface topography can impact cellular behavior including adhesion, migration, morphology, and orientation in addition to focal adhesion, the development of cytoskeleton, and differentiation (50). Surface modifications on implant surfaces can be manipulated by etching (51), plasma deposition (52), sintering powders (53), machining/micro-machining (54), and ion-beam assisted deposition (22).

When an implant is placed in the body, a multi-step process occurs. First, serum/plasma proteins adsorb on the implant surface and cells attach to the protein layer by integrins which recognize presented extracellular ligands and mediate the initial interactions of cells and the implant material (55). After the cells adhere, there is a rearrangement of cytoskeleton proteins, formation of tight focal adhesion contacts, activation of focal adhesion kinase, and the induction of several intracellular signal transduction pathways, which leads to proliferation and differentiation of the cells (55, 56). Jager *et al.* and Stevens *et al.* have shown that roughened Ti surfaces can increase the focal contacts for cellular adhesion and they are able to guide membrane receptor organization and cytoskeletal assembly (57, 58). *In vitro* experiments have shown that rough implant surfaces promote the adsorption of FN and albumin (59, 60). *In vivo* osteointegration has also been improved on roughened surfaces compared to smoother surfaces, which may suggest that the surface modulates the response including osteoblast differentiation, ECM deposition, and calcification (61, 62). Hence, if there is an improvement in the symbiosis of the implant and osteointegration, it

should accelerate the healing time, increase the implant longevity, and reduce the necessity of revision surgery (55).

In the present work, osteoblast functions including cell adhesion, growth, and differentiation on different nano-samples were investigated. Cell responses to surfaces were examined using SAOS-2 osteoblast-like cells. We studied a correlation between the surface topography and the cell growth by characterizing the SAOS-2 cells with immunofluorescence and measuring the alizarin red concentration produced after 7 and 14 days.

MATERIALS AND METHODS

3.1.1 Sample Preparation

The scientific community has been actively pursuing the study of IBAD for specific applications such as tri-biological coatings, anti-corrosion coatings, optical coatings, superconducting buffer layers, and coatings for temperature sensitive substrates such as polymer. IBAD (Figure 3-1) combines evaporation with concurrent ion beam bombardment in a high vacuum environment. Energetic ions (with a depth penetration of typically less than 20 nm) were employed to produce engineered nano-crystals "stitched" to a substrate (utilizing billions and billions of directed and parallel ionic hammers). Ion bombardment is also the crucial factor for controlling other film properties such as surface morphology, density, stress level, crystallinity, grain size, grain orientation, and chemical composition (22).
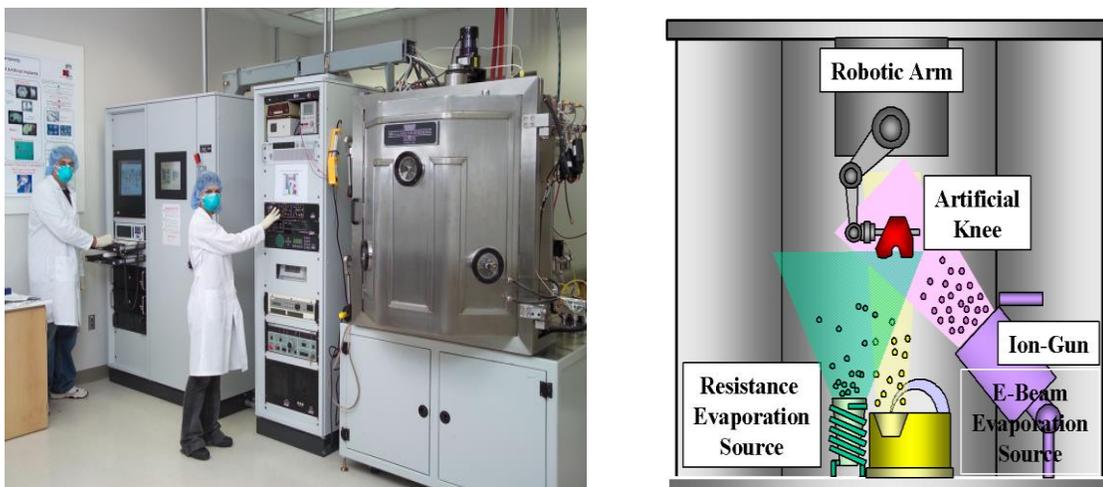
Figure 3-1: (a) IBAD system and (b) schematic. The process combines physical vapor deposition (evaporation) with concurrent ion beam bombardment to produce a wide range of nano-crystalline and coating (22).

The nano-crystalline TiO_2 and Ti samples were prepared by IBAD technique at the Nano-technology Laboratory of the University of Nebraska Medical Center (Figure 3-1). The IBAD system is composed of a Veeco 12 cm RF ion gun that supplies ions at energies up to 1500 eV with a total current density of 500 mA, which provides a broad uniform ion beam of O, N, and Ar. IBAD experiments were carried out in an ultrahigh vacuum environment at a base pressure of 10^{-8} Torr. Using this ion beam technique, we can easily create a gradual transition between the substrate material and the deposited film with less built-in stress than other techniques. These properties result in films with a much more durable adhesion to the substrate, even at room temperature. Ion bombardment also aids the production of stress-free films, eliminating stress-induced problems such as buckling, micro-cracking, or peeling. IBAD samples were cut into 1 cm^2 sections and placed in a 50:50 mixture of acetone: methanol. Samples were sonicated for 1 hour at room temperature, rinsed in ethanol, and dried under N2 air. Samples were wrapped in foil and autoclaved before use.

3.1.2 Cell Culture and Cell Seeding

A human osteoblast-like cell line (SAOS-2) was used in this research. SAOS-2 cells were purchased from ATCC. Cells were grown in McCoy's 5A medium (ATCC) supplemented with 15% FBS and 1% gentamycin (Invitrogen) in a humidified 5% CO_2 atmosphere at 37°C. Cells were seeded at a cell density of 10,000, 25,000, 50,000, and 75,000 cells/ml/cm2 for cell adhesion and cell growth.

For differentiation experiments, cells were incubated in the standard McCoy's medium (supplemented with FBS and antibiotics) for 4 days. On day 4, 0.3 mM ascorbic acid and 10 mM glycerol phosphate were added to the medium (differentiating medium). The medium was changed every 3rd day and the cells were incubated for 7 and 14 days (mineralization).

3.1.3 Cell Adhesion and Fluorescence Imaging

The number of adherent cells was determined by means of nuclei quantification on the TiO_2-nano, Ti-nano, and Ti-micro substrates. Therefore, after 48 hours of incubation, SAOS-2 cells were washed with PBS. Then the cells were fixed with 4% formaldehyde for 10 minutes and stained with 300 nM DAPI (6-diamidino-2-phenylindole) for 5 minutes and rinsed. From each sample, 10 digital images were randomly taken with a Nikon camera using a planar 10x/0.25 objective. DAPI-stained cells were automatically counted after single-channel image segmentation and binary masking. The analysis was performed with Image J (Rasband, W.S., Image J, U. S. NIH, Bethesda, Maryland, USA, http://imagej.nih.gov/ij/, 1997-2012).

The morphology of focal adhesions and actin of SAOS-2 cells cultured on the samples were characterized by microscopy after immunofluorescent staining of actin (5:200, Invitrogen, CA, USA Alexa Fluor 546 Phalloidin) and DAPI (300 nM, Invitrogen, CA, USA 6-diamidino-2-phenylindole). Briefly, samples were rinsed in PBS and fixed with 4% formaldehyde for 10 minutes at room temperature. After another rinse in 1% PBS/BSA, cells were permeabilized with 0.1%

Triton-X 100 solution in PBS. Samples were washed with PBS 3 times for 5 minutes at room temperature. Actin stain was added to each sample at a dilution of 5:200 for 30 minutes and rinsed with PBS 3 times for 5 minutes at room temperature. DAPI was added to each sample (300 nM) for 5 minutes and washed with PBS 3 times for 5 minutes at room temperature. Samples were mounted to slides and cover-slipped until further examination.

3.1.4   Alizarin Red Staining and Quantification

Alizarin red staining was used in order to determine the calcium deposition of SAOS-2 osteosarcoma cells incubated on the nano-samples at day 7 and 14 using the Millipore Osteogenesis Assay Kit (ECM815) according to the manufacturer. Briefly, medium was removed from the samples and rinsed with PBS. The nano-samples were fixed in 10% formaldehyde and stained with alizarin red stain for 20 minutes. The nano-samples were placed in 10% acetic acid for 30 minutes to remove the monolayer, placed in a microcentrifuge tube, and heated to 85°C for 10 minutes and centrifuged. The supernatant was neutralized with 150 μl of 10% ammonium hydroxide and the absorbance was read at 405 nm.

3.1.5   Statistical Analysis

All data presented were derived from three independent experiments (n = 3) and within one experiment three separate samples were analyzed. The results are presented as mean ± SD. Statistical significant differences between three different substrates for alizarin red experiments were evaluated using ANOVA with post-hoc Bonferroni's multiple comparison tests.

RESULTS

Morphology of IBAD nano-crystalline Ti and TiO_2 determined by atomic force microscopy (AFM) and is shown in Figure 3-2.
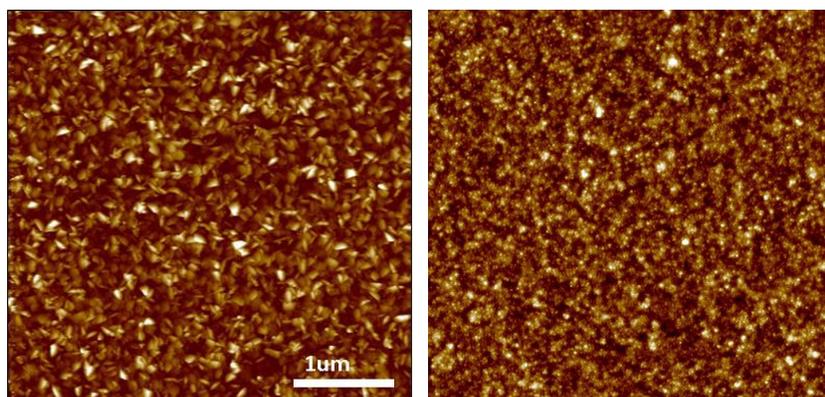
Figure 3-2: AFM images (5μm scan size) of ion beam deposited nano-crystalline Ti and TiO$_2$ deposited at room temperature (a) Ti with a RMS of 6.1 nm (b) TiO$_2$ with a RMS of 1.3 nm.

3.1.6 Cell Adhesion

SAOS-2 cells were monitored for adhesion to the nano-crystalline TiO$_2$, Ti, and medical grade of Ti substrates at 48 hours. The number of adherent cells was determined by nuclei quantification with DAPI in Figure 3-3. Figure 3-3a shows a higher number of cells on nano-structured surfaces compared to biomedical grade Ti, which indicates more adhesion and growth on nano-surfaces. However, by only observing DAPI stained cells, it is impossible to know if cells are healthy and prolific on the surface or not; besides DAPI staining, we also monitored actin fiber shapes (Figure 3-3b and 3-3c) that show a significant difference in cell shape on nano-crystalline TiO$_2$ and Ti as compared to micro-crystalline Ti.
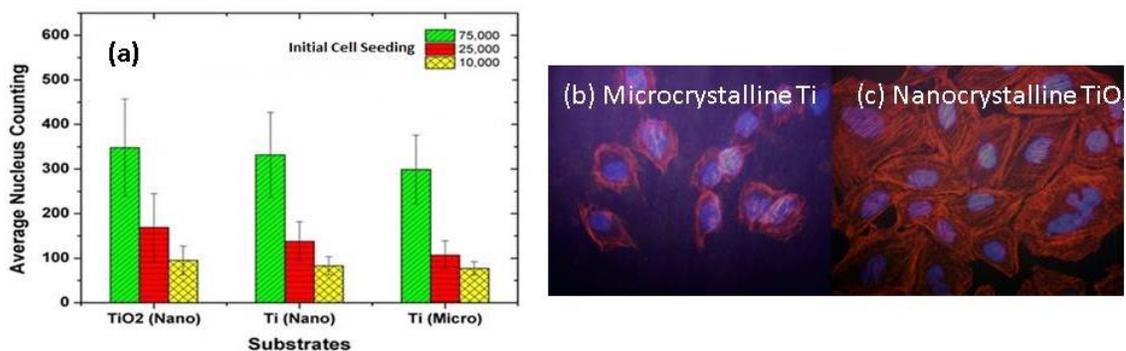
Figure 3-3: (a) Comparing the number of nuclei of SAOS-2 cells on different substrates using DAPI at 48 hours, (b) and (c) merged actin and DAPI stained cells on micro-crystalline Ti and nano-crystalline TiO2, respectively.

3.1.7 Cell Morphology

In order to evaluate the morphology of cells adherent to the various substrates, the attached cells were labeled with actin and DAPI. Pronounced, large focal adhesions or thin, round shapes with actin staining indicate larger surfaces available for adhesion and thus stronger adhesion contacts between cell and material (63). From Figure 3-4, the overall cell morphology is flattened, cells are well spread on the substrate, and the used timing (48 hours of incubation) allowed the cell to go through one cell cycle, which is also an indicator of the suitability of the substrate.
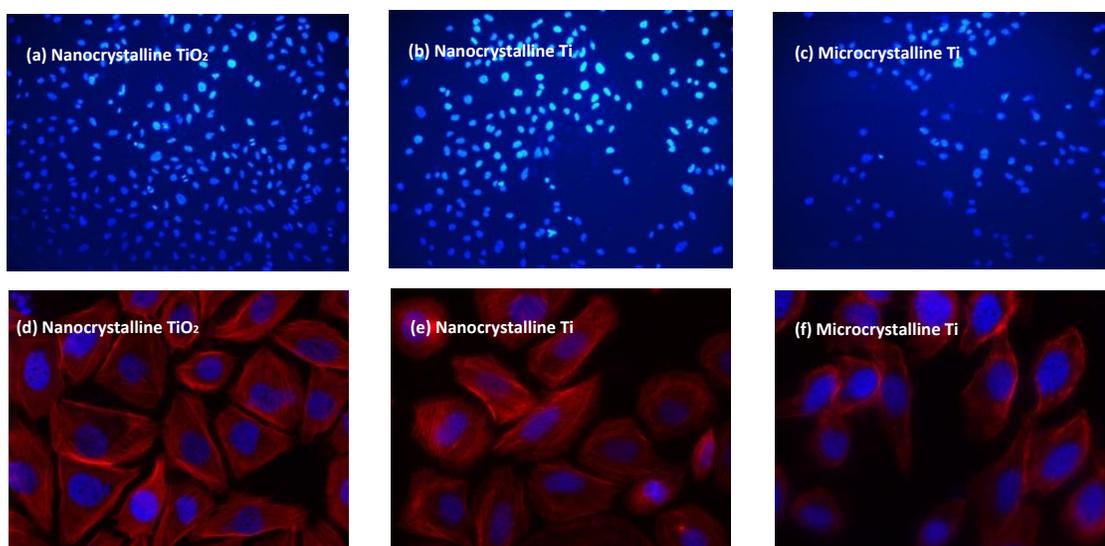
Figure 3-4: Comparing cell adhesion on nano-crystalline TiO_2, Ti, and biomedical grade of Ti by fluorescence images microscopy. 50000 cells were incubated for 48 hours. (a), (b) and (c) are DAPI and (d), (e) and (f) are actin stain experiments.

3.1.8 Alizarin Red Quantification

In order to determine the calcium deposition of SAOS-2 on osteosarcoma cells incubated on different substrates on the 7th day and 14th day of the culture, alizarin red staining was performed. Alizarin Red-S Staining (ARS) is a dye that binds selective calcium salts and is ideally

used for calcium mineral Histochemistry (64). Results of a typical experiment performed in quadruplicate are shown. Values are given as means ± SD.
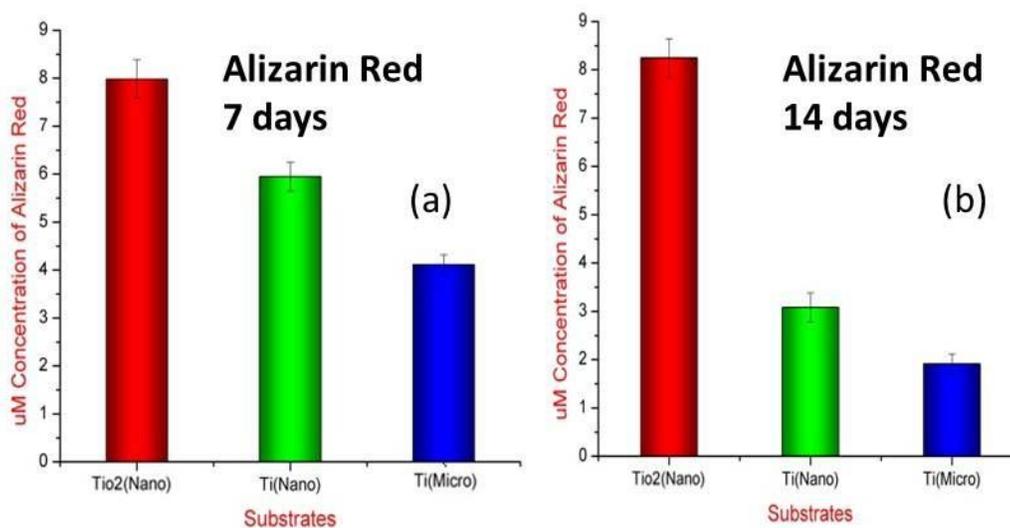
Figure 3-5: Comparing calcium deposition on different substrates using Alizarin Red Assay which indicates that more calcium deposited on IBAD nano-crystalline TiO_2 and Ti as compared to biomedical Ti.

CONCLUSION

Fluorescence images presented in Figure 3-4 show that cell body shape is dependent on the surface of the substrate. If the cell appears round, it is possible that the cells recognize the surface as "flat" and unstructured. However, the nano-roughness of the nano-substrate surfaces appears comparable in size and structure, causing the cells to attach only slightly and to search for suitable places for optimal anchoring (65). Figure 3-5 shows the observed matrix mineralization (Calcium) in SAOS-2 cells. Osteoblastic cells deposit calcium in order to support bone construction. The cells cultured on the nano-surfaces clearly show bright orange-red staining which implies a higher degree of differentiation of the cells. Therefore, enhanced bone formation ability can be expected from the

developed nano-structured surfaces. Our statistical analysis indicates that calcium deposition on nano-crystalline TiO_2 is significantly different from biomedical grade of Ti after 7 days. These results indicate that the surface nano-structures affect cell interactions at the surface and alter cell behavior when compared to conventional (microstructures) size topography. Nano-structured surfaces possess unique properties that alter cell adhesion by direct (cell– surface interactions) and indirect (affecting protein–surface interactions) mechanisms (65). Indeed, in recent work, we have shown that the nano-engineered cubic ZrO_2 is superior in supporting growth, adhesion, and proliferation as compared to the micro-structured one (23). Since cell attachment is mediated by adhesive proteins such as FN, we performed a comparative analysis of adsorption energies of FN fragment using quantum mechanical calculations and Monte Carlo (MC) simulation, both on smooth and nano-structured surfaces. We have found that an FN fragment adsorbs significantly more strongly on the nano-structured surface than on the smooth surface (24).

4   CHAPTER FOUR: EFFECTS OF NANO-ENGINEERED SURFACES ON OSTEOBLAST ADHESION, GROWTH, DIFFERENTIATION, AND APOPTOSIS

ABSTRACT

Modifying implant surfaces to improve their biocompatibility by enhancing osteoblast activation, growth, differentiation, and induction of greater bone formation with stronger attachments should result in improved outcomes for total joint replacement surgeries. This study tested the hypothesis that nano-structured surfaces, produced by the IBAD method, enhance osteoblast adhesion, growth, differentiation, bone formation, and maturation. The IBAD technique was employed to deposit ZrO_2 films on glass substrates. The effects of the IBAD technique on cellular functions was investigated by comparing adhesion, proliferation, differentiation, and apoptosis of the human osteosarcoma cell line SAOS-2 on coated *vs.* uncoated surfaces. IBAD-deposited nano-coatings enhanced initial cell adhesion assessed by the number of DAPI-stained cells on ZrO_2 nano-coated surfaces compared to glass surfaces. This nano-modification also increased cell proliferation as measured by mitochondrial dehydrogenase activity. Moreover, the IBAD technique improved cell differentiation as determined by the formation of mineralized bone nodules and by the rate of calcium deposition, both of which are *in vitro* indicators of the successful bone formation. However, programmed cell death assessed by Annexin V staining and flow cytometry was not statistically significantly different between nano-surfaces and glass surfaces. Overall, the results indicate that nano-crystalline ZrO_2 surfaces produced by the IBAD technique are superior to uncoated surfaces in supporting bone cell adhesion, proliferation, and differentiation. Thus, surface properties altered by the IBAD technique enhanced bone formation and may increase the biocompatibility of bone-cell associated surfaces.

INTRODUCTION

Degenerative joint problems due to inflammatory joint disease, obesity, aging, and other injuries cause irreversible damage and ultimately have no solution other than total joint replacement (TJR). More than one million patients in the United States undergo joint replacement surgery each year, and total Medicare expenses for knee and hip replacements alone exceed three billion dollars per year (66). The number of Americans who need TJR is expected to increase in the near future, with a projection of over four million annually by 2030 (3). In addition to first-time TJR surgeries, 10-20% of patients need revision surgeries due to implant failures (3). Currently, orthopedic implant lifetimes are only 10–15 years with failures due to multiple causes including infection, inflammation, and poor osseointegration (67-69). These statistics highlight the need to develop better technologies for TJR procedures and to produce implants that stimulate host cell adhesion and growth. Improving osseointegration properties of bone implants decreases healing time and increases implant longevity (69, 70). Implant surface properties, including chemical, physical, and mechanical properties, are known to affect the responses of the cells that attach to these surfaces (71). Surface modifications can be achieved by various techniques (72) including etching, physicochemical coating, machining, plasma surface engineering, radiation grafting, ion beam processing, and surface patterning. Even though these modifications have been identified, there is still a continuing search for an optimal surface modification method to improve the biocompatibility of implants, to enhance osteoblast activation and differentiation, and thus extend implant longevity (69).

In 2008, Namavar *et al.* (22) adopted the IBAD technique to generate nano-crystalline films with combined properties of hardness and wettability; both of which are critical determinants of implant success and durability. Limited preliminary studies showed that these films had improved osseointegration and other biomedical properties, due to their ultra-hydrophilic properties (22).

Therefore, this study hypothesized that the IBAD technique would additionally improve implant surface properties by increasing osteoblast adhesion, proliferation, differentiation, bone formation, and maturation. To test this hypothesis, osteoblast cell adhesion, growth, differentiation, and apoptosis of a human osteosarcoma cell line were compared between IBAD-generated ZrO_2 nano-coated and uncoated glass surfaces. The results presented here suggest the likely utility of these nano-coatings for improving orthopaedic implants.

MATERIAL AND METHODS

4.1.1   Suppliers

The ZrO_2 powder for making nano-coatings was purchased from Alfa Aesar (#36319, Tewksbury, MA) and glass substrates were Fisherfinest premium plain glass microscope slides (#125441, Waltham, MA). The human osteosarcoma cell line SAOS-2 was obtained from the ATCC (#HTB-85, ATCC, Manassas, VA), and cultured in McCoy's 5A medium (#30-2007, ATCC, Manassas, VA). The medium was supplemented with FBS (#S11550, Atlanta Biologicals, Flowery Branch, GA) and gentamycin (#15750060, Life Technologies, Grand Island, NY). For mounting samples to the slides and coverslips, Fluormount-G (#0100-01, SouthernBiotech, Birmingham, AL) was used. Metabolic activity was measured using CellTiter 96 AQueous One solution cell proliferation assay from Promega (#G3582, Madison, WI). An Alexa Fluor 488 Annexin V/Dead cell apoptosis kit was purchased to measure the programmed cell death with Alexa Fluor 488 Annexin V and PI for flow cytometry from Invitrogen (#V13241, Eugene, OR). The osteogenesis assay kit was obtained from Millipore (#ECM81, Billerica, MI) and employed according to the manufacturer's instructions.

4.1.2   Nano-fabrication

Nano-surfaces were prepared using the IBAD technique precisely as described by Namavar *et al.* (22). This technique utilizes a combination of an electron beam evaporation system with

concurrent ion beam bombardment in a very high vacuum environment (10^{-8} Torr). These energetic ions attach a nano-crystalline thin film of ZrO_2 to the substrate. Ion bombardment is the critical factor for controlling film properties including morphology, density, stress level, crystallinity, grain size, grain orientation, and chemical composition (22). Using the IBAD technique to modify surface properties was previously shown to result in stress-free films with more durable adhesion to a Ti substrate (73). Glass substrates were tested here to eliminate inherent surface properties of metal surfaces, allowing the focus solely on the specific nano-coating properties.

4.1.3   Sample Preparation

Both nano-coated and uncoated glass surfaces were cut into 1 cm x 1 cm samples, sonicated for 2 hours in 50:50 acetone:methanol mixture, and rinsed in ethanol. The samples were wrapped in aluminum foil and autoclaved to ensure sterile surfaces for cell culture studies.

4.1.4   Cell Culture

Cell culture studies were performed using the human osteosarcoma cell line SAOS-2, which was derived from the primary osteosarcoma of an 11-year-old Caucasian girl (74). Cells were grown in McCoy's 5A medium supplemented with 15% heat-inactivated FBS and 1% gentamycin in a humidified 5% CO_2 atmosphere at 37°C.

For differentiation experiments, cells were grown in McCoy's medium supplemented with FBS and gentamycin for 4 days. From day 4, cell cultures were maintained in the same medium supplemented with 0.3 mM ascorbic acid and 10 mM glycerol phosphate (differentiation medium). The cells were incubated for 7, 14, or 21 days, with fresh medium changes every 3 days.

4.1.5   Survival

To compare programmed cell death of SAOS-2 cells on uncoated and ZrO_2 nano-coated glass surfaces, an Annexin V kit with PI staining was used. Preparation of 1X Annexin-binding

buffer and 100 µg/mL working solution of PI was prepared based on the manufacturer's protocol. Three samples of each substrate were placed in 12-well plates, and 500,000/ml cell with 2 ml of suspension medium was seeded on the top of each sample (1 million cells per well) and incubated for 24 hours in a CO_2 incubator at 37°C. After 24 hours, all samples were transferred to a fresh 12-well plate, fresh medium was added, and incubated for 3 more days. At day 4 after plating, the medium was removed, samples were washed with 1 ml PBS, and 500 µl of Accutase was added to each well. The samples were incubated for 10 minutes at room temperature, 2 ml of medium was added to each well, and detached cells were transferred to separate 15-ml conical tubes, and centrifuged. The cells were washed with cold PBS, re-centrifuged, and re-suspended in 1X Annexin-binding buffer. To each 100 µL of cell suspension, 5 µL Alexa Fluor 488 Annexin V and 1 µL 100 µg/mL PI working solution. Following incubation at room temperature for 15 minutes in the dark, 400 µL of 1X Annexin-binding buffer was added to each tube and mixed gently. Samples were placed on ice and analyzed within 1 hour by flow cytometry measuring the fluorescence emission at 530 nm and 575 nm or equivalent using 488 nm excitation. A total, 10,000 events were collected for each sample. The population was separated into three groups: live cells showed only a low level of fluorescence, apoptotic cells showed green fluorescence, and dead cells showed both red and green fluorescence. Data are expressed as the average percent viability.
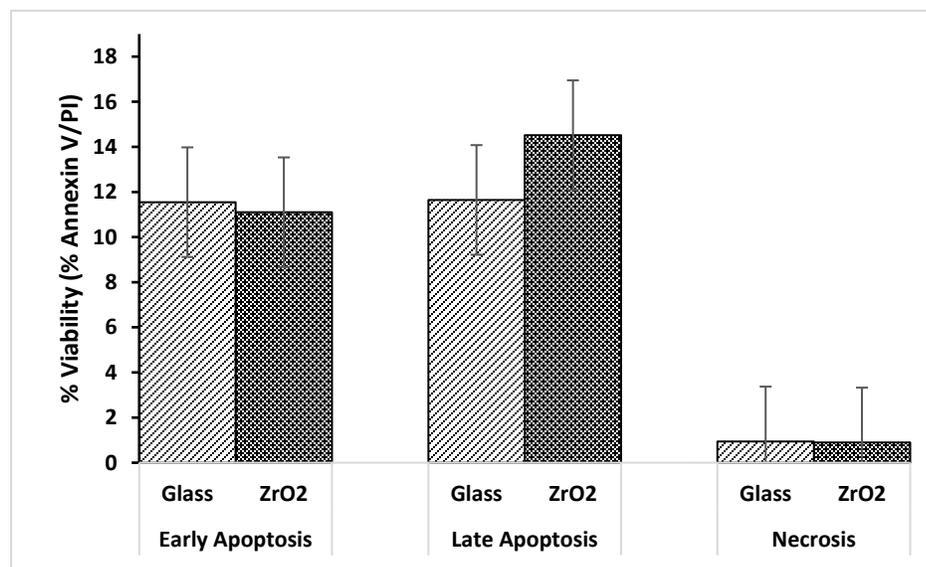
Figure 4-1: Comparison of viability (early apoptosis, late apoptosis, and necrosis) of coated and uncoated surfaces. The percentage of viable SAOS-2 cells was quantified by measuring fluorescence using flow cytometry (n = 3, means $\pm$ SD).

4.1.6 Adhesion

For quantifying adherent cells, different densities of SAOS-2 cells were cultured as described above in 12-well plates. After 24 hours, samples were washed with 1x PBS containing 1% BSA, fixed with 1 ml of 4% formaldehyde for 10 minutes, and permeabilized with 1 ml of 0.1% Triton-X-100 for 5 minutes, all at room temperature. Samples were stained with DAPI (1 ml of a 300 nM stock solution of 4', 6- diamidino-2-phenylindole dihydrochloride in PBS per sample) for 5 minutes in the dark at room temperature. Between all steps above, cells were washed twice with PBS/1% BSA buffer. Samples were fixed to the slides and coverslips were attached with Fluormount-G. Cells were quantified using ImageJ software (IJ 1.45 m, National Institutes of Health, Bethesda, MD), and data are expressed as the average number of DAPI-stained cells in 15 random fields captured at 10x.
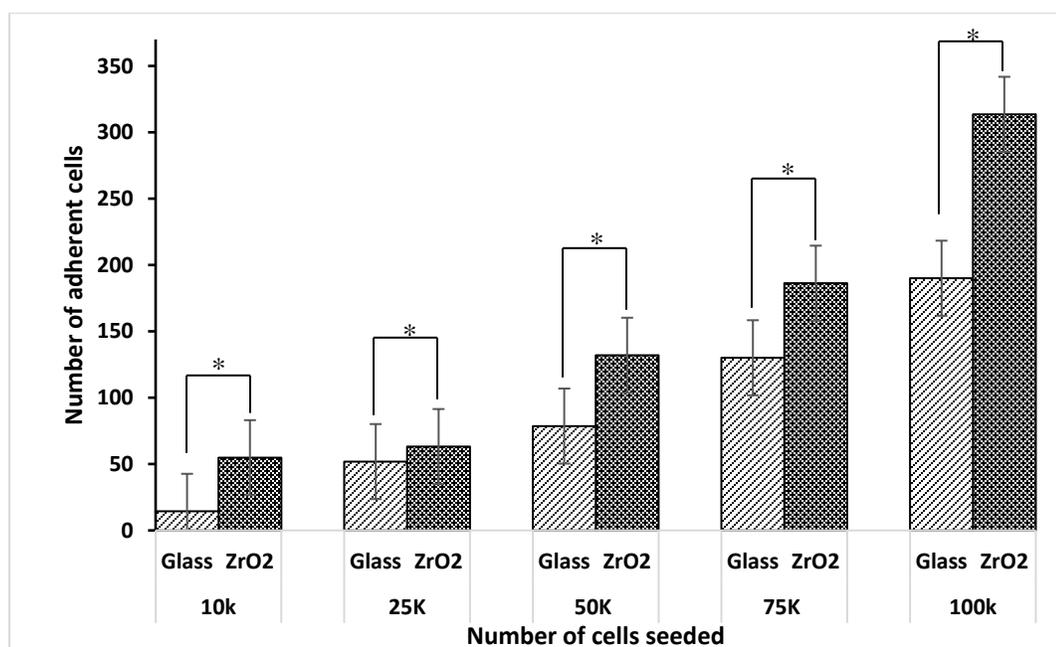
Figure 4-2: Comparison of initial cell adhesion on coated and uncoated surfaces

Different cell numbers were seeded on nano-ZrO_2 and glass surfaces. The number of adherent SAOS-2 cells 24 hours after seeding was quantified by counting DAPI-stained cells from 15 random images captured at 10x (n = 3, means $\pm$ SD).

Table 4-1: Number of adherent SAOS-2 cells on coated and uncoated
surfaces 24 hours after seeding

Cell seeding	Cell attachment mean +/- SD		Ratio	*P-value*
	Glass	**ZrO$_2$**		
10,000	14 ± 03	55 ± 18	3.9	.0001
25,000	52 ± 09	63 ± 09	1.2	.0020
50,000	79 ± 09	132 ± 17	1.7	.0001
75,000	130 ± 10	186 ± 30	1.4	.0001
100,000	190 ± 18	314 ± 22	1.7	.0001

4.1.7 Proliferation

- <u>Metabolic Activity</u>

As an indicator of cell viability and proliferation, the metabolic activity of SAOS-2 cells on coated and uncoated surfaces was determined using an MTS assay. Culturing 500,000/ml cell with 2 ml of suspension added to samples was performed as previously. After 24 hours, all samples were transferred to a fresh 12-well plate, fresh medium was added, and incubated for 3 more days. At day 4 after plating, the medium was removed from the samples, 200 µl of fresh medium, and 40 µl MTS dye solution was added to each sample. The plates were incubated in a CO$_2$ incubator at 37°C for 3 h. After this incubation period, 100 µl of supernatant was transferred into each well of a 96-well plate and absorbance of the MTS formazan dye product was measured photometrically at 490 nm with an Infinite M200 (Tecan, Morrisville, NC) plate reader. The cells in each well were stained with DAPI and visualized at 10x by fluorescence microscopy as described in the cell counting section.
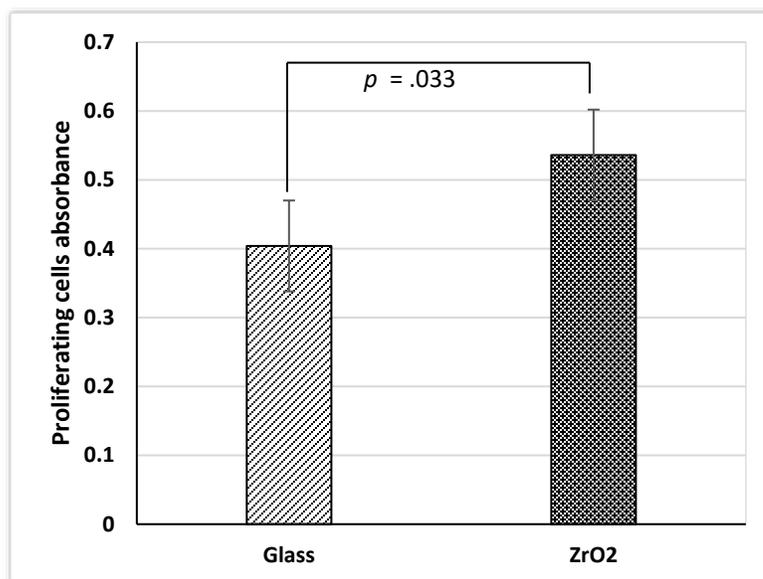
Figure 4-3: Comparison proliferating cells absorbance on coated and
uncoated surfaces based on MTS assay.

SAOS-2 cells were plated on either uncoated or ZrO_2 nano-coated glass surfaces (1 million

cells per sample), and proliferation was assessed after 4 days using MTS assays (n = 3,

means $\pm$ SD). The statistical differences were evaluated using independent samples t-test.
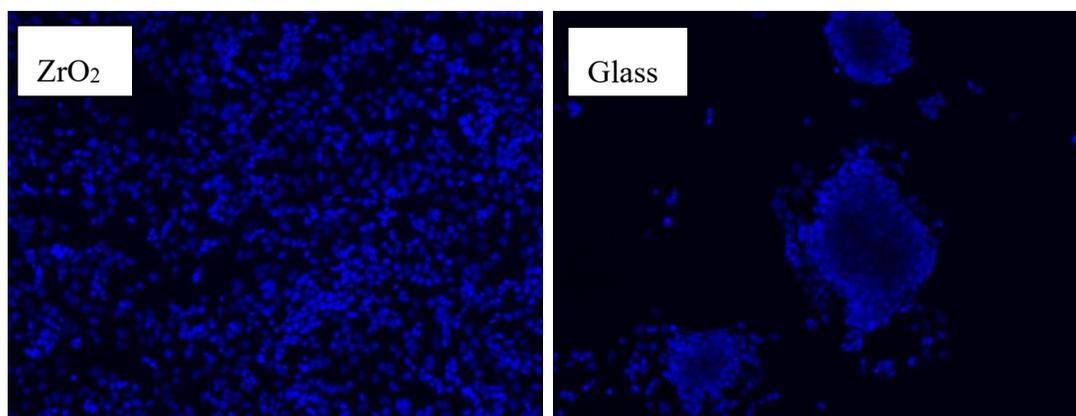
Figure 4-4: Visualization of SAOS-2 cells at day 4 to assess adhesion and proliferation on coated and
uncoated surfaces.

SAOS-2 cells were plated on ZrO_2 nano-coated and uncoated glass substrates (1 million cells per sample), and allowed 24 hours to adhere, followed by 3 additional days of proliferation. After 4 days, cells were stained with DAPI (blue). Results are from one experiment representative of those from 3 independent experiments with random images taken at 10x magnification. The statistical differences were evaluated using the independent sample T-test.

4.1.8 Differentiation

- Alizarin Red Assay

To determine calcium deposition, SAOS-2 cells were cultured as described previously, incubated on the different surfaces for 7 days in 24-well plates, and alizarin red staining was performed as follows. After removing medium from the samples and rinsing with PBS, samples were transferred to fresh plates and fixed with 10% formaldehyde at room temperature for 15 minutes. Samples were rinsed 3 times with de-ionized water, 1 ml alizarin red stain solution was added to each well, followed by incubation at room temperature for 20 minutes. Excess dye was removed by 4 washes with de-ionized water, 400 µl of 10% acetic acid was added to each well, the plates were incubated for 30 minutes with shaking, and the mixtures were transferred to 1.5-ml centrifuge tubes. To remove the cell monolayer, samples were vortexed for 30 seconds and then incubated at 85°C for 10 minutes in a block heater. Tubes were placed on ice for 5 minutes and then centrifuged at 20,000 g for 15 minutes. A 400-µl portion of the supernatant was transferred to a fresh 1.5-ml centrifuge tube, and the pH was neutralized with 150 μl of 10% ammonium hydroxide (pH 4.1-4.5). Finally, 150 µl of the mixture in each tube was transferred to one well of a 96-well plate, and the absorbance at 405 nm was quantified.

4.1.9   Statistical Analysis

Statistical analysis was performed using data from three independent experiments (n = 3), and the results are presented as means ± SD. The statistical significance of differences between surfaces was evaluated using the Mann-Whitney test or the 2-sample t-test with independent samples.

RESULTS

The program cell death of SAOS-2 cells assessed by Annexin V kit with PI staining (Figure 4-1) showed no differences between uncoated and ZrO_2 nano-coated glass surfaces in early apoptosis ($p = .842$), late apoptosis ($p = .074$), and necrosis ($p = .853$) suggesting that differential toxicities of the surfaces was not a factor in outcomes.

Adherence of SAOS-2 cells to coated and uncoated surfaces 24 hours after culturing on the top of surfaces at different densities assessed by counting DAPI-stained cells was 1.3- to 3.9-fold greater on ZrO_2 nano-coated compared to uncoated glass surfaces (Figure 4-2 and Table 4-1), indicating greater adhesion on nano-surfaces.

The proliferation of SAOS-2 cells assessed by metabolic activity in MTS assays was 1.6-fold higher for cells on ZrO_2 nano-coated *vs.* uncoated glass surfaces at day 4 after culturing (Figure 4-3), indicating higher metabolic activities of those cells.

Similarly, the proliferation of cells visualized by DAPI staining at day 4 after plating appeared to show greater adhesion and proliferation for cells plated on ZrO_2 nano-coated than *vs.* uncoated glass surfaces (Figure 4-4). These data indicated not only greater proliferation on nano-surfaces but also a more uniform distribution of the cells on those surfaces.

Calcium deposition, assessed by alizarin red staining, was 1.2-fold higher for cells on ZrO_2 nano-coated *vs.* uncoated glass surfaces on day 7 of culture, indicating higher calcium deposition in differentiation, by cells grown on these nano-surfaces.

DISCUSSION

Early and late apoptosis and also necrosis of SAOS-2 cells on uncoated and ZrO_2 nano-coated glass surfaces showed no difference. The viability percentage for these data is a combination of the survival of the cells on the substrates, and their death because of apoptosis/necrosis as a response to surfaces or a combination of both. The Annexin V kit with PI staining cannot differentiate between these assumptions and but was used as a starting point for further investigation.

Both adhesion and proliferation of SAOS-2 cells assessed by counting DAPI-stained cells were greater on ZrO_2 nano-coated compared with uncoated glass surfaces, indicating that nano-coating enhance cell interactions with the surface and altered cell behavior. Moreover, cell distributions on the coated and uncoated surfaces were different. Cells showed a more uniform distribution on ZrO_2 nano-coated compared with uncoated glass surfaces, where the cells adhered in the form of clumps. This difference indicates that adhesion of these cells is more compatible with nano-coated surface compared to the uncoated ones and it appears on the glass surfaces; they prefer to stick to each other (potentially to maintain viability) than adhere to the surface.

The metabolic activity in MTS assays was 1.3-fold higher for cells on ZrO_2 nano-coated *vs.* uncoated glass surfaces at day 4 after plating, and independent samples t-test showed a *P value* = .033. This result indicates that cells seeded on nano-coated surfaces showed increased metabolic activity and growth rates when compared with the uncoated glass surface as a control.

These data show that cells not only attached and proliferated more on the ZrO_2 nano-coated surface compared with the uncoated surface, but that they also appeared healthier. Taken together, these data suggest that ZrO_2 nano-coatings can accelerate and increase adhesion, proliferation, and subsequent metabolic activity of osteoblasts compared with uncoated surfaces. Increasing the extent of host cell adhesion and the rate of growth could likely lead to accelerated integration and decreased healing time for patients and increased longevity for implants.

Calcium deposition, assessed by alizarin red staining, is an indicator of late differentiation and bone formation capability of the osteoblast-like cells that are responsible for bone formation (75). Calcium deposition measured on day 7 of culture was 1.2-fold higher for cells on ZrO_2 nano-coated *vs.* uncoated glass surfaces. Osteoblastic cells deposit calcium to support bone formation. Therefore, in a clinical setting, the enhanced bone formation would be expected from cells grown on nano-crystalline ZrO_2 compared to uncoated glass surfaces.

Although this study tested nano-coatings on glass substrates, our previous study using Ti substrates showed similar results (73). The main reason for choosing glass substrates for the current study was to avoid the effect of any surface roughness other than the nano-roughness produced by the IBAD technique. The natural micro-roughness of Ti and its oxides improve its biocompatibility, and this is a major reason that Ti-based materials are an optimal choice for implants (49). Using smooth glass substrates instead of any other material with inherent micro-scale roughness and porosity made it possible for us to isolate the specific effects of the nano-roughness produced by the IBAD technique from other factors that might influence cell interactions with surfaces. Glass surfaces are also neutral, another advantageous property for *in vitro* experiments.

The results here document that nano-crystalline ZrO_2 surfaces improve the adhesion, proliferation, and differentiation of SAOS-2 bone-forming cells *in vitro* compared with the same cells on uncoated glass surfaces. These findings indicate the importance of the unique properties of

IBAD-produced nano-films for surface biocompatibility. There are additional unique properties of these surfaces that make them ideal for osseointegration applications and beneficial for increasing the biocompatibility of implant materials; the most important are grain size, wettability, and hardness (22). An ideal biomaterial should have several fundamental properties simultaneously, including biocompatibility, high strength, bone-bonding ability, and resistance to fatigue, corrosion, and wear (69). However, no known materials possess these combined properties. For example, ceramics have high biocompatibility and enhanced corrosion resistance, but they are brittle and can fracture because of their low plasticity. Moreover, as they become oxidized, they release ions into the body that can lead to immune system reactions and implant degradation (76). Aluminum and Zr are suitable for load-bearing applications because they possess high wear resistance, but there are cases of mechanical failures with these materials (76). Because interactions with foreign bodies are very complicated, more studies are needed to understand the *in vivo* behavior of implant materials better. Hence, research continues to develop new coating technologies and to make advanced implant materials that reduce failure by addressing these many challenges, simultaneously. The promising *in vitro* results presented here provide support for further testing of IBAD-generated surface modifications in animal models for potential future use as significantly improved materials for human implants.

5 CHAPTER FIVE: SURFACE NANO-MODIFICATION BY ION BEAM ASSISTED DEPOSITION ALTERS THE EXPRESSION OF OSTEOGENIC GENES IN OSTEOBLASTS

ABSTRACT

Biomaterials with enhanced biocompatibility are favored in implant studies to improve the outcomes of total joint replacement surgeries. This study tested the hypothesis that nano-structured surfaces, produced by the IBAD method, would enhance osteointegration by altering the expression of bone-associated genes in osteoblasts. The IBAD technique was employed to deposit nano-films on glass or Ti substrates. The effects of the IBAD technique on the human osteosarcoma cell line SAOS-2 at the molecular level was investigated by assays of adhesion, proliferation, differentiation, and apoptosis on coated surfaces *vs.* uncoated CoCr as the control. IBAD nano-coatings enhanced bone-associated gene expression at initial cell adhesion, proliferation, and differentiation compared to CoCr surfaces as assessed by PCR techniques. Increased cell proliferation was observed using a nuclear cell proliferation-associated antigen. Moreover, enhanced cell differentiation was determined by ALP activity, an indicator of bone formation. In addition, programmed cell death assessed by annexin V staining and flow cytometry was lower on nano-surfaces compared to CoCr surfaces. Overall, the results indicate that nano-coated surfaces produced by the IBAD technique are superior to orthopaedic grade CoCr in supporting bone-cell adhesion, proliferation, differentiation, and reducing apoptosis. Thus, surface properties altered by the IBAD technique should enhance bone formation and increased the biocompatibility of bone-cell associated surfaces.

INTRODUCTION

Total joint replacement (TJR) is among the top ten most costly and rapidly increasing procedures in the United States due to the aging population, bone fractures, and increasing obesity (77). In addition, biomaterial studies also have shown a rapid growth rate in the face of the challenge of finding biomaterials with the optimal physical, mechanical, and wear properties necessary for orthopaedic purposes (78, 79). The biomaterials used in implants are usually metals, polymers, ceramics, and composites (79). There are several metallic biomaterials with sufficient hardness, strength, corrosion resistance, and biocompatibility, including stainless steel, Ti alloys, and CoCr alloys, that make them a good option for TJR (78). Stainless steel was the first material used in this category regarding its easy casting and proper mechanical properties. However, some alloying elements including nickel and molybdenum are problematic, mainly due to corrosion (79). Ti and Ti-based alloys are light, biocompatible, and have good mechanical and chemical properties. However, they have the weak shear strength that limits their applications (79). CoCr alloys are highly resistant to corrosion and therefore considered the safest biomaterials for orthopedic prostheses (79, 80). The biocompatibility of the implants can also be modified using a variety of surface modification techniques (69). Understanding the impact of these modifications and also the role of surface chemistry and topography on the osseointegration require many standardized *in vitro* and *in vivo* tests (59).

This study evaluated, at the molecular level, the approach of Namavar *et al.* (22) that introduced the IBAD technique to coat nano-crystalline films with combined controllable properties of hardness and wettability on different substrates. Our previous study showed that IBAD-produced nano-crystalline ZrO_2 surfaces improved the adhesion, proliferation, and differentiation of SAOS-2 bone-forming cells *in vitro* compared with the same cells growing on uncoated glass surfaces.

This study evaluated these differences at the molecular level by investigating gene expression modifications and protein generation. Therefore, we hypothesized that the IBAD technique would improve implant surface properties by optimizing the expression of bone-associated genes. To test this hypothesis, bone-associated gene expression of a human osteosarcoma cell line were compared between IBAD-generated nano-surfaces and uncoated CoCr surfaces in the processes of adhesion, proliferation, and differentiation. In addition, protein generation was studied using ELISA and flow cytometric assays. The results presented here suggest the likely utility of these nano-coatings for improving the integration of orthopaedic implants.

MATERIAL AND METHODS

5.1.1 Suppliers

The ZrO_2 and TiO_2 powder used as source materials for nano-coatings were purchased from Alfa Aesar (#36319 and #36199, Tewksbury, MA), Ti and CoCr substrates were orthopaedic grades purchased from Edge International (CoCrMo ASTM F1537, Dayton, Ohio), and glass substrates used for coating were Fisherfinest premium plain glass microscope slides (#125441, Waltham, MA). The SAOS-2 cell line that is a human osteosarcoma was purchased from the ATCC (#HTB-85, ATCC, Manassas, VA), cultured in McCoy's 5A medium (#30-2007, ATCC, Manassas, VA) , and supplemented with FBS (#30-2020, ATCC, Manassas, VA) and gentamycin (#15750060, Life Technologies, Grand Island, NY). Proliferation was measured using PE Mouse Anti-Human Ki-67 Set (RUO) from Biosciences (#556027, San Jose, CA). The alexa fluor 488 annexin V/Dead cell apoptosis (programmed cell death) kit including alexa fluor 488 annexin V and PI (propidium iodide) for flow cytometry was purchased from Invitrogen (#V13241, Eugene, OR). The SensoLyte pNPP ALP assay kit was obtained from Anaspec (#AS-72146, Fremont, CA) and employed according to the manufacturer's instructions. To normalize data from ALP assay, the BCA protein assay was employed. The Quant-iT PicoGreen dsDNA assay kit was obtained from Invitrogen

(#P11496, Eugene, OR) and Pierce BCA protein assay kit from Thermo Scientific (#23227, Rockford, IL).

5.1.2   Nano-fabrication

All nano-surfaces including ZrO_2 on Glass, ZrO_2 on Ti and TiO_2 on Ti were coated using IBAD technique as described by Namavar *et al.* (22). A combination of an electron beam evaporation system with a simultaneous ion beam bombardment in a high vacuum environment (10^{-8} Torr), stitches a nano-film of the source material to the desired substrate material. The unique characteristics of this nano-film affect mechanical properties and the wettability by controlling the crystallinity, chemical composition, grain size, density, and grain orientation (22).
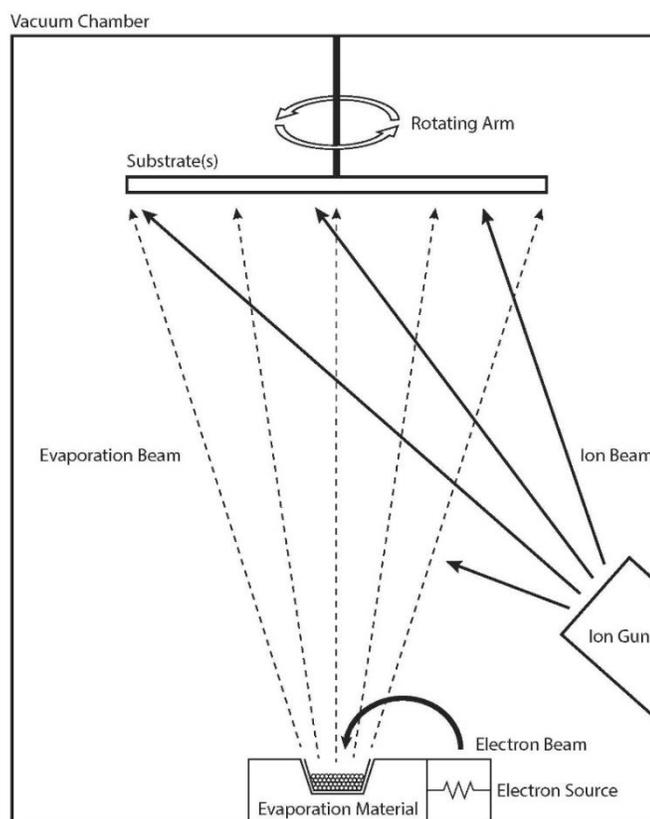
Figure 5-1: Schematic of the IBAD system

5.1.3 Sample Preparation

Nano-coated surfaces were cut into 10 mm by 10 mm squares (area = 100 mm^2), and CoCr samples were cut into disks with 12.7 mm diameter (area = 127 mm^2), polished, sonicated for 1 hour in 50:50 acetone:methanol mixture, wrapped in aluminum foil and autoclaved.

5.1.4 Cell Culture

The cell line used for this study was SAOS-2, a primary human osteosarcoma obtained from the ATCC and originally derived from an 11-year-old Caucasian girl (74). Based on the ATCC protocol, cells were cultured in McCoy's 5A medium, supplemented with 15% heat-inactivated FBS and 1% gentamycin in a humidified 5% CO_2 atmosphere at 37°C.

The differentiation medium, used for ALP and PCR experiments, employed the same medium as above, supplemented with 0.3 mM ascorbic acid and 10 mM glycerol phosphate.

5.1.5 Cellular Responses to Surfaces

5.1.5.1 Proliferation

For comparing osteosarcoma cell proliferation on different surfaces, the Ki-67 assay was used. Ki-67, a nuclear cell proliferation-associated antigen expressed by all proliferating human cells, can be recognized at all stages of the cell cycle (late G1, S, M, and G2 phases) except for G0 phase (39). About 30 flasks of cells were harvested at 50% confluency using trypsin, detached cells were adjusted to 500,000 cells per 2 ml (250,000/ml), 3 samples of each surface were placed in a 12-well plate, and each sample was seeded with 500,000 cells (2 ml for each well), and incubated for 24 hours. After 24 hours, samples were transferred to a fresh 12-well plate, fresh medium was added and incubated for 3 more days. At day 4 after plating, samples were washed with 1 ml PBS once, 500 µl of accutase were added to each well, and incubated for 10 minutes at room temperature. After 10 minutes, 2 ml of medium was added to the each well, detached cells were collected in separate 15-ml conical tubes, centrifuged at 200 g for 5 minutes, the supernatant

was discarded, 5 ml of cold 70% - 80% ethanol was added drop by drop into the cells pellet in each

tube, mixed well and were incubated at -20°C for 24 hours. For Ki-67 staining by flow cytometry,10

ml wash buffer (PBS with 1% FBS, 0.09% NaN3 pH7.2) was added to the fixed cells in each tube,

centrifuged for 5 minutes at 200 g and supernatant was aspirated. One more wash was performed

as described; cells were resuspended in 100 µl wash buffer, 20 µl of antibody was added into the

tubes and mixed gently. Tubes were incubated at room temperature for 30 minutes in the dark,

washed with 2 ml of PBS washing buffer, centrifuged at 200 g for 5 minutes, and 0.5 ml of PBS

wash buffer was added into each tube. The samples were analyzed by FACS.
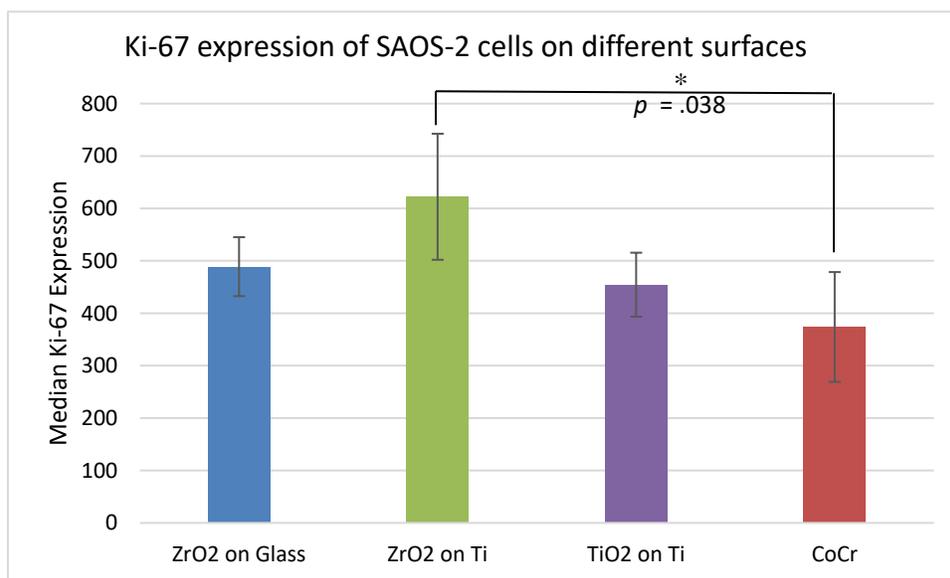
Figure 5-2: Comparison of proliferating cells on coated nano-surfaces and uncoated CoCr
based on Ki-67 expression.

SAOS-2 cells were plated on either uncoated or nano-coated surfaces (1 million cells per

sample), and proliferation was assessed after 4 days using ki-67 assays (n = 3, means $\pm$ SD). The

statistical differences were evaluated using independent samples t-test.

5.1.5.2 Apoptosis

To compare programmed cell death of SAOS-2 cells on different surfaces, an annexin V kit with PI staining was used. In the early stages of apoptosis, PS is translocated from the inner to the outer layer of the cytoplasmic membrane. This translocation marks it for recognition and phagocytosis by macrophages (42). Annexin V is a protein with high affinity for PS that is labeled with a fluorophore. This kit also includes red fluorescent propidium iodide (PI) nucleic acid binding dye that is impermeable to live cells and apoptotic cells, but stains dead cells with red fluorescence. Therefore, apoptotic cells show green fluorescence, dead cells show red and green fluorescence, and live cells show little or no fluorescence. These populations can be distinguished using a flow cytometer with a 488 nm excitation laser. About 30 flasks of cells were harvested at 50% confluency using trypsin, and the detached cells were adjusted to 1,000,000 cells per 2 ml (500,000/ml), 3 samples of each surface were placed in a 12-well plate and each sample was seeded with 1,000,000 cells (2 ml for each well), and incubated for 24 hours. After 24 hours, samples were transferred to a fresh 12-well plate; fresh medium was added and incubated for 3 more days. At day 4 after plating, 1X annexin-binding buffer, and PI working solution were prepared based on the manufacturer's protocol. Subsequently, samples were washed with 1 ml PBS, 500 µl of accutase was added to each well, and incubated for 10 minutes at room temperature. After 10 minutes, 2 ml of medium was added to each well; detached cells were collected in separate 15-ml conical tubes, centrifuged at 200 g for 5 minutes, supernatant was discarded, cells were washed with cold PBS, and resuspended in 1X annexin-binding buffer, and 5 µL alexa fluor 488 annexin V and 1 µL 100 µg/mL PI working solution were added to each 100 µL of cell suspension and incubated at room temperature for 15 minutes in the dark. After the incubation period, 400 µL 1X annexin-binding buffer was added to the samples, mixed gently, and kept on ice for analysis within 1 hour by flow cytometry, measuring the fluorescence emission at 530 nm and 575 nm or equivalent, using 488 nm excitation. From each sample, 10,000 events were collected, and the population was separated

into three groups: live cells (little or no fluorescence), apoptotic cells (green fluorescence), and dead cells (red and green fluorescence). Data are expressed as the average percent viability. Controls that were used included unstained cells, cells stained with annexin V conjugate only (no PI), and cells stained with PI only (no annexin V conjugate).

Figure 5-3: Comparison of viability (late apoptosis) of nano-coated and uncoated CoCr surfaces.

The percentage of viable SAOS-2 cells was quantified by measuring fluorescence using flow cytometry (n = 3, means ± SD).
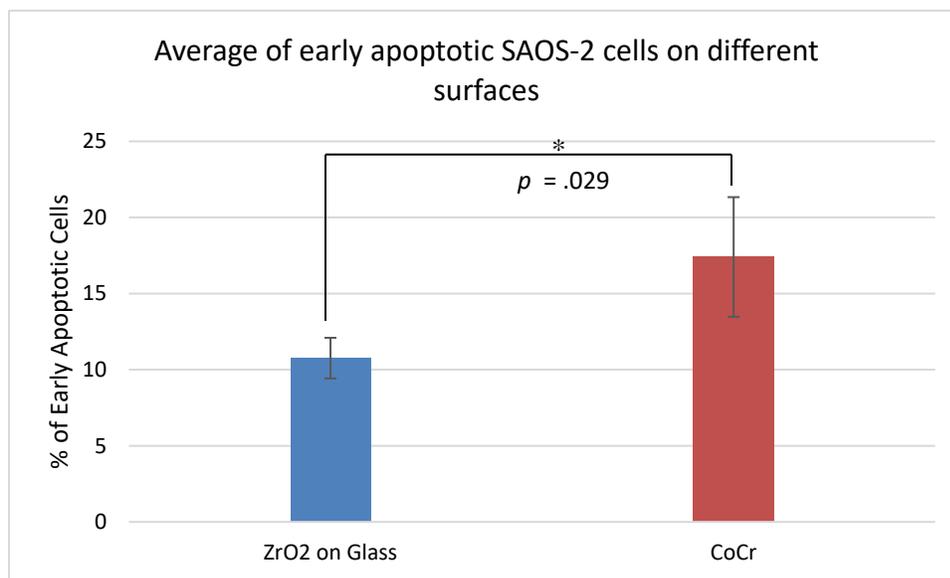
Figure 5-4: Comparison of viability (early apoptosis) of nano-coated and uncoated CoCr surfaces.

The percentage of viable SAOS-2 cells was quantified by measuring fluorescence using flow cytometry (n = 3, means ± SD).
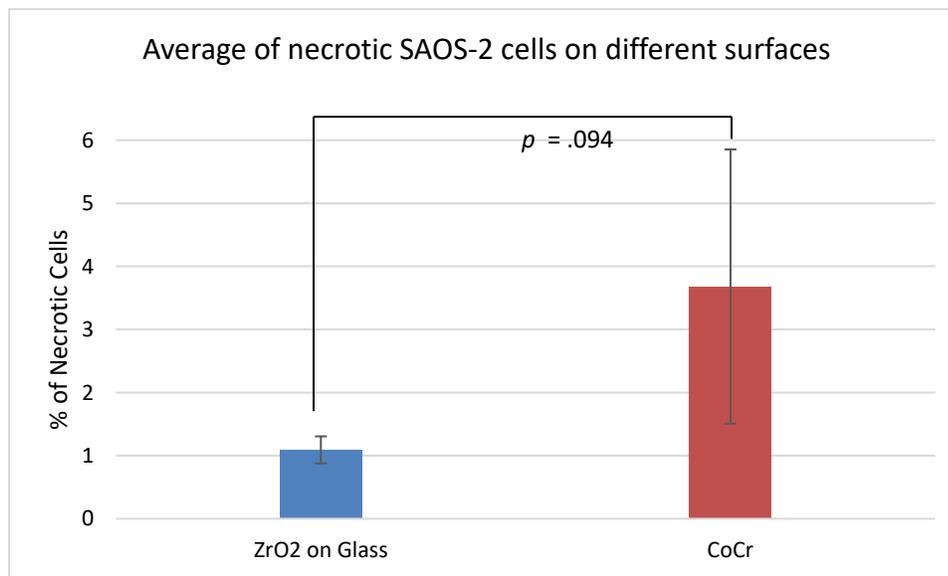
Figure 5-5: Comparison of viability (necrosis) of nano-coated and uncoated CoCr surfaces.

The percentage of viable SAOS-2 cells was quantified by measuring fluorescence using flow cytometry (n = 3, means $\pm$ SD).

5.1.5.3 Differentiation

In order to compare osteosarcoma cell differentiation on the different surfaces, an ALP assay was used. A bone-specific isoform of ALP is found on the cell surface of osteoblasts that are responsible for the synthesis of the new bone matrix and its mineralization. The SensoLytepNPP ALP assay kit can detect ALP by ELISA using colorimetric pNPP phosphatase substrate at absorbance 405 nm. About 30 flasks of cells were harvested at 50% confluency using trypsin, and detached cells were brought to the 500,000 cells per 2 ml (250,000/ml) density, 3 samples of each surface were placed in a 12-well plate, and each sample was seeded with 500,000 cells (2 ml for each well), and incubated for 24 hours. After 24 hours, samples were transferred to a fresh 12-well plate. Fresh medium was added and incubated for another day. At day 2 after plating, differentiating medium was added and incubated for 3 more days. At day 5 after plating, 1X assay buffer, pNPP ALP substrate working solution, and Triton X buffer were prepared according to the manufacturer's instructions. To prepare cell extracts, 500 µl of the Triton X buffer was added to each sample, cell suspensions were incubated the at 4°C for 10 minutes under agitation (100 rpm), collected in a microcentrifuge tube, centrifuged at 2500 g for 10 minutes at 4°C, and the supernatant was collected for ALP assay. To detect ALP activity, 100 µL of pNPP substrate working solution was added into each well, mixed by gently shaking the plate for 30 seconds, and incubated at room temperature for 60 minutes in the dark. After the incubation period, 50 µL of stop solution was added into each well, and the absorbance was measured at 405 nm using Epoch (Biotek, Winooski, VT) microplate spectrophotometer. ALP activity of cell lysates was extrapolated from the ALP standard curve, and the ALP activity was normalized according to the number of cells in the cell lysates using BCA protein assay. This assay is based on BCA for the colorimetric detection and quantitation of total

protein. One cuprous ion forms a complex with two BCA molecules, producing a purple-colored water-soluble complex that absorbs light at 562 nm. The absorbance data were plotted against the standard curve to calculate the concentration of protein in samples.
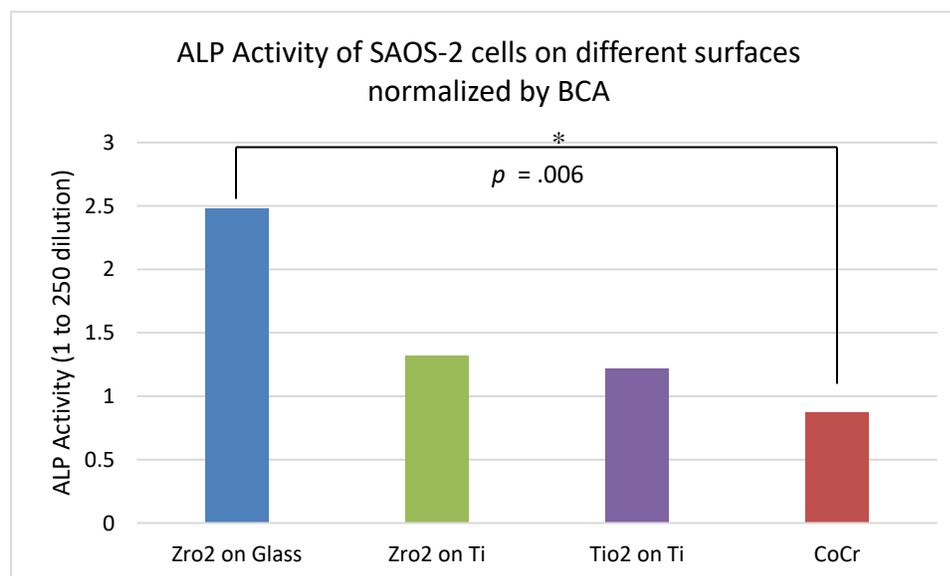
Figure 5-6: Comparison of differentiation on coated and uncoated surfaces based on ALP activity.

SAOS-2 cells were seeded on nano-coated and CoCr surfaces (1 million cells per sample), and differentiation was assessed after 5 days using ALP assay (n = 3, means $\pm$ SD). The statistical differences were evaluated using independent samples t-test.

5.1.6 Gene Expression Modified by the Cell to Surface Interactions

In order to determine the responses of human osteoblast cells to implant surfaces, the gene expression profiles as modified by the cell to surface interactions such as initial adhesion, proliferation, and differentiation were measured using PCR techniques. RNA from cells cultured on the various surfaces was extracted and evaluated by real-time PCR for the osteogenic markers and matrix proteins listed in Table 5-1.

Table 5-1: List of genes used for PCR experiments

Target Gene	Abbreviation	Implication
RUNX 2	RUNX 2	Early osteoblastic transcription factor
Osterix	SP7	Transcription factor in osteoblast differentiation
Alkaline phosphatase	ALPL	Marker for bone mineralization (initial stage)
Osteopontin	SPP1	Marker for middle stage osteogenic differentiation
Fibronectin	EGFLAM	Promoting cell attachment and migration
Ki-67	MKI67	Proliferation marker
Bone morphogenetic protein 2	BMP2	Stimulates the production of bone
GAPDH	GAPDH	Control (housekeeping gene)

About 130 flasks of cells were harvested at 50% confluency using trypsin, and detached cells were adjusted to 500,000 cells per 2 ml (250,000/ml) density. For each adhesion, proliferation and differentiation set, 3 samples of each surface were placed in separate 12-well plates. Each sample was seeded with 500,000 cells (2 ml for each well) and incubated for 24 hours. After 24 hours, adhesion set samples were harvested, but the samples from proliferation and differentiation samples were transferred to fresh 12-well plates, and fresh medium was added. The proliferation samples were incubated for 3 more days and harvested on day 4. For differentiation samples, at day 2 after plating, differentiation medium was added, samples were incubated for 3 more days, and

were harvested at day 5 after plating. Cells were harvested using accutase as previously described. Detached cells were placed in separate centrifuge tubes, centrifuged at 14,000 rpm for 5 minutes, and the supernatant was discarded. To isolate RNA, QIAGEN RNeasy mini kits were used. Cells were resuspended in 350μL RLT buffer, vortexed for 5 seconds, pipetted onto a QIAshredder spin column, centrifuged at 14,000 rpm for 2 minutes and the lysate was transferred to a gDNA eliminator spin column, centrifuged at 10,000 rpm for 30 seconds, and the flowthrough was saved. Then, 350μL of 70% ethanol was added to the lysate, mixed well by pipetting, 700μL of the sample was applied to an RNeasy mini column, centrifuged at 10,000 rpm for 20 seconds and the flowthrough was discarded. Next, 700μL Buffer RW1 was added to the column, centrifuged at 10,000 for 20 seconds, the flowthrough was discarded, and columns were transferred to new 2-mL collection tubes. Subsequently, 500μL Buffer RPE was pipetted onto the column, centrifuge at 10,000 for 20 seconds, flowthrough was discarded, 500μL buffer RPE was added to the column, centrifuged at 10,000 rpm for 2 minutes. Columns were transferred to a new 1.5-mL collection tube, 50μL RNase-free water was pipetted onto the column membrane and centrifuged at 10,000 rpm for 1 minute. RNA quantification was performed at this stage to ensure successful isolation. For reverse transcription, cDNA master mix was made by adding 6 µl of 10x RT Buffer, 6 µl of 10x Random Primer, 3 µl of Multiscribe, 2.4 µl of 25x dNTPs, and 12.6 µl of nuclease-free water per reaction. Then, 30 µl of RT master mix and 30 µl of each RNA sample were added in separate centrifuge tubes, incubated at room temperature for 10 minutes in an incubator at 37°C for 2 hours, and then in a heat block at 85°C for 5 minutes, and stored at 4°C in the dark. To achieve the desired volume for each PCR, 70 µl of nuclease-free water was added to each cDNA sample. The PCR master mix for each sample and each primer was generated by adding 50 µl of TaqMan Master Mix, 5 µl of specific primer, 10 µl of cDNA Sample, and 35 µl of Nuclease-free water to a small tube. Then, 25 µl of the mix was added into 96-well PCR plate in triplicate, and the plate was covered with an optical cover, centrifuged at 520 rpm for 30 seconds, placed in the PCR machine

(Biosystems 7500 Real-time PCR System). Relative quantification was used, and the primers that correspond to the plate were chosen (GAPDH as the endogenous control). After reading the plate, PCR program was used for analyzing the data. The baseline was set for CoCr, and the amplification plots were acquired. The outliers/missing wells were omitted during the analysis.
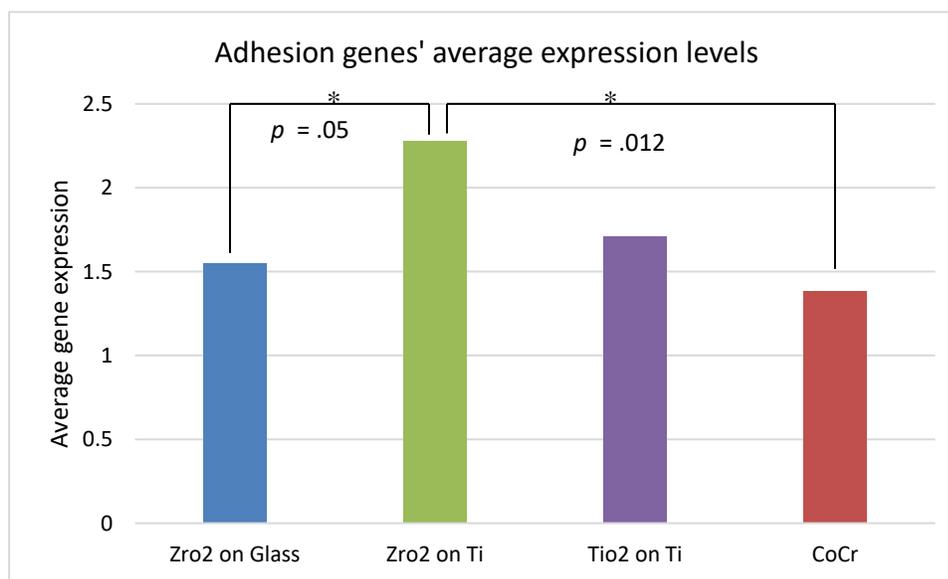
Figure 5-7: Comparison of average gene expression in the adhesion experiments

Comparison of average gene expression in the adhesion experiments on coated nano-surfaces and uncoated CoCr, using PCR technique. SAOS-2 cells were plated on either uncoated or nano-coated surfaces (1 million cells per sample), and RNA was harvested after 24 hours (n = 3, means $\pm$ SD). The statistical differences were evaluated using independent samples t-test.
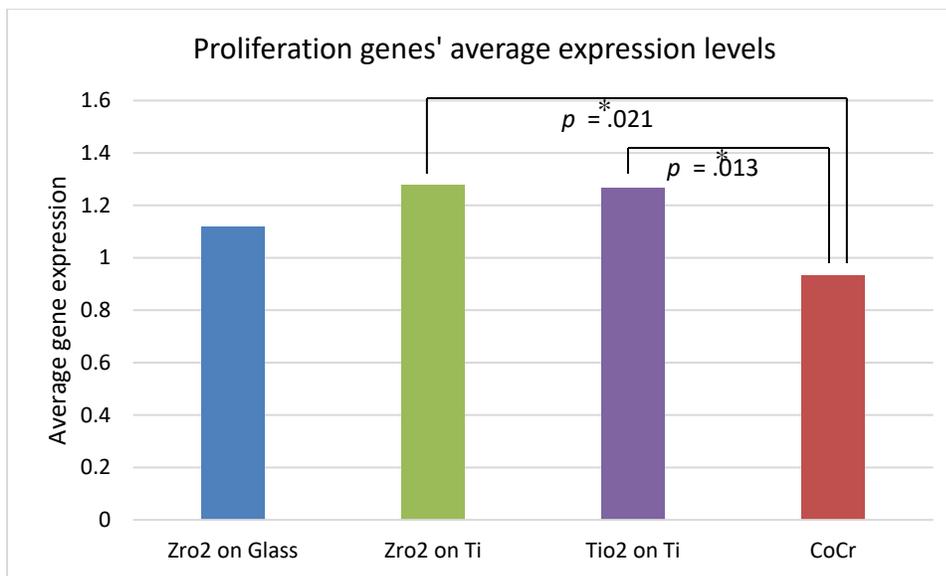
Figure 5-8: Comparison of average gene expression in the proliferation experiments

Comparison of average gene expression in the proliferation experiments on coated nano-surfaces and uncoated CoCr, using PCR technique. SAOS-2 cells were plated on either uncoated or nano-coated surfaces (1 million cells per sample), and RNA was harvested after 4 days (n = 3, means $\pm$ SD). The statistical differences were evaluated using independent samples t-test.
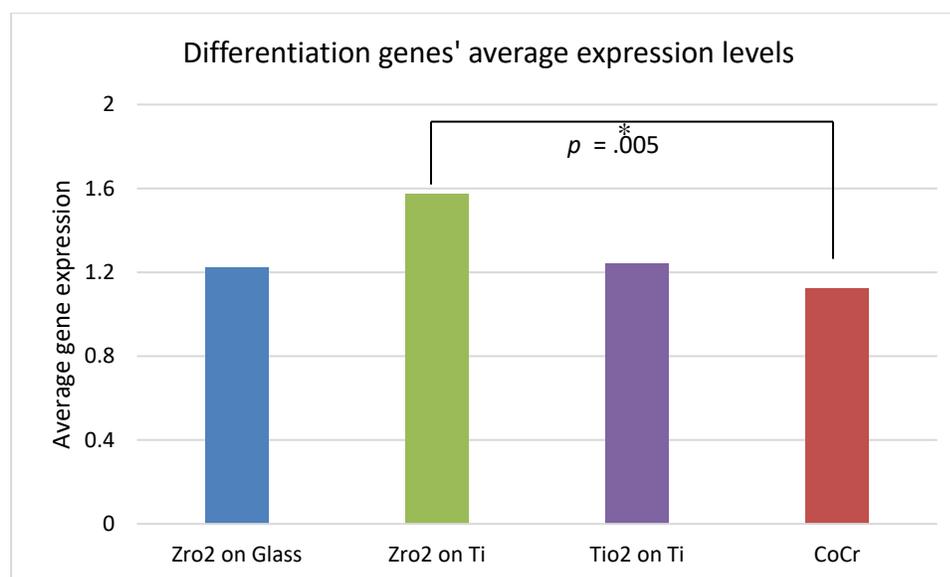
Figure 5-9: Comparison of average gene expression in the differentiation experiments

Comparison of average gene expression in the differentiation experiments on coated nano-surfaces and uncoated CoCr, using PCR technique. SAOS-2 cells were plated on either uncoated or nano-coated surfaces (1 million cells per sample), and RNA was harvested after 5 days (n = 3, means $\pm$ SD). The statistical differences were evaluated using independent samples t-test.

5.1.7 Data Analysis and Statistics

Statistical analysis was performed using data from three independent experiments (n = 3), and the results are presented as means $\pm$ SD. The statistical significance of differences between surfaces was evaluated using the 2-sample t-test with independent samples.

RESULTS

The proliferation of SAOS-2 cells assessed by nuclear cell proliferation-associated antigen Ki-67 was higher for cells on nano-coated surfaces *vs.* uncoated CoCr surfaces at day 4 after culturing (Figure 5-2). Median Ki-67 expression for ZrO_2 on the glass, ZrO_2 on Ti, and TiO_2 on Ti

were 1.3, 1.7, and 1.2 fold higher than CoCr relatively, indicating higher proliferation of SAOS-2 cells on those surfaces. Also, statistical analysis showed a significant difference in Ki-67 expression of the cells between nano-ZrO_2 on Ti *vs.* CoCr ($p = .038$).

Programmed cell death of SAOS-2 cells assessed using an annexin V kit with PI staining (Figure 5-3, 5-4, 5-5) showed significant differences between uncoated CoCr and ZrO_2 nano-coated glass surfaces in both early apoptosis ($p = .029$) and late apoptosis ($p = .007$), suggesting that differential toxicity of the surfaces and cellular stress induced by those surfaces were factors in outcomes. No significant differences between uncoated CoCr and ZrO_2 nano-coated glass surfaces were observed for necrosis ($p = .094$).

Osteoblastic differentiation measured by ALP activity was 2.8, 1.5, and 1.4 -fold higher for cells on nano-coated ZrO_2 on the glass, ZrO_2 on Ti, and TiO_2 on Ti *vs.* uncoated CoCr surfaces on day 5 of culture, indicating higher differentiation and mineralization by cells grown on these nano-surfaces. Also, as shown by statistical analysis, the difference between nano-coated ZrO_2 on glass and CoCr was significant ($p = .006$).

Average gene expression levels for adhesion, assessed by PCR techniques, showed a significant difference between nano surfaces ZrO_2 on Ti *vs.* ZrO_2 on glass ($p = .05$)., and also between nano-ZrO_2 on Ti *vs.* CoCr ($p = .012$). Average gene expression levels in the proliferation experiments showed significant differences between nano-ZrO_2 on Ti *vs.* CoCr ($p = .021$), and also between nano-TiO_2 on Ti *vs.* CoCr ($p = .013$). Average gene expression levels in the differentiation experiments showed significant differences between nano-ZrO_2 on Ti *vs.* CoCr ($p = .005$). In addition, some individual genes, including EGFLAM, ALPL, SPP1, and SP7 and their ranks among all other 7 genes at different experiments were studied separately (data are not shown). EGFLAM was ranked 1 and 2 for nano-surfaces in adhesion, while it was 7 for CoCr. The rank numbers for different surfaces were almost the same in the proliferation experiments (3, 4, and 5), but for the

differentiation experiments, the ranks changed (rank 1, 2 and 5 for nano-surfaces and 7 for CoCr). ALPL was almost the same for all the surfaces in the adhesion and proliferation experiments (average of 2), while in the differentiation experiments, the ALPL rank was 6 and 7 for nano-surfaces and 1 for CoCr. SPP1 was ranked 5, 6, and 7 for nano-surfaces in adhesion experiments, while it was 3 for CoCr. In the proliferation experiments, the rank was 1 and 2 for nano-surfaces but 7 for CoCr. Moreover, for the differentiation experiments, the rank was 1, 2, and 3 for nano-surfaces and 6 for CoCr. SP7 was ranked 5, 6, and 7 for nano-surfaces in adhesion experiments, while it was 3 for CoCr. In the proliferation experiments, the ranks were almost similar as in the adhesion experiments (7 for nano-surfaces and 4 for CoCr). For differentiation experiments, the ranks were different and became 1, 3, and 4 for nano-surfaces and 5 for CoCr.

DISCUSSION

The Ki-67 expression was 1.3, 1.7, and 1.2 fold higher for cells on nano-coated surfaces ZrO_2 on glass, ZrO_2 on Ti, and TiO_2 on Ti *vs.* uncoated CoCr surfaces at day 4 after plating, and an independent samples t-test showed a *P-value* = .038 for Ki-67 expression differences of the cells between nano-ZrO_2 on Ti *vs.* CoCr. This result indicated that cells seeded on nano-coated surfaces proliferated more and showed increased growth rates when compared with the uncoated control CoCr surface. Also, among nano-surfaces, ZrO_2 on Ti shared the significant difference with control surface CoCr, suggesting that substrate used for coating may also play a role, along with the coated material, and this needs further investigation. For this experiment, cells were harvested at 50% confluency which was in the middle range confluency. Since we measured proliferative activity, it was essential to harvest cells when they were in the log phase of growth, before they started changing their gene expression patterns due to contact inhibition and nutrient limitations or became quiescent. In the experiment at higher confluency (i.e., 70-80%), the fold changes between nano-

surfaces and CoCr decreased, and significant differences between ZrO_2 on Ti and CoCr were not observed (data is not shown).

Since ZrO_2 on glass had the lowest Ki-67 expression, it was selected to be compared with uncoated CoCr, and both early and late apoptosis of SAOS-2 cells on uncoated CoCr and ZrO_2 nano-coated glass surfaces showed significant differences. The viability percentage is a combination of the survival of the cells on the surfaces and their death because of apoptosis as a response to the surface. The differences in apoptosis obtained from the nano-surfaces with the lowest proliferation activity indicated that survival of SAOS-2 cells is as0ciated with nano-coated surfaces compared to the uncoated CoCr.

Osteoblastic differentiation measured by ALP activity is an indicator of the initial stages of differentiation of osteoblast-like cells. The experiment was performed with different ALP dilutions including 1 to 100 and 1 to 250. The data was consistent internally. However, the 1 to 250 dilution shows differences with higher fold changes, suggesting this dilution was optimal for the standard curve (in the linear part of the curve). Normalization using BCA was also performed with 1 to 1 and 1 to 4 dilutions. The data was consistent from both dilutions, and the 1 to 1 dilution data is presented here. ALP activity measured on day 5 of culture was 2.8, 1.5, and 1.4 -fold higher for cells on nano-coated ZrO_2 on the glass, ZrO_2 on Ti, and TiO_2 on Ti *vs.* uncoated CoCr surfaces. In addition, as shown by statistical analyses, the differences between nano-coated ZrO_2 on glass and CoCr was significant (p = .006). Osteoblastic cells differentiate to produce bone. Therefore, in a clinical setting, enhanced bone formation and mineralization would be expected from cells grown on nano-crystalline surfaces compared to CoCr surfaces.

Taken together, the Ki-67 and ALP data suggest that nano-coatings can accelerate and increase proliferation and differentiation of osteoblasts compared with uncoated CoCr surfaces. However, it is clear that some nano-surfaces favor proliferation while others favor differentiation.

This fits the cell differentiation paradigm that well-differentiated cells proliferate at a lower rate while less differentiated cells are highly proliferative (81).

Increasing the rate of growth, maturation, and mineralization leading to bone formation could decrease healing time for patients, reduce the chance of systemic infection, and increase the longevity of implants.

Overall, data from PCR experiments showed that for all adhesion, proliferation and differentiation experiments, nano-surfaces are better than CoCr. Average gene expression levels for adhesion showed that nano-coatings enhanced cell interactions with the surface and altered cell behavior (specifically the difference between nano-ZrO_2 on Ti *vs.* CoCr). Also, a significant difference between nano surfaces ZrO_2 on Ti *vs.* ZrO_2 on glass was observed suggesting that in adhesion experiments substrates that were used for nano-coatings also played a role. Therefore, the differences between nano-surfaces and CoCr was a combination effect of nano-coatings and substrate materials, and it was shown that Ti is a better substrate than glass. It also has been shown that the natural micro-roughness of Ti and its oxides improve its biocompatibility (49) and this may explain why Ti is a better substrate. However, to avoid the effects of any surface roughness, other than the IBAD nano-roughness, our previous study was designed to use only smooth glass substrates.

Similarly, differences in average gene expression levels for proliferation indicated that the proliferation of SAOS-2 cells was more compatible with nano-coated surfaces, compared to the CoCr. It also appears that only nano-coated surfaces on Ti substrates showed significant differences with CoCr and this could be either effect of Ti substrate on proliferation genes, or having more cells due to increased initial adhesion levels. Data for the proliferation marker (MKI-67) did not show any difference among nano-surfaces. Therefore, the effect of the substrate on proliferation appears small. In the differentiation experiments, differences between average gene expression

levels for nano-coatings and CoCr were observed, while there was no difference between the Ti and glass substrates.

In addition, some individual genes and their ranks among all other 7 genes were studied in different experiments, in case any specific regulation could be observed among nano-surfaces *vs.* CoCr. EGFLAM is FN that promotes initial cells attachments to surfaces and regulates their migration during tissue differentiation. Therefore, its ranking should be highest in adhesion and differentiation experiments. Indeed, it was ranked 1 and 2 for nano-surfaces in adhesion experiments while it was 7 for CoCr, which fits with the higher level for cell attachments to the nano-surfaces. For the proliferation experiments, the ranks showed no differences between different surfaces (3, 4, and 5), but again for differentiation experiments, it was highest for nano-surfaces (rank 1, 2 and 5) while CoCr showed no increase in transcribing this particular gene (rank 7 for CoCr). ALPL is ALP gene, that is essential for bone mineralization, and it marks the initial stage of differentiation. Its gene transcription starts from early stages and decreases later; therefore we expected to see high ranks in the adhesion and proliferation experiments, but a lower rank for the differentiation experiments. In the adhesion and proliferation experiments, the rank was almost the same for all the surfaces (average of 2), but in later stages (differentiation experiments) ALPL transcription was reduced for nano-surfaces (rank 6 and 7), but it was still high for CoCr (rank 1), potentially indicating delayed differentiation of SAOS-2 cells on CoCr. SPP1 represents osteopontin that is a marker for the middle stage of osteoblast differentiation. Based on the timing of experiments, the increase in rank was expected in the proliferation and differentiation experiments, but not in the adhesion experiments. Again, this pattern was observed among nano-surfaces (ranked 5, 6, and 7 in adhesion experiments, 1 and 2 in the proliferation experiments, and 1, 2, and 3 in the differentiation experiments) while SPP1 rank CoCr was 6. SP7 is Osterix, a critical transcription factor in osteoblast differentiation. For nano-surfaces, its rank in adhesion was 5, 6,

and 7, in the proliferation experiments 7, and for differentiation experiments, it became 1, 3, and 4. For CoCr the rank was 3, 4, and 5 relatively. Taken together, it showed that cells on CoCr either started differentiation very early or very late. If they started differentiation very early, it means they were not very proliferative and could not cover the surface rapidly, and this could affect the healing time. If the second alternative is the explanation and they started differentiation later, this could delay the mineralization and the bone-forming process.

The results presented in this study indicate that nano-crystalline surfaces produced via the IBAD technique improved adhesion, proliferation, and differentiation of SAOS-2 bone-forming cells *in vitro* compared with the same cells growing on uncoated CoCr surfaces, by altering their gene expression profiles. This indicates the biocompatibility of the nano-coatings produced by IBAD technique, along with their other known properties, such as wettability and hardness makes them promising candidates for osseointegration applications (22). However, additional studies including *in vivo* experiments using animal models, are needed to understand the behavior of these materials in more detail, in particular, their interactions with the *in vivo* environment, e.g., corrosion and potential toxicities, although there is, currently, no evidence that these will be issues.

6   CHAPTER SIX: DISCUSSION

GENERAL DISCUSSION AND SUMMARY

It has been shown that the selection of implant biomaterials directly impacts the effectiveness and success of TJR. One of the crucial factors that influence this selection is material properties and biocompatibility (79). Osseointegration is determined by the design, chemical composition, surface topography, and coating of the implants (69), and many studies have been conducted to investigate the effect of surface modifications on the TJR outcomes. Although some data are available from animal models, most of these studies have been limited to *in vitro* experiments. Unfortunately, there are no standardized *in vitro* methods being utilized for assessing the new surfaces in TJR. Thus, the present study developed and described standard methods to establish a model system that may be extended to other studies. After a comprehensive search to evaluate a proper model for osteoblast functions, we decided on the use of the SAOS-2 cell line. In addition, we developed experiments to investigate many of the essential cellular events including adhesion, proliferation, cell morphology, apoptosis, and differentiation. Moreover, experiments were devised to compare different nano-samples and different control samples, including non-coated, polished metallic surfaces to investigate the impact of nano-coatings along with the effect of coatings' chemistry and substrates on outcomes**.** Furthermore, during preliminary optimization studies, we identified the optimized timing for experiments, cell seeding densities, appropriate cell detachment agents, volumes and timing as well as appropriate surface cleaning methods.

Our first series of studies "Compared Biocompatibility of Nano-Crystalline Titanium and Titanium-Oxide with Micro-Crystalline Titanium" (chapter 3), which evaluated adhesion, morphology, and differentiation of SAOS-2 cells on those surfaces. The adhesion experiment showed a higher number of cells on nano-structured surfaces compared to biomedical grade Ti, which indicated more adhesion and growth on nano-surfaces. Besides DAPI staining, actin fiber

shapes were monitored and a significant difference in cell shape was observed on nano-crystalline TiO_2 and Ti (large focal adhesions) compared to micro-crystalline Ti (thin and round shapes). The alizarin red assay for observing calcium deposition of SAOS-2 cells showed that the cells cultured on the nano-surfaces had a higher degree of differentiation. Therefore, enhanced bone formation ability was expected from those surfaces. These were important observations that showed nano-structured surfaces possess unique properties that alter cell adhesion, growth, and differentiation by direct (cell–surface interaction) mechanisms. However, we did not observe the effects of substrates' roughness and coatings' chemistry on cell–surface interactions. Also, preliminary data showed that the timing for adhesion and morphology experiments was best accomplished at 48 hours. In this period, adhesion and growth occurred consecutively, and thus there was no chance to identify the effect of surfaces on initial adhesion.

Therefore, we designed a new series of experiments (adhesion, proliferation, metabolic activity, and differentiation) for a new study "The Effects of Nano-engineered Surfaces on Osteoblast Adhesion, Growth, Differentiation, and Apoptosis" (chapter 4). Previously, it has been shown that the natural micro-roughness of Ti and its oxides improve its biocompatibility (49). Thus in this study, we included nano-coatings of ZrO_2 on glass compared to glass substrates to avoid the effect of any surface properties other than the nano-roughness. Using smooth glass substrates instead of Ti with inherent roughness, made it possible for us to isolate the specific effects of the nano-roughness produced by the IBAD technique from other factors that might influence cell interactions with surfaces. The outcomes were consistent with the previous study, and we showed that adhesion and proliferation of SAOS-2 cells were greater on nano-ZrO_2 compared with uncoated glass surfaces, indicating that nano-coatings enhanced cell interactions with the surface. Moreover, cells showed a more uniform distribution on nano-ZrO_2 compared with uncoated glass surfaces where they formed clumps to maintain viability, which indicated cell adhesion was more

compatible with the nano-coated surface. The metabolic activity using the MTS assays showed significantly higher levels for cells on nano-ZrO_2 as compared to uncoated glass surfaces, indicating increased growth rates for cells on those surfaces. Calcium deposition assessed by alizarin red staining, an indicator of late differentiation and bone formation capability, was higher for cells on nano-ZrO_2 *vs.* uncoated glass surfaces. Thus, enhanced bone formation would be expected from cells grown on those surfaces. The findings of this study showed that unique properties of IBAD-produced nano-films increased surface biocompatibility, although only a specific nano-coating (ZrO_2) was studied and the effects of other coatings' chemistry was not examined. Despite the fact that essential cellular events were investigated in this study, none of them were evaluated at the molecular level. Thus, further studies were planned to evaluate the mechanisms behind the outcomes of the current study.

In the next study, "Surface Nano-Modification by Ion Beam Assisted Deposition Alters the Expression of Osteogenic Genes in Osteoblasts" (chapter 5), the effects of IBAD-produced nano-structured surfaces on SAOS-2 cells at the molecular level (investigated by assays of adhesion, proliferation, differentiation, and apoptosis) and gene expression level (assessed by PCR techniques at initial cell adhesion, proliferation, and differentiation) were evaluated. To imitate a realistic scenario, the control surfaces were chosen to be orthopaedic grade CoCr. In this study, we also extended our observations to a comparison between different surface coatings' chemistry (ZrO_2 and TiO_2) and different substrates' roughness (glass and Ti). The proliferation of SAOS-2 cells assessed by nuclear cell proliferation-associated antigen Ki-67 was higher for cells on nano-coated surfaces *vs.* uncoated CoCr surfaces indicating higher proliferation and increased growth rates on those surfaces. Since nano-ZrO_2 on Ti only showed a significant difference with control surface CoCr, the substrate used for coating may play a role, along with the coated material. Since nano-ZrO_2 on glass had the lowest Ki-67 expression, it was selected to be used for apoptosis

experiments. Programmed cell death of SAOS-2 cells assessed by annexin V kit with PI staining showed significant differences between uncoated CoCr and nano-ZrO_2 surfaces in both early apoptosis and late apoptosis, suggesting that differential toxicities of the surfaces and cellular stress induced by them, were associated with survival. Osteoblastic differentiation, measured by ALP activity, was higher for cells on nano-surfaces *vs.* uncoated CoCr surfaces, indicating higher differentiation and mineralization by cells grown on those surfaces. Taken together, the Ki-67 and ALP data suggested that nano-coatings can accelerate and increase proliferation and differentiation of osteoblasts, compared with uncoated CoCr surfaces. However, it is clear that some nano-surfaces favor proliferation while others favor differentiation, indicating the effect of coatings' chemistry on these cellular events. Since CoCr is mainly employed for articular components of the prosthesis, its properties are consistent with such use.

Gene expression experiments assessed by PCR techniques were performed at initial cell adhesion, proliferation, and differentiation levels. Overall, data from PCR experiments showed that for all adhesion, proliferation, and differentiation experiments, nano-surfaces were better than CoCr. Average gene expression levels for adhesion showed that nano-coatings enhanced cell interactions with the surface and altered cell behavior. Also, a significant difference between nano-ZrO_2 on Ti *vs.* nano-ZrO_2 on glass suggested that substrates used for nano-coatings played a role in adhesion. Therefore, the differences between nano-surfaces and CoCr appears to have a combination effect due to nano-coatings and substrate materials. Clearly, Ti was shown to be a better substrate than glass, which may be due to the natural micro-roughness of Ti and its oxides. Similarly, differences in average gene expression levels for proliferation indicated that the proliferation of SAOS-2 cells was more compatible with nano-coated surfaces, compared to CoCr. It also appears that only nano-coated surfaces on Ti substrates showed significant differences with CoCr. This could be due to either the effect of Ti substrate on proliferation genes, or having more

cells due to increased initial adhesion levels, or both. Data for the proliferation marker (MKI-67) did not show any difference among nano-surfaces. Therefore, the effect of the substrate on proliferation appears small or negligible. In the differentiation experiments, differences between average gene expression levels for nano-coatings and CoCr were observed, while there was no difference between the Ti and glass substrates.

Evaluating some individual genes and their ranks among the other 7 genes in different experiments indicated interesting differences among nano-surfaces *vs.* CoCr. EGFLAM is FN that promotes initial cell attachments to surfaces and regulates their migration during tissue differentiation. Therefore, its ranking should be highest in adhesion and differentiation experiments. Indeed, this was the case for nano-surfaces, but not for CoCr, which fits with the higher level of cell attachments to nano-surfaces. ALPL is ALP gene, which is essential for bone mineralization and marks the initial stage of differentiation. ALPL gene transcription begins from early stages and decreases later; therefore we expected to see high ranks in the adhesion and proliferation experiments, but a lower rank for the differentiation experiments. In the adhesion and proliferation experiments, the rank was almost the same for all the surfaces, but in differentiation experiments ALPL transcription was reduced for nano-surfaces and stayed high for CoCr, potentially indicating a delayed differentiation of SAOS-2 cells on CoCr. SPP1 represents osteopontin that is a marker for the middle stage of osteoblast differentiation. Based on the timing of experiments, the increase in rank was expected in the proliferation and differentiation experiments, but not in the adhesion experiments. This pattern was observed among nano-surfaces but not for CoCr. SP7 is Osterix, which is a critical transcription factor in osteoblast differentiation and was expected to rank high in differentiation experiments; this was true for nano-surfaces, but not for CoCr. Putting together the observation from SPP1 and SP7, showed that cells on CoCr either started differentiation very early or very late. If they started differentiation very early, it

means they were not very proliferative and could not cover the surface rapidly, and this could affect (delay) the healing time. If the alternative is the explanation and they started differentiation later, this could delay mineralization and thus bone-forming processes.

All the outcomes presented here from the studies were internally consistent with each other and indicated that nano-crystalline surfaces produced via the IBAD technique improved adhesion, proliferation, and differentiation of SAOS-2 bone-forming cells *in vitro* compared with the same cells growing on uncoated surfaces, by altering their gene expression profiles.

FUTURE DIRECTIONS

From our studies, we reported that surface modifications using the IBAD technique enhanced biocompatibility of SAOS-2 osteosarcoma (osteoblast) cells. However, additional studies in the future are needed to understand the behavior of these materials in more detail and to address questions raised by our studies. Some of the possible future studies are discussed below:

1. In PCR studies, we evaluated the differences between surfaces based on 3 different time course events. These timings were chosen based on previous studies and preliminary data. However, it is likely that because this timeline was used, some changes might have been missed or incompletely characterized. Further time-dependent studies are needed to address these questions.

2. We observed the differences between surfaces in gene expression profiles and molecular level. Except for actin staining, we did not characterize proteins localizations. It is possible that some proteins produced by cells were not localized in the appropriate place and thus may not be functional. Future studies should characterize both proteins translation and localizations.

3. There were significant differences between nano-coated surfaces and uncoated surfaces which made nano-surfaces appears to be the better option for the bone contact component of future implants. However, this observation raises the question as to whether nano-surfaces are still superior when they are compared to other modified surfaces. This question can be addressed in future studies involving several modified surfaces besides control surfaces.

4. We analyzed the expression profile of limited genes to understand the biologic differences that were observed on different surfaces at the genetic levels. These genes were selected based on preliminary data and other studies in the literature. To conduct a more comprehensive study, RNA seq or microarray would make a more complete characterization of molecular differences. However, they are currently beyond the scope of this dissertation.

5. Since interactions with foreign bodies are very complicated, these promising *in vitro* results presented here are the first step in the further testing of IBAD-modified surfaces in animal models for potential future use for human implants.

6. Although the IBAD-modified surfaces are believed to possess enhanced corrosion resistance, future studies are needed to test whether they release toxic metallic ions into the body as they become oxidized, which can lead to immune reactions and implant degradation.

7. Many studies have been shown that bacterial coverage increases on different surfaces as roughness increases (82). However, roughness parameters do not have equal effects on

this promoted coverage, and sometimes different parameters or variant topography lead to biofilm inhibition. Potential future studies can determine how IBAD- modification affects bacterial adhesion and outcomes.

References

1. Farlex Partner Medical Dictionary. 2012.

2. Ethgen O, Bruyere O, Richy F, Dardennes C, Reginster J. Health-related quality of life in total hip and total knee arthroplasty: a qualitative and systematic review of the literature. JBJS. 2004;86(5):963-74.

3. Kurtz S, Ong K, Lau E, Mowat F, Halpern M. Projections of primary and revision hip and knee arthroplasty in the United States from 2005 to 2030. J Bone Joint Surg Am. 2007 Apr;89(4):780-5.

4. Ren K, Dusad A, Zhang Y, Purdue PE, Fehringer EV, Garvin KL, et al. Early diagnosis of orthopedic implant failure using macromolecular imaging agents. Pharm Res. 2014;31(8):2086-94.

5. Sloan M, Premkumar A, Sheth NP. Projected Volume of Primary Total Joint Arthroplasty in the U.S., 2014 to 2030. J Bone Joint Surg Am. 2018 Sep 5;100(17):1455-60.

6. Wilson NA, Schneller ES, Montgomery K, Bozic KJ. Hip and knee implants: current trends and policy considerations. Health Aff. 2008;27(6):1587-98.

7. Kurtz SM, Ong KL, Schmier J, Mowat F, Saleh K, Dybvik E, et al. Future clinical and economic impact of revision total hip and knee arthroplasty. JBJS. 2007;89:144-51.

8. Demierre M, Castelao E, Piot-Ziegler C. The long and painful path towards arthroplasty: A qualitative study. Journal of health psychology. 2011;16(4):549-60.

9. Junker R, Dimakis A, Thoneick M, Jansen JA. Effects of implant surface coatings and composition on bone integration: a systematic review. Clin Oral Implants Res. 2009;20:185-206.

10. Wang W, Poh CK. Titanium alloys in orthopaedics. In: Titanium Alloys-Advances in Properties Control. InTech; 2013.

11. Anil S, Anand P, Alghamdi H, Jansen J. Dental implant surface enhancement and osseointegration. In: Implant dentistry-A rapidly evolving practice. InTech; 2011.

12. Saini M, Singh Y, Arora P, Arora V, Jain K. Implant biomaterials: A comprehensive review. World J Clin Cases. 2015 Jan 16;3(1):52-7.

13. Aherwar A, Singh AK, Patnaik A. Cobalt Based Alloy: A Better Choice Biomaterial for Hip Implants. Trends in Biomaterials & Artificial Organs. 2016;30(1).

14. Hirschmann MT. 2 Biology of the Knee After Total Knee Replacement: Neglected Potential or Source of Failure? In: The Unhappy Total Knee Replacement. Springer; 2015. p. 17-27.

15. Christen B. 11 Material Failure of Total Knee Replacement. In: The Unhappy Total Knee Replacement. Springer; 2015. p. 127-33.

16. Chen Q, Thouas GA. Metallic implant biomaterials. Materials Science and Engineering: R: Reports. 2015;87:1-57.

17. Lewallen EA, Riester SM, Bonin CA, Kremers HM, Dudakovic A, Kakar S, et al. Biological strategies for improved osseointegration and osteoinduction of porous metal orthopedic implants. Tissue Engineering Part B: Reviews. 2014;21(2):218-30.

18. Nowakowski AM, Vavken P, Pagenstert G, Valderrabano V. 8 Design, Shape, and Materials of Total Knee Replacement. In: The Unhappy Total Knee Replacement. Springer; 2015. p. 85-97.

19. Sidambe AT. Biocompatibility of advanced manufactured titanium implants—A review. Materials. 2014;7(12):8168-88.

20. Voisin M, Ball M, O'Connell C, Sherlock R. Osteoblasts response to microstructured and nanostructured polyimide film, processed by the use of silica bead microlenses. Nanomedicine: Nanotechnology, Biology and Medicine. 2010;6(1):35-43.

21. Wang G, Zreiqat H. Functional coatings or films for hard-tissue applications. Materials. 2010;3(7):3994-4050.

22. Namavar F, Cheung CL, Sabirianov RF, Mei W, Zeng XC, Wang G, et al. Lotus effect in engineered zirconia. Nano letters. 2008;8(4):988-96.

23. Namavar F, Rubinstein A, Sabirianov RF, Thiele GM, Sharp JG, Pokharel U, et al. Engineered Nanostructured Coatings for Enhanced Protein Adsorption and Cell Growth. MRS Proceedings; Cambridge Univ Press; 2012.

24. Sabirianov R, Rubinstein A, Namavar F. Enhanced initial protein adsorption on engineered nanostructured cubic zirconia. Physical Chemistry Chemical Physics. 2011;13(14):6597-609.

25. Rubinstein A, Sabirianov R, Namavar F. Enhanced cell growth by nanoengineering zirconia to stimulate electrostatic fibronectin activation. Nanotechnology. 2014;25(6):065101.

26. Namavar F, Jackson JD, Sharp JG, Mann EE, Bayles K, Cheung BCL, et al. Searching for smart durable coatings to promote bone marrow stromal cell growth while preventing biofilm formation. MRS Online Proceedings Library Archive. 2006;954.

27. Dusad A, Chakkalakal DA, Namavar F, Haider H, Hanisch B, Duryee MJ, et al. Titanium implant with nanostructured zirconia surface promotes maturation of peri-implant bone in osseointegration. Proc Inst Mech Eng H. 2013 May;227(5):510-22.

28. Tuljapurkar SR, Jackson JD, Brusnahan SK, O'Kane BJ, Sharp JG. Characterization of a mesenchymal stem cell line that differentiates to bone and provides niches supporting mouse and human hematopoietic stem cells. Stem Cell Discovery. 2012;2(01):5.

29. Czekanska E, Stoddart M, Richards R, Hayes J. In search of an osteoblast cell model for in vitro research. Eur Cell Mater. 2012;24(4):1-17.

30. Wang G, Brewer JR, Namavar F, Sabirianov RF, Haider H, Garvin KL, et al. Structural Study of Titanium Oxide Films Synthesized by Ion Beam-Assisted Deposition. Scanning: The Journal of Scanning Microscopies. 2008;30(2):59-64.

31. Rodan SB, Imai Y, Thiede MA, Wesolowski G, Thompson D, Bar-Shavit Z, et al. Characterization of a human osteosarcoma cell line (Saos-2) with osteoblastic properties. Cancer Res. 1987 Sep 15;47(18):4961-6.

32. Pautke C, Schieker M, Tischer T, Kolk A, Neth P, Mutschler W, et al. Characterization of osteosarcoma cell lines MG-63, Saos-2 and U-2 OS in comparison to human osteoblasts. Anticancer Res. 2004 Nov-Dec;24(6):3743-8.

33. Mosmann T. Rapid colorimetric assay for cellular growth and survival: application to proliferation and cytotoxicity assays. J Immunol Methods. 1983;65(1-2):55-63.

34. Tada H, Shiho O, Kuroshima K, Koyama M, Tsukamoto K. An improved colorimetric assay for interleukin 2. J Immunol Methods. 1986;93(2):157-65.

35. Hansen MB, Nielsen SE, Berg K. Re-examination and further development of a precise and rapid dye method for measuring cell growth/cell kill. J Immunol Methods. 1989;119(2):203-10.

36. Denizot F, Lang R. Rapid colorimetric assay for cell growth and survival: modifications to the tetrazolium dye procedure giving improved sensitivity and reliability. J Immunol Methods. 1986;89(2):271-7.

37. Carmichael J, DeGraff WG, Gazdar AF, Minna JD, Mitchell JB. Evaluation of a tetrazolium-based semiautomated colorimetric assay: assessment of chemosensitivity testing. Cancer Res. 1987 Feb 15;47(4):936-42.

38.   PE   Mouse   Anti-Ki-67   Set (RUO)   [Internet].   Available   from: http://www.bdbiosciences.com/us/applications/research/intracellular-flow/intracellular-kits-sets-and-cocktails/pe-mouse-anti-ki-67-set/p/556027.

39. Gerdes J, Lemke H, Baisch H, Wacker HH, Schwab U, Stein H. Cell cycle analysis of a cell proliferation-associated human nuclear antigen defined by the monoclonal antibody Ki-67. J Immunol. 1984 Oct;133(4):1710-5.

40. Urruticoechea A, Smith IE, Dowsett M. Proliferation marker Ki-67 in early breast cancer. Journal of clinical oncology. 2005;23(28):7212-20.

41. Lin H, Hwang S, Wu S, Hsu L, Liao Y, Sheen Y, et al. The osteoblastogenesis potential of adipose mesenchymal stem cells in myeloma patients who had received intensive therapy. PloS one. 2014;9(4):e94395.

42. Vermes I, Haanen C, Steffens-Nakken H, Reutellingsperger C. A novel assay for apoptosis flow cytometric detection of phosphatidylserine expression on early apoptotic cells using fluorescein labelled annexin V. J Immunol Methods. 1995;184(1):39-51.

43. Koopman G, Reutelingsperger CP, Kuijten GA, Keehnen RM, Pals ST, van Oers MH. Annexin V for flow cytometric detection of phosphatidylserine expression on B cells undergoing apoptosis. Blood. 1994 Sep 1;84(5):1415-20.

44. Alexa Fluor® 488 annexin V/Dead Cell Apoptosis Kit with Alexa® Fluor 488 annexin V   and   PI   for   Flow   Cytometry   [Internet].;   2010.   Available   from: https://www.thermofisher.com/document-connect/document-connect.html?url=https://assets.thermofisher.com/TFS-Assets/LSG/manuals/mp13241.pdf&title=Alexa%20Fluor%20488%20annexin%20V/Dead%20Cell%20Apoptosis%20Kit%20with%20Alexa%20Fluor%20488%20annexin%20V%20and%20PI%20for%20Flow.

45. Jensen ED, Gopalakrishnan R, Westendorf JJ. Regulation of gene expression in osteoblasts. Biofactors. 2010;36(1):25-32.

46. Czekanska EM, Stoddart MJ, Ralphs JR, Richards R, Hayes J. A phenotypic comparison of osteoblast cell lines versus human primary osteoblasts for biomaterials testing. Journal of biomedical materials research Part A. 2014;102(8):2636-43.

47. Tognarini I, Sorace S, Zonefrati R, Galli G, Gozzini A, Sala SC, et al. In vitro differentiation of human mesenchymal stem cells on Ti6Al4V surfaces. Biomaterials. 2008;29(7):809-24.

48. Sila-Asna M, Bunyaratvej A, Maeda S, Kitaguchi H, Bunyaratavej N. Osteoblast differentiation and bone formation gene expression in strontium-inducing bone marrow mesenchymal stem cell. Kobe J Med Sci. 2007;53(1-2):25-35.

49. Namavar F, Sabirianov R, Marton D, Rubinstein A, Garvin K. Biocompatibility of Titanium. APS March Meeting Abstracts; ; 2012.

50. Lord MS, Foss M, Besenbacher F. Influence of nanoscale surface topography on protein adsorption and cellular response. Nano Today. 2010;5(1):66-78.

51. Webster TJ, Ergun C, Doremus RH, Lanford WA. Increased osteoblast adhesion on titanium-coated hydroxylapatite that forms CaTiO3. Journal of Biomedical Materials Research Part A: An Official Journal of The Society for Biomaterials, The Japanese Society for Biomaterials, and The Australian Society for Biomaterials and the Korean Society for Biomaterials. 2003;67(3):975-80.

52. Svehla M, Morberg P, Bruce W, Zicat B, Walsh W. The effect of substrate roughness and hydroxyapatite coating thickness on implant shear strength. J Arthroplasty. 2002;17(3):304-11.

53. Klokkevold PR, Johnson P, Dadgostari S, Davies JE, Caputo A, Nishimura RD. Early endosseous integration enhanced by dual acid etching of titanium: a torque removal study in the rabbit. Clin Oral Implants Res. 2001;12(4):350-7.

54. Brunette D, Chehroudi B. The effects of the surface topography of micromachined titanium substrata on cell behavior in vitro and in vivo. J Biomech Eng. 1999;121(1):49-57.

55. Kalbacova M, Rezek B, Baresova V, Wolf-Brandstetter C, Kromka A. Nanoscale topography of nanocrystalline diamonds promotes differentiation of osteoblasts. Acta Biomaterialia. 2009;5(8):3076-85.

56. Kim J, Leucht P, Luppen CA, Park YJ, Beggs HE, Damsky CH, et al. Reconciling the roles of FAK in osteoblast differentiation, osteoclast remodeling, and bone regeneration. Bone. 2007;41(1):39-51.

57. Jager M, Zilkens C, Zanger K, Krauspe R. Significance of nano- and microtopography for cell-surface interactions in orthopaedic implants. J Biomed Biotechnol. 2007;2007(8):69036.

58. Stevens MM, George JH. Exploring and engineering the cell surface interface. Science. 2005 Nov 18;310(5751):1135-8.

59. Le Guéhennec L, Soueidan A, Layrolle P, Amouriq Y. Surface treatments of titanium dental implants for rapid osseointegration. Dental materials. 2007;23(7):844-54.

60. Francois P, Vaudaux P, Taborelli M, Tonetti M, Lew DP, Descouts P. Influence of surface treatments developed for oral implants on the physical and biological properties of

titanium.(II) Adsorption isotherms and biological activity of immobilized fibronectin. Clin Oral Implants Res. 1997;8(3):217-25.

61. Boyan B, Bonewald L, Paschalis E, Lohmann C, Rosser J, Cochran D, et al. Osteoblast-mediated mineral deposition in culture is dependent on surface microtopography. Calcif Tissue Int. 2002;71(6):519-29.

62. Wu Y, Zitelli JP, TenHuisen KS, Yu X, Libera MR. Differential response of Staphylococci and osteoblasts to varying titanium surface roughness. Biomaterials. 2011;32(4):951-60.

63. Babchenko O, Kromka A, Hruska K, Kalbacova M, Broz A, Vanecek M. Fabrication of nano-structured diamond films for SAOS-2 cell cultivation. physica status solidi (a). 2009;206(9):2033-7.

64. Sasmazel HT. Novel hybrid scaffolds for the cultivation of osteoblast cells. Int J Biol Macromol. 2011;49(4):838-46.

65. Mendonça G, Mendonça DB, Aragao FJ, Cooper LF. Advancing dental implant surface technology–from micron-to nanotopography. Biomaterials. 2008;29(28):3822-35.

66. Kane RL, Saleh KJ, Wilt TJ, Bershadsky B. The functional outcomes of total knee arthroplasty. J Bone Joint Surg Am. 2005 Aug;87(8):1719-24.

67. II GEA. Enhanced osteoblast adhesion to drug-coated anodized nanotubular titanium surfaces. International journal of nanomedicine. 2008;3(2):257-64.

68. Raphel J, Holodniy M, Goodman SB, Heilshorn SC. Multifunctional coatings to simultaneously promote osseointegration and prevent infection of orthopaedic implants. Biomaterials. 2016;84:301-14.

69. Rahyussalim AJ, Marsetio AF, Saleh I, Kurniawati T, Whulanza Y. The Needs of Current Implant Technology in Orthopaedic Prosthesis Biomaterials Application to Reduce Prosthesis Failure Rate. Journal of Nanomaterials. 2016;2016.

70. Kalbacova M, Rezek B, Baresova V, Wolf-Brandstetter C, Kromka A. Nanoscale topography of nanocrystalline diamonds promotes differentiation of osteoblasts. Acta Biomaterialia. 2009;5(8):3076-85.

71. Olivares-Navarrete R, Raz P, Zhao G, Chen J, Wieland M, Cochran DL, et al. Integrin alpha2beta1 plays a critical role in osteoblast response to micron-scale surface structure and surface energy of titanium substrates. Proc Natl Acad Sci U S A. 2008 Oct 14;105(41):15767-72.

72. Qiu Z, Chen C, Wang X, Lee I. Advances in the surface modification techniques of bone-related implants for last 10 years. Regenerative biomaterials. 2014;1(1):67-79.

73. Miralami R, Koepsell L, Premaraj T, Kim B, Thiele GM, Sharp JG, et al. Comparing Biocompatibility of Nanocrystalline Titanium and Titanium-Oxide with Microcrystalline Titanium. MRS Proceedings; Cambridge Univ Press; 2013.

74. Fogh J, Fogh JM, Orfeo T. One hundred and twenty-seven cultured human tumor cell lines producing tumors in nude mice. J Natl Cancer Inst. 1977 Jul;59(1):221-6.

75. Spreafico A, Frediani B, Capperucci C, Chellini F, Paffetti A, D'Ambrosio C, et al. A proteomic study on human osteoblastic cells proliferation and differentiation. Proteomics. 2006;6(12):3520-32.

76. Manivasagam G, Dhinasekaran D, Rajamanickam A. Biomedical Implants: Corrosion and its Prevention-A Review. Recent patents on corrosion science. 2010.

77. Losina E, Thornhill TS, Rome BN, Wright J, Katz JN. The dramatic increase in total knee replacement utilization rates in the United States cannot be fully explained by growth in population size and the obesity epidemic. J Bone Joint Surg Am. 2012 Feb 1;94(3):201-7.

78. Aherwar A, Singh A, Patnaik A. A study on mechanical behavior and wear performance of a metal–metal Co–30Cr biomedical alloy with different molybdenum addition and optimized using Taguchi experimental design. Journal of the Brazilian Society of Mechanical Sciences and Engineering. 2018;40(4):213.

79. Aherwar A, Singh AK, Patnaik A. Current and future biocompatibility aspects of biomaterials for hip prosthesis. AIMS Bioeng. 2016;3(1):23-43.

80. Aherwar A, Singh AK, Patnaik A. Cobalt Based Alloy: A Better Choice Biomaterial for Hip Implants. Trends in Biomaterials & Artificial Organs. 2016;30(1).

81. Ruijtenberg S, van den Heuvel S. Coordinating cell proliferation and differentiation: Antagonism between cell cycle regulators and cell type-specific gene expression. Cell Cycle. 2016;15(2):196-212.

82. Chung KK, Schumacher JF, Sampson EM, Burne RA, Antonelli PJ, Brennan AB. Impact of engineered surface microtopography on biofilm formation of Staphylococcus aureus. Biointerphases. 2007;2(2):89-94.

83. Annexin V, FITC Apoptosis Detection Kit [Internet]. Available from: https://www.dojindo.com/store/p/847-Annexin-V-FITC-Apoptosis-Detection-Kit.html.

84. Karachalios T. Bone-implant interface in orthopedic surgery: basic science to clinical applications. Springer Science & Business Media; 2013.

APPENDIX A: PRELIMINARY DATA

1. Cell detachment methods

This experiment was aimed to compare different cell detachment methods to figure out which method affected the cells viability less in an optimized time frame. In this regard, 3 different known detergents were used.

Trypsin: Trypsin is the most common treatment to remove adherent cells from a culture surface. In this experiment, 1X Trypsin solutions 0.025% was used to avoid any damages to cell membranes.

Accutase: Accutase is another cell dissociation used for the routine detachment of cells from standard tissue culture. Compared to trypsin, accutase maintains higher cell viability following detachment of cells.

Cellstripper: Cellstripper is a non-enzymatic cell dissociation solution that gently detaches adherent cells in culture. Cells can be exposed to cellstripper for extended periods of time without the risk of damage associated with protein-digestive enzymes like trypsin.

To measure the detached cells' viability, a live/dead fixable stains kit was used. Using flow cytometry, this kit assessed cell viability in samples via the reaction of fluorescent reactive dyes with amines (cellular proteins). These dyes cannot penetrate live cell membranes and only react to cell surface proteins resulting in faint staining. However, the dyes can permeate the damaged membranes of dead cells and stain both the interior and exterior amines, resulting in intense staining. Therefore, the difference in fluorescence intensity discriminated between the live and dead cells.

In this regard, 3 flasks of cells were collected at 50% confluency. After aspirating medium and washing with 2 ml PBS, 1 ml of trypsin, accutase, or cellstripper was added to each flask.

Incubated for 2 minutes, 10 minutes, and 25 minutes relatively (these timings were when half of the cells were detached, checked using a microscope), 5 ml of medium were added to each flask, cells were filtered, counted, and centrifuge at 300 rpm for 5 minutes. Cells were resuspended in 2 ml of PBS for experiment and in 2 ml of PBS for control. Dyes were prepared based on the manufactural protocol, 1 μL of which were added to 1 mL of the cell suspension, mixed well, and incubated in room temperature in the dark for 30 minutes. Cells were washed twice with 1 mL of PBS with 1% BSA, resuspended in 1 mL of PBS with 1% BSA and were analyzed by flow cytometry using the appropriate detection channel (450/50 nm or similar).
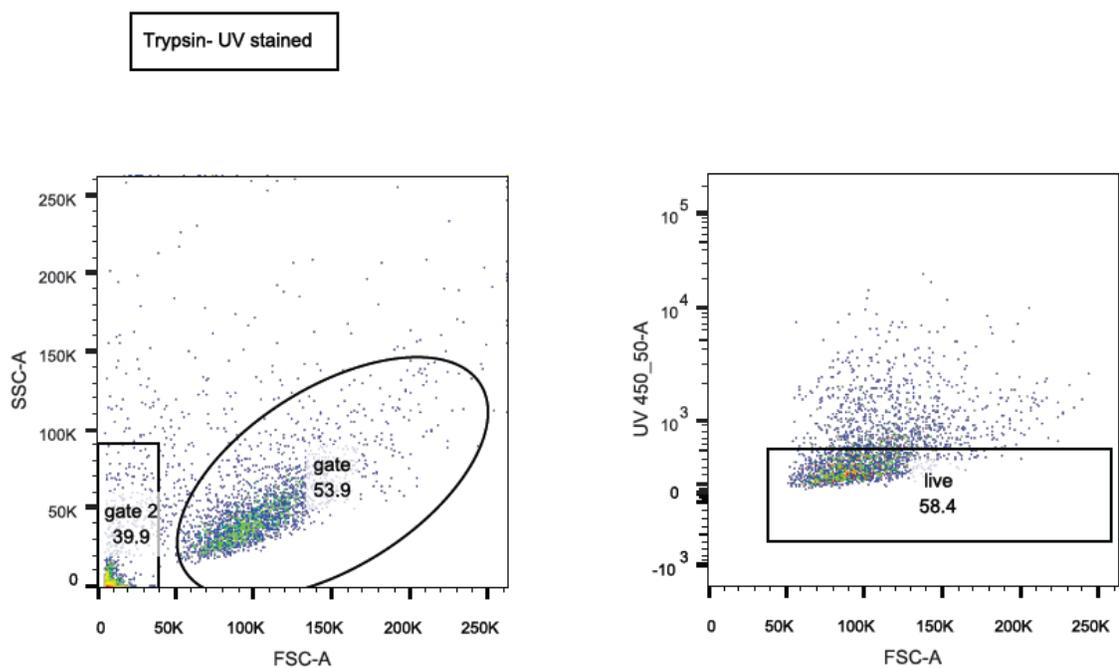
Trypsin- UV stained

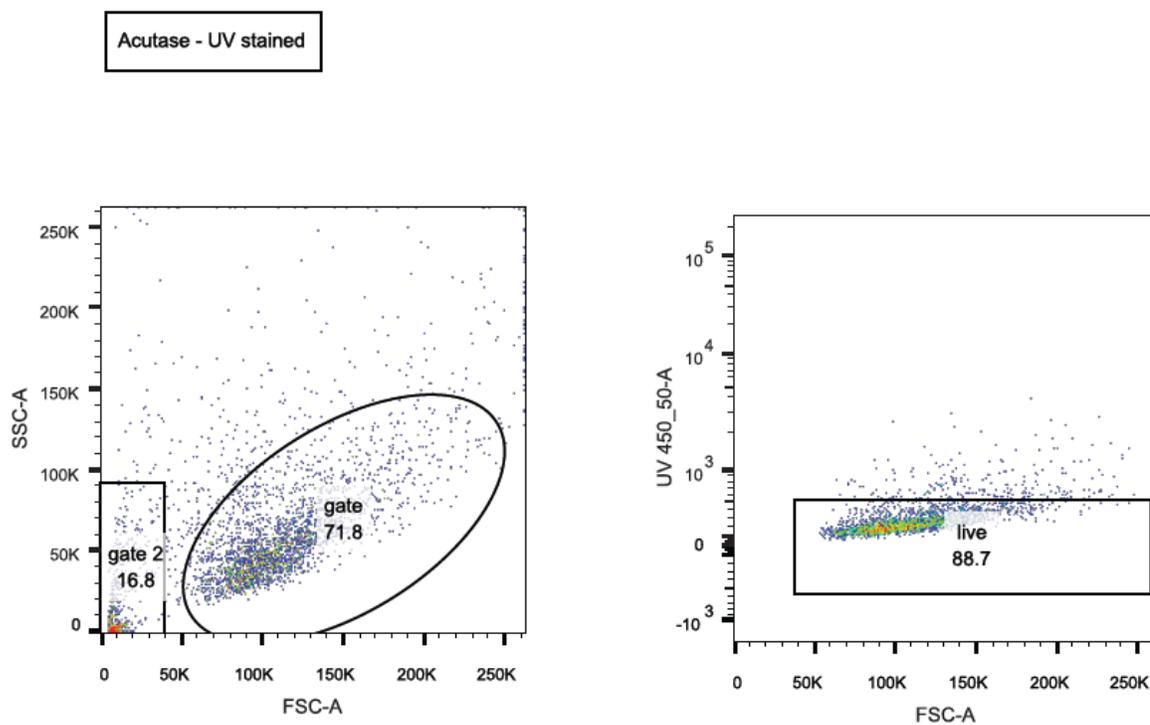Figure A-1: Percentage of viable cells detached by trypsin measured by flow cytometry

Acutase - UV stained

Figure A-2: Percentage of viable cells detached by accutase measured by flow cytometry
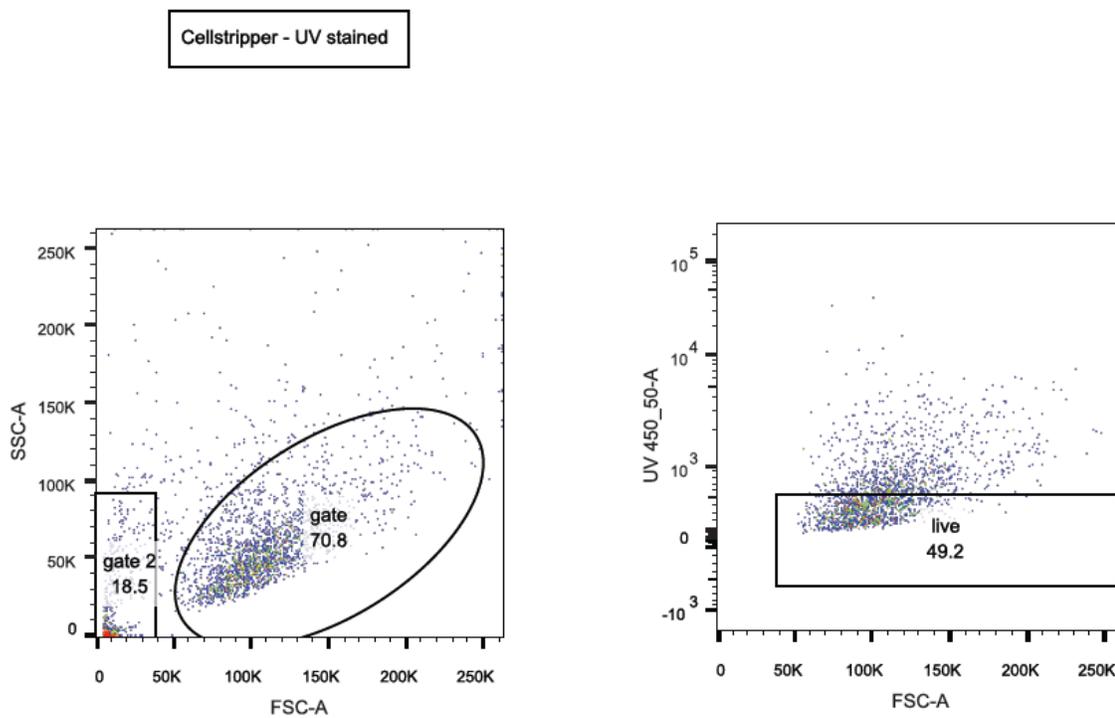
Cellstripper - UV stained

Figure 0A-3: Percentage of viable cells detached by cellstripper measured by flow cytometry

The result showed more dead/damaged cells detached by trypsin while accutase method showed the least dead cells and debris (highest viability percentage). In addition, cellstripper was not a viable option, since time was an important factor and 20 minutes seemed to be too long.

2. Accutase timing

After choosing accutase to be the detachment detergent, the next step was to find the optimal timing for cells' detachment with the least amount of damage and the highest viability. This experiment was done using glass samples (actual size). In this regard, 10 flasks of cells were harvested at 50% confluency using trypsin, detached cells were adjusted to 500,000 cells per ml, 8 samples were placed in a 12-well plate, and each sample was seeded with 500,000 cells. After 24 hours incubation, samples were transferred to a fresh 12-well plate, and 1 ml fresh medium was added and incubated for another 24 hours. After aspirating medium, samples were washed with 0.5 ml PBS, 300 µl of accutase were added to each sample, and samples were incubated for 5 minutes, 10 minutes, 15 minutes, and 30 minutes in duplicates. Detached cells were put in 4 separate 15-ml conical tubes, and the other 4 samples were fixed and stained with DAPI, and counted as described in previous methods. Detached cells were filtered, counted, and centrifuge at 300 rpm for 10 minutes. Cells were resuspended in 0.5 ml of PBS for experiment and in 0.5 ml of PBS for control. Prepared based on the manufactural protocol, 1 µ of dyes was added to 1 mL of the cell suspension, mixed well, and incubated in room temperature in the dark for 30 minutes. Cells were washed twice with 1 mL of PBS with 1% BSA, resuspended in 1 mL of PBS with 1% BSA, and were analyzed by flow cytometry using the appropriate detection channel (450/50 nm or similar).

The results from flow cytometry indicated that 10 minutes had the highest amount of harvested cells with highest viability percentage. Therefore, the 10-minutes incubation time was chosen to be the optimal timing for the accutase detaching method.
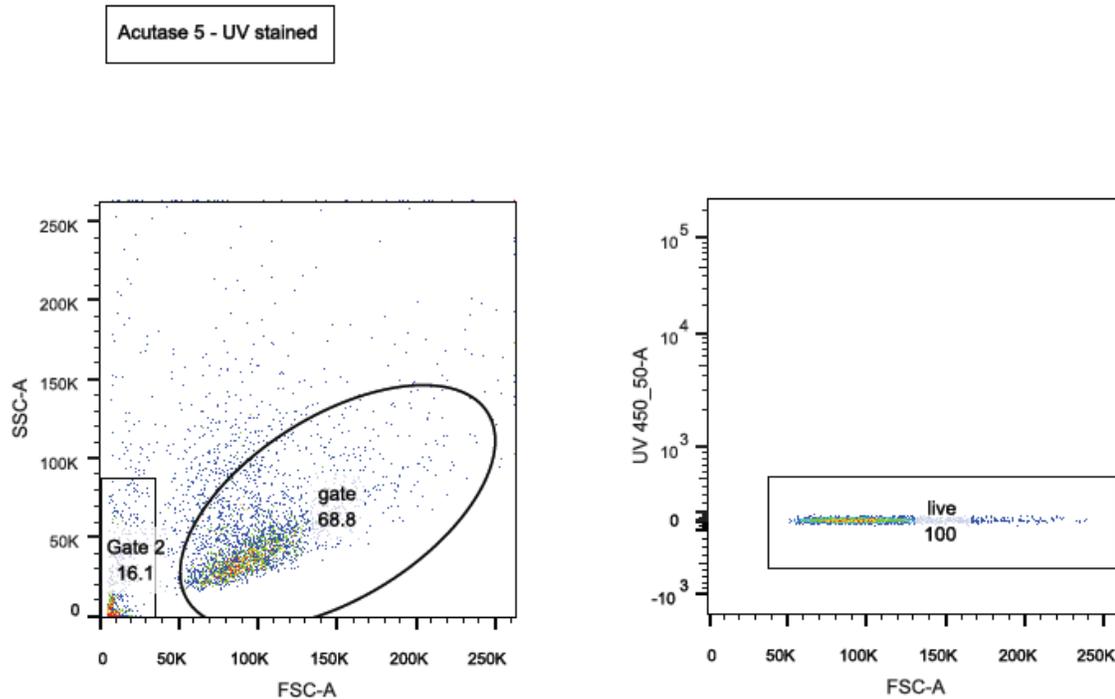
Figure A-4: Detached cells using accutase after 5 minutes incubation time
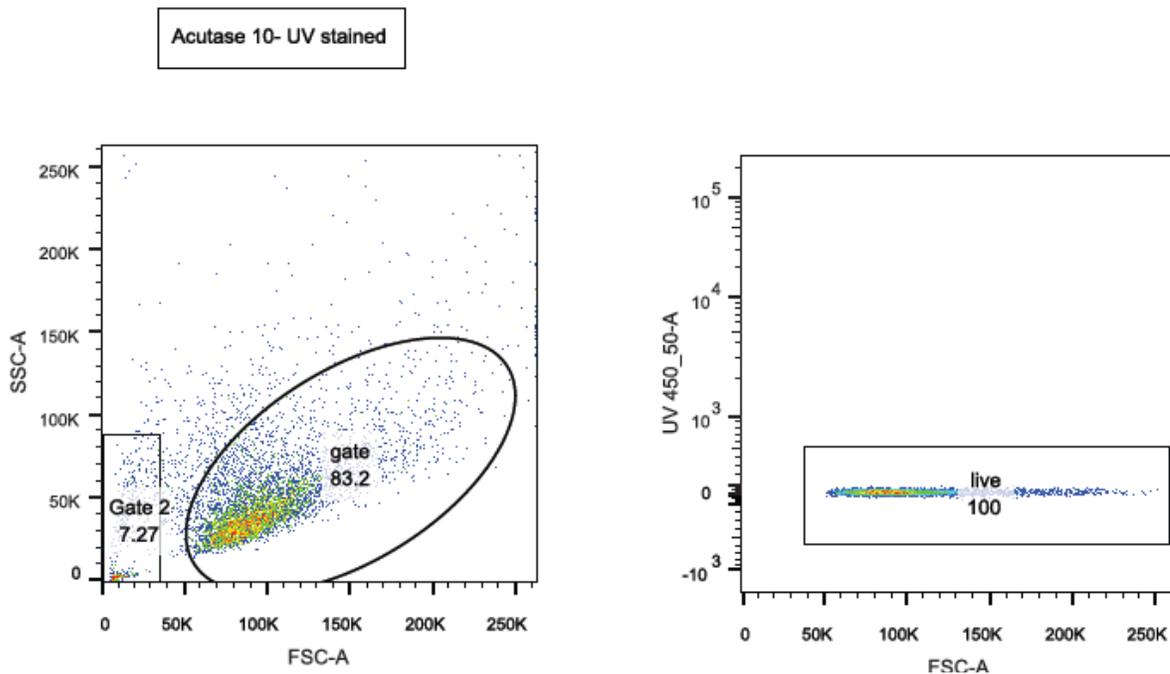

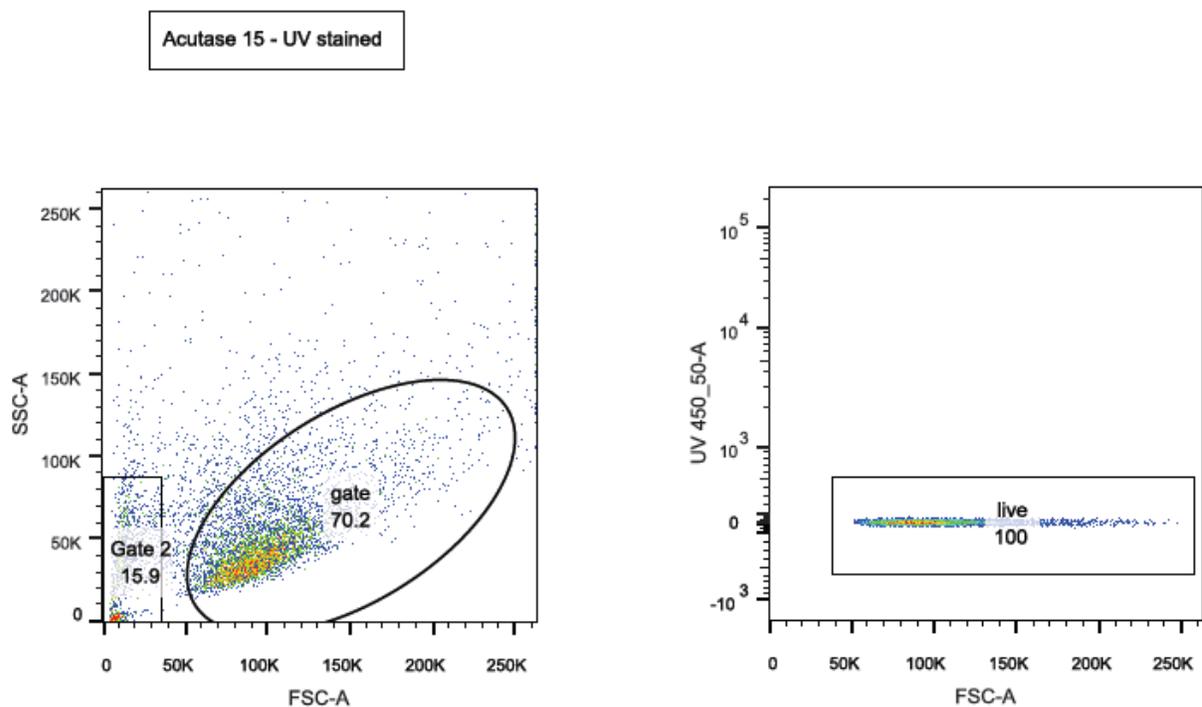Figure A-5: Detached cells using accutase after 10 minutes incubation time

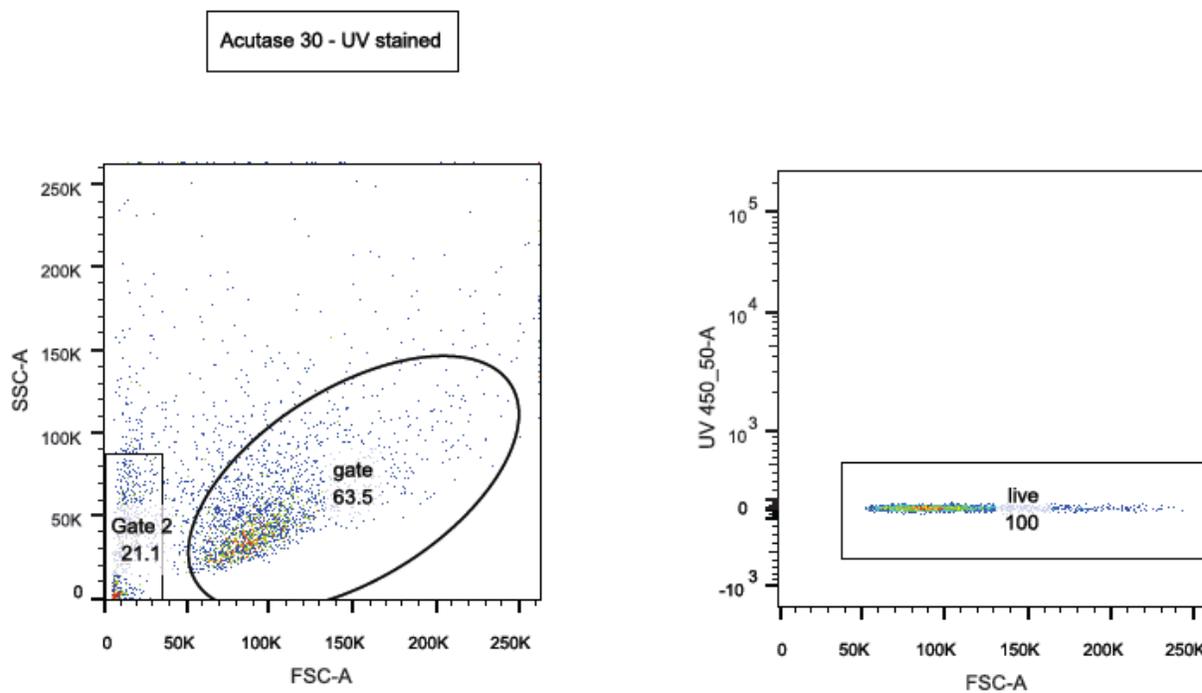Figure A-6: Detached cells using accutase after 15 minutes incubation time

Figure A-7: Detached cells using accutase after 30 minutes incubation time

3. Cleaning detergents

Due to a shortage of nano-samples, some samples had to be reused for a limited number of experiments. In order to find the best detergent to clean proteins and residuals on used samples, without interfering with surface properties, liquinox and tergazyme were chosen.

Liquinox: it is an FDA certified cleaning liquid detergent with a wide application range from healthcare instruments to industrial parts. It is phosphate free, biodegradable, with a corrosion inhibited formulation that leaves no interfering residues.

Tergazyme: it is an FDA certified enzyme-active powdered detergent with a wide application range from healthcare instruments to industrial parts. It is biodegradable, with a corrosion inhibited formulation that leaves no interfering residues, and contains protease enzyme to remove proteinaceous.

To test the toxicity of these detergents, apoptosis experiment (as explained previously) was performed using the fresh ZrO_2 sample, used-ZrO_2 sample washed with liquinox, used-ZrO_2 sample washed with tergazyme, and used-ZrO_2 sample without any detergent wash. The data showed no significant differences between the fresh sample and detergent-washed samples. Although, liquinox seemed to be more similar to the fresh samples. Therefore liquinox has been selected as a cleaning detergent for reusing samples if it is necessary.